Missouri S&T Library and Learning Resources

Scholars' Mine

Doctoral Dissertations | Student Theses and Dissertations

Fall 2013

Interacting stress concentration factors and their effect on fatigue of metallic aerostructures

David Warren Whitley

Follow this and additional works at: https://scholarsmine.mst.edu/doctoral_dissertations

 Part of the Aerospace Engineering Commons

Department: Mechanical and Aerospace Engineering

Recommended Citation

Whitley, David Warren, "Interacting stress concentration factors and their effect on fatigue of metallic aerostructures" (2013). *Doctoral Dissertations*. 1830.
https://scholarsmine.mst.edu/doctoral_dissertations/1830

This thesis is brought to you by Scholars' Mine, a service of the Missouri S&T Library and Learning Resources. This work is protected by U. S. Copyright Law. Unauthorized use including reproduction for redistribution requires the permission of the copyright holder. For more information, please contact scholarsmine@mst.edu.

INTERACTING STRESS CONCENTRATION FACTORS AND THEIR EFFECT ON FATIGUE OF METALLIC AEROSTRUCTURES

by

DAVID WARREN WHITLEY

A DISSERTATION

Presented to the Faculty of the Graduate School of the

MISSOURI UNIVERSITY OF SCIENCE AND TECHNOLOGY

In Partial Fulfillment of the Requirements for the Degree

DOCTOR OF PHILOSOPHY

in

AEROSPACE ENGINEERING

2013

Approved by

Dr. Lokeswarappa R. Dharani, Advisor

Dr. Victor Birman, Co-Advisor

Dr. K. Chandrashekhara

Dr. Daniel Stutts

Dr. Jefferey Thomas

ABSTRACT

During fabrication of certain aerostructure components, a situation can arise where a hole is mislocated so that it interferes with a radius, chem-mill step, machined step, or some other similar detail. The interaction of stress concentration effects between a hole and step are not well understood and the resulting impact on fatigue performance is difficult to predict. There exists a need for fatigue data that can be used to determine the analysis methods for evaluation of the interaction of machined steps and fastener holes.

In this dissertation, the effect of stress concentrations placed in close proximity to each other and their impact on fatigue performance is studied. Unique cases of interaction between a hole and radius are analyzed. Physical testing and finite element analysis methods are used to derive thestress concentration factor (SCF, K_t) modification factors (K_{tf}) for open hole and joint assembly structures. The most conservative factors derived are recommended for use in fatigue analysis for these instances of holes located at or near radii.

The SCF mod factors increase as distance between the hole and radius tangent decreased. For associated geometry, loading and materials similar to those presented within this research, a K_{tf} value of 1.22 is suggested for use in fatigue analysis of these situations of holes intersecting a radius.K_t and K_{tf} values have a significant effect on fatigue lifetimes and resulting fatigue margins of safety. Based on a pass/fail experiment, the corrosion specimen passed the test as no fatigue cracking failures associated with the bolt in radius condition were observed.

ACKNOWLEDGEMENTS

I would like to express thanks to my dissertation advisor Dr. L. R. Dharani for his guidance during the course of this research. I would also like to thank Dr. Victor Birman, Director of the Missouri S&T Engineering Education Center for his continued assistance with my graduate studies. To the remaining members of my advisory committee, thank you for your interest and participation.

Also, to my parents Ron and Nancy Whitley and my sister Christine Whitley, I appreciate your ongoing support. Your love and encouragement helped motivate me to conduct this research.

The cooperation of my employer, Spirit AeroSystems, Inc., in particular my colleague Mark Ofsthun, should be acknowledged. The resources and testing capabilities provided by Spirit made this study possible. Thank you Mark for your expert input and guidance.

TABLE OF CONTENTS

LIST OF ILLUSTRATIONS

LIST OF TABLES

1. INTRODUCTION

1.1. METAL FATIGUE

1.1.1. Definition of Fatigue. A standard definition of the term fatigue, as it applies to metals, from ASTM E1823 [1] is, *the process of progressive localized permanent structural change occurring in a material subjected to conditions that produce fluctuating stresses and strains at some point or points and that may culminate in cracks or complete fracture after a sufficient number of fluctuations*. A more straightforward definition for fatigue is the nucleation of cracks in a structure resulting from cyclic loading.

Voids or slip planes that are inherent in the material join together to form these cracks. The three chronological stages a fatigue crack undergoes are

1. Crack Nucleation
2. Fatigue Crack Growth
3. Ductile Separation

The fatigue strength of a material differs from the static strength in that the static strength is related to a single applied load while the fatigue strength is dependent upon repeated loading that varies over time.

Classical fatigue theory is typically considered valid for metals only. Composite materials exhibit fatigue related properties that cannot necessarily be covered by typical fatigue analysis methods and relationships. The study of the phenomenon of fatigue in composites is ongoing and more research is needed to come to a better understanding of how these complex materials react to repeated loading. Although composites are used

extensively in aerostructures, the research contained in this study is limited strictly to metals.

Some commonly used terms and equations related to a typical cyclic fatigue loading profile are presented. Figure 1.1 shows a representative fatigue loading cycle.

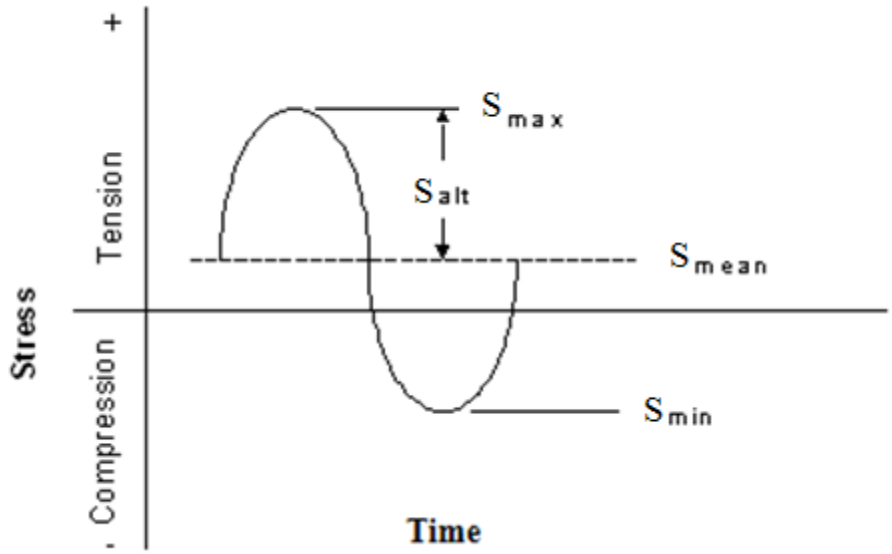

Figure 1.1. Cyclic Fatigue Loading Profile

Stress Range: $$\Delta S = S_{\max} - S_{\min} \quad (1)$$

Stress Amplitude: $$S_{alt} = \frac{S_{\max} - S_{\min}}{2} \quad (2)$$

Mean Stress: $$S_{mean} = \frac{S_{\max} + S_{\min}}{2} \quad (3)$$

Stress Ratio: $$S = \frac{S_{\min}}{S_{\max}} \quad (4)$$

Fatigue analysis and fracture mechanics, the science behind damage tolerance, are sometimes grouped together. However, it should be noted that fatigue and fracture mechanics are actually separate disciplines. The goal of proper fatigue analysis for design is to ensure that a crack will not initiate or nucleate for a desired life. In fracture mechanics, it is assumed that a crack of a certain specified length already exists and the amount of time it takes, or number of cycles needed, to grow the existing crack to a critical length is determined. Each discipline has its own unique methods and set of commonly used relationships. Fatigue is concerned with concepts including S-N curves and stress concentrations while the theory and study of fracture mechanics includes the use of da/dN curves and stress intensity factors.

1.1.2. A Historical Perspective of Fatigue. The first study of fatigue, relating to a structural change in metals due to repeated loading, dates back to 1838 when Wilhelm Albert [2] conducted research on hoisting chains used in mining. Jean-Victor Poncelet, a French engineer and mathematician, coined the term *fatigue* to describe the wearing down of a material due to changes in loading in 1839 during lectures at a military school in Metz, France. The first in-depth fatigue analysis involving testing and the development of S-N curves is credited to August Wöhler [3] in 1860 for a study of failures of railroad axles.

Much of this early fatigue-related research was conducted due to a need to analyze metallic machinery that was used extensively during the Industrial Revolution of the 19th century. A large amount of new information has been generated and many

original analysis methods have been developed relating to fatigue subsequent to these early studies. Research on fatigue in aerostructures, important because of the typical loading and unloading conditions that exist, has played a critical role in the development of the science of metal fatigue since the advent of flight in the early 20th century. Many fatigue failures and disasters in aerostructures have been recorded. The in-flight disintegration of a Comet I airplane in 1954 after a long service history is one of the first notable failure events in aerospace that was attributed to fatigue. The particular airplane that failed was actually the first passenger plane with a jet engine to go in to active service. Just a few weeks after the first Comet I event, another Comet I disintegrated in-flight. All service of the aircraft was then immediately suspended. Subsequent testing, as detailed in the Federal Aviation AdministrationDamage Tolerance Assessment Handbook [4], revealed that the cause of the disasters was a fatigue failure originating at the cabin windows.

The widespread fatigue damage (WFD) failure of Aloha Airlines Flight 243 in 1988 is another catastrophic event attributed to the effects of cyclical loading. In this accident, an entire section of the upper cabin was blown out. The Boeing 737 aircraft was actually well beyond the certified design service goal when the fatigue failure occured. A passenger is reported to have noticed a crack in the fuselage skin prior to the flight. The plane was forced to make an emergency landing and one person was killed. The National Transportation Safety Board accident report [5] identified corrosion as the primary cause of the fatigue cracking in this incident. A picture of the Aloha airplane just after landing, which illustrates the massive damage caused by metal fatigue, is shown in Figure 1.2.

Figure 1.2. Aloha Airlines Flight 243 - Fatigue Failure Due to Corrosion [6]

There have been many other disasters and events involving fatigue in aerostructures, some of them very recent. TheLos Angeles Times [7] reported that in April of 2011, a Southwest Airlines Boeing 737 was forced to make an emergency landing after a visible tear opened in the upper fuselage skin causing some cabin depressurization. Subsequent inspections found fatigue cracking in the critical region. These incidents indicate the necessity of proper and detailed fatigue analysis in the design and maintenance of aircraft as well as a need for continued research related to the effects of loading and unloading on aerostructures.

1.1.3 Stress-Life Approach. There are different methods commonly used to conduct fatigue analysis of metals. Stress-Life, Strain-Life, and some applications of Linear Elastic Fracture Mechanics (LEFM) can all be employed when attempting to predict the nucleation of cracks in metals. The Stress-Life or S-N approach is the most frequently used and well established method of fatigue life prediction.

The Wöhler diagram, more commonly referred to as the S-N curve, provides the basis for the Stress-Life method of fatigue analysis. This plot, which is derived from empirical test data for a specified material, shows a relationship between the alternating stress and cycles to failure. Bannantine, Comer and Handrock [8] note that S-N curves are usually plotted on a log-log scale. An example of a S-N curve is displayedin Figure 1.3.

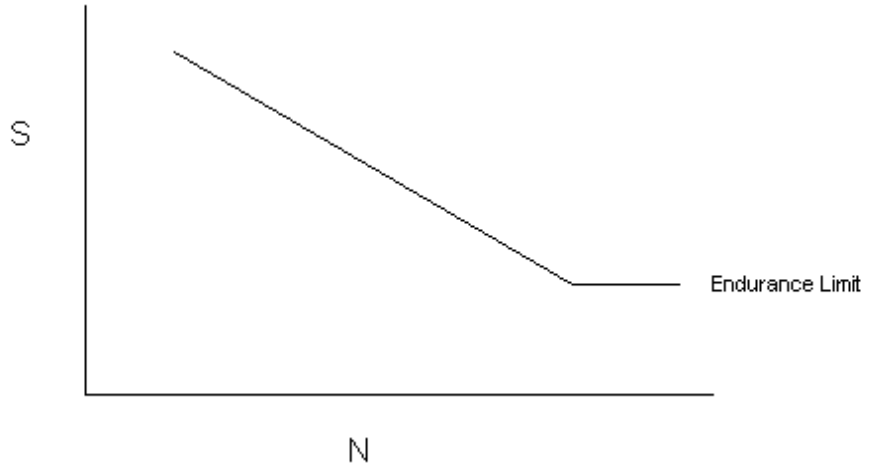

Figure 1.3. Typical S-N Curve

The test data used to generate a S-N curve is good for a specified R value. The endurance limit is an alternating stress for which a certain metal will never experience fatigue failure as long as the stress remains below this value.

Figure 1.4 illustrates the effect that notches have on a typical S-N curve. The notched specimen will have a shorter fatigue life at the same stress level compared to the unnotched specimen.

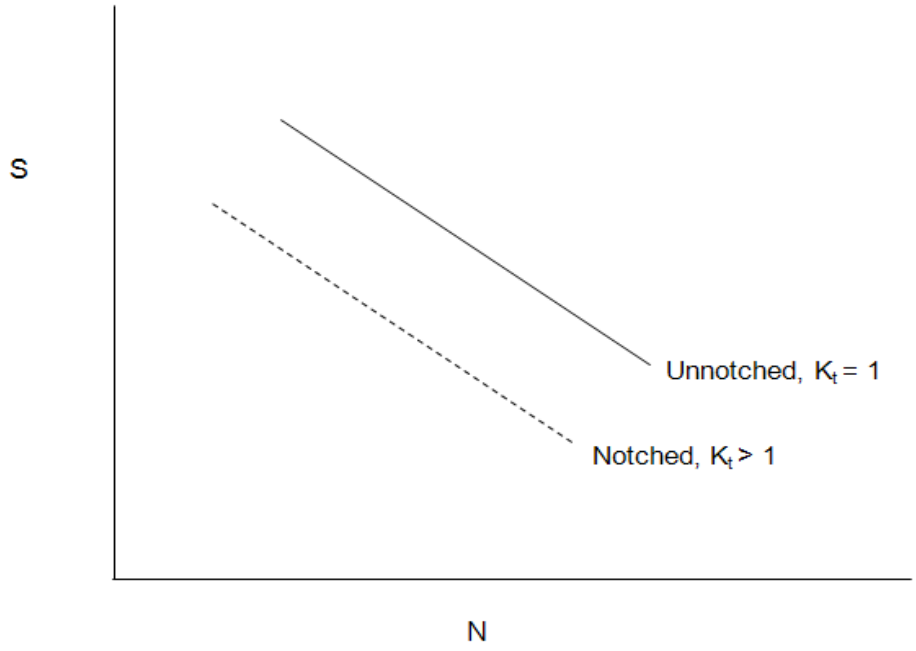

Figure 1.4. Unnotched vs. Notched S-N Curves

1.1.3. Variable Amplitude Loading. Fatigue loading is generally represented as a spectrum, which is a series of maximum and minimum cycles of loading that are grouped together. These loading cycles have varying stress amplitudes. This is true especially in aerostructures, that are often subjected to complex load patterns. A diagram of a simplified spectrum is shown in Figure 1.5.

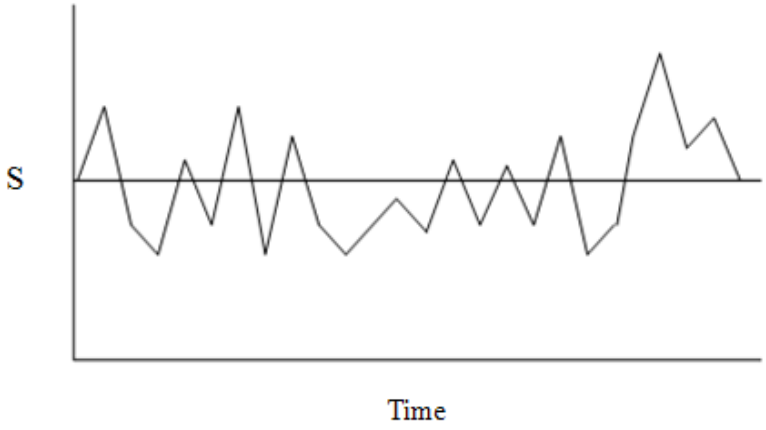

Figure 1.5. Fatigue Spectrum Loading

To analyze a structure for variable amplitude loading, the concept of a damage ratio is introduced. The damage ratio, D_i, at a particular stress level in the spectrum is defined as

$$D_i = \frac{n_i}{N_i} \tag{5}$$

where n_i is the number of cycles at a certain stress and N_i is the number of cycles to failure at that same stress.

Miner [9] has developed an important relationship in metal fatigue analysis that can be used for life prediction. Miner's rule states that fatigue failure will occur when the sum of the damage ratios for all of the stress levels in a given spectrum is greater than or equal to one. Miner's rule is given by Equation (6).

$$\sum D_i = \sum \frac{n_i}{N_i} \geq 1 \tag{6}$$

For variable amplitude loading in aerostructures, the ground-air-ground , or GAG,stresses are the maximum and minimum stresses reached in the entire spectrum. The GAG Damage Ratio can be defined as

GAG Damage Ratio = GAG Damage / Total Damage (7)

If it is assumed that the spectrum represents variable loading for one flight then the predicted fatigue life in number of flights for a critical detail can be found using the concept of GAG stresses and GAG damage by applying Equation (8).

Number of Flights = 1 / (GAG Damage / GAG Damage Ratio) (8)

This predicted fatigue life can then be used to determine a fatigue margin of safety based on a pre-defined service life objective.

1.2. STRESS CONCENTRATIONS

1.2.1. Definition of a Stress Concentration. ESDU Data Item 64001 [10], *Guide to Stress Concentration Data,* states that a stress concentration, also sometimes referred to as a stress raiser or stress riser, is defined as *a local stress increase in the intensity of a stress field due to discontinuity*. Stress concentrations are measured by

stress concentration factors, typically denoted by the symbol K_t. In [10], the stress concentration factor, or SCF, is defined as *the ratio of the highest stress to a reference stress calculable from simple theory*.

Many different sources and references provide K_t charts for various geometries and loading conditions involving features such as notches, radii, fillets, holes, grooves, etc. However, Peterson's Stress Concentration Factors [11,12] acts as the preferred handbook for SCF values.

The situation of a hole in a plate loaded in axial tension is displayed in Figure 1.6. The stress distribution in the plate at the hole location is shown. As D/W goes to zero, for an infinitely wide plate, $K_t = 3$.

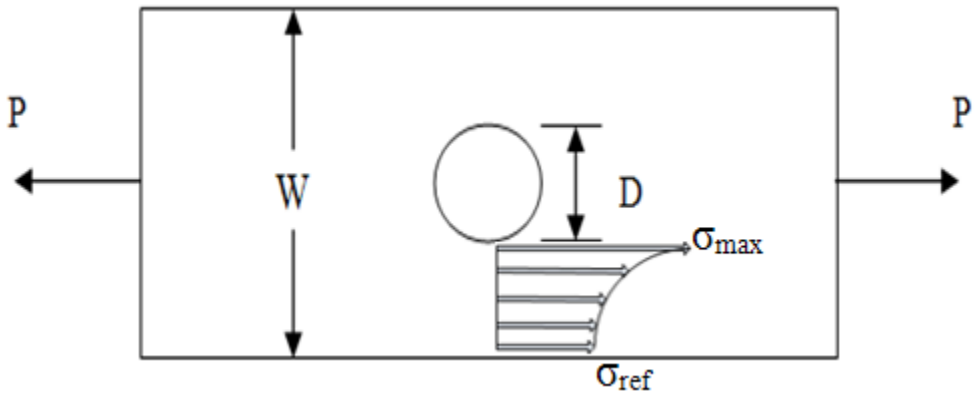

Figure 1.6. Plate with a Hole Loaded in Axial Tension

A bar with shoulder fillets loaded in tension is shown in Figure 1.7. As r/b decreases or as W/b increases, the stress concentration factor goes up. This means that a small radii, or sharp corner, will have a high K_t.

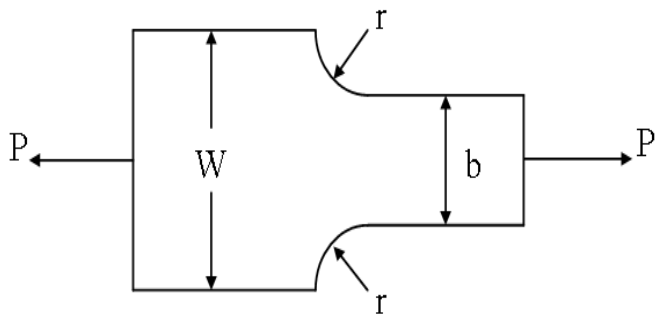

Figure 1.7. Flat Bar in Tension with Shoulder Fillets

Now consider the case a flat bar with a double notch loaded in tension, as shown in Figure 1.8. As r/b decreases or W/b increases, the value of K_t rises. Smaller radii in the notches or deeper notches will cause the stress concentration factor for this case to increase.

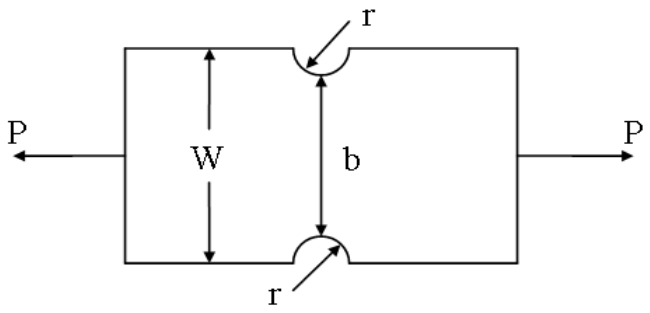

Figure 1.8. Flat Bar in Tension with Double Notch

Stress concentration factors are always dependent upon the specific case of geometry and loading being considered. Engineers must always reference the K_t charts

in sources like Peterson [11,12] to ensure that they are using accurate SCF values in their analysis of metallic structures.

1.2.2. Use of Stress Concentrations in Fatigue Analysis. Stress concentration factors play a critical role in any detailed metal fatigue analysis. Within a structure, fatigue cracks are most likely to nucleate in the region where the stress is at its peak. The highest stresses in a body will occur at geometric features including holes, radii, notches, etc. These peak stresses are calculated from stress concentration factors. Therefore it is essential that accurately determined SCFs are used to ensure that a proper fatigue life prediction of any structure has been performed. The use of stress concentration factors in aerostructures is particularly important due to the high number of stress raising features that exist in aerospace part design, in particular fastener holes.

For fatigue analysis, the net stress concentration factor, denoted with the symbol K_{tn}, is used. This net stress concentration factor must be calculated to accurately determine the maximum stress at the critical feature.

Consider a plate loaded in tension with a hole at the center as shown in Figure 1.9. The critical points at the hole where the peak stress is located are labeled C. The plate has a thickness of h.

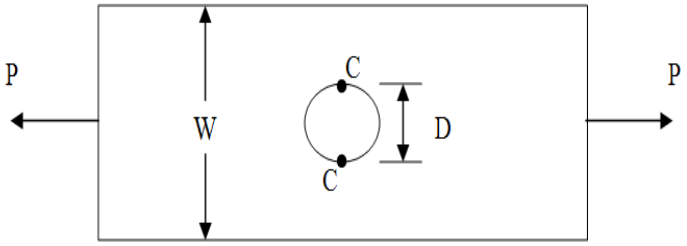

Figure 1.9. Plate with a Hole Loaded in Tension

K_{tn} takes in to account the net cross-sectional area in the body at the point of interest. The net stress concentration factor can be written as a function of the gross stress concentration factor, denoted with the symbol K_{tg}, which does not account for the net cross-sectional area in the body at the critical point. For the case presented in Figure 1.9, the difference between K_{tn} and K_{tg} is found in the formula used to the determine the reference stress for each factor.

$$K_{tn} = \frac{\sigma_{\max}}{\sigma_{ref,net}} = \frac{\sigma_{\max}(W-D)h}{P} \tag{9}$$

$$K_{tg} = \frac{\sigma_{\max}}{\sigma_{ref,gross}} = \frac{\sigma_{\max}Wh}{P} \tag{10}$$

$$K_{tn} = K_{tg}\frac{W-D}{W} \tag{11}$$

Equations (9-11) are used to calculate gross and net stress concentration factors throughout this research.

1.2.3. Concept of Interacting Stress Concentrations. In certain situations, two or more stress concentrations may interact causing an increase or decrease in the stress concentration factor for each detail. The interaction of these stress risers is dependent upon the geometric proximity of the features with respect to each other as well as loading conditions. Some of these situations may be relatively simple to analyze and accurate stress concentration factors can be easily developed. Other times, the combined effects are complex and predicting stress concentrations factors for cases of interaction can be challenging.

The word *interacting* is sometimes substituted with other terms including *multiple*, *superimposed*, *intersecting*, *combined* or *compounding*to describe these situations. All of these descriptions have the same meaning and for the purposes of consistency within this research the term *interacting*is predominantly used.

Interacting stress concentrations can occur in aerostructures as a result of a design that specifies two or more geometric features such as holes, radii, notches etc. be placed in close enough proximity to each other that interaction may occur depending upon loading conditions. Circumstances may also arise during fabrication and repair of parts and assemblies that can or will cause stress concentrations of separate details to combine. Mistakes made by manufacturing such as mislocated holes, extra holes, overly sharp radii, holes drilled in radii, extra notches, etc. can be the origin of interacting stress concentrations. Many times these fabrication errors can turn single geometric details

with easily determined stress concentration factors in to complex situations of multiple critical features that experience the effects of interaction stress concentrations.

These interacting stress concentrations and their associated stress concentration factors are important to fatigue analysts. The potential rise in stresses caused by the proximity of multiple details considering loading criteria needs to be taken in to account to adequately predict the fatigue life of the structure being studied. The interaction of stress concentrations can cause a significant increase in stresses when compared to situations where only a single stress raiser is being considered. Consequently, interacting stress concentrations can reduce expected fatigue life in aerostructures.

Fatigue analysts may use knowledge relating to interacting stress concentrations to suggest and help design details and repairs that will attempt to mitigate the negative effects these interacting features can potentially have on the overall life of a particular structure. Coordination with static stress analysts may also be required. The use of K_t values is not necessarily limited to fatigue analysis. Stress concentration factors can be used to design and study parts and assemblies to ensure that stress allowables are not exceeded.

1.3. PREVIOUS STUDIES OF INTERACTING STRESS CONCENTRATIONS

1.3.1. Overview of Previous Research on Interacting Stress Concentrations.

There have been numerous studies of situations involving the interaction of stress concentrations due to the proximity of various geometric features with respect to certain applied loading conditions. Some of these studies are simplistic while others are very complex, involving extensive testing and the use of finite element models to predict stress

values at critical locations. The majority of previous research on the phenomenon of K_t interactions is based on a detailed study of a specific situation or situations involving closely spaced features subjected to a particular loading profile. Also, many of the earlier studies on this specific topic are related to aerostructures or have been completed with the goal of being used in the aerospace industry. These instances seem to arise or occur in this field more frequently than in any other engineering discipline.

Ling [13] is typically recognized for having conducted the first full-scale research on interacting stress concentrations.In Ling's study, combined K_t effects were analyzed for two circular holes in a plate. This situation tends to be the most common example of stress concentration interaction found in aerostructures.

Peterson [11] includes a section concerning the effects of multiple stress concentrations. A simplified relationship is presented to attempt to account for the interaction of two stress raising features.

$$K_{t1,2} = K_{t1} \cdot K_{t2} \tag{12}$$

However, Equation (12) is approximate and in most cases considered overly conservative in that the combined stress concentration factor, $K_{t1,2}$, is found to be much larger than the actual value that can be derived through means of testing or applied finite element analysis.

Other relationships have been proposed to account for combined stress concentrations including the root sum squared method identified in Equation (13).

$$K_{t1,2} = \sqrt{K_{t1}^{\,2} + K_{t2}^{\,2}} \tag{13}$$

Another simple relationship, presented by Eccles [14], that can be used in the analysis of two interacting stress concentrations is

$$K_{t1,2} = K_{t1}\sqrt{K_{t2}} \quad \text{, where } K_{t1} \geq K_{t2}\,. \tag{14}$$

The above K_t interaction Equations (12-14) are limited to only two combined features. Specific relationships must be developed and unique data generated for various cases of geometry and loading related to interacting K_t effects for more than two details.

1.3.2. Two Closely Spaced Holes in an Infinite Plate. One of the most commonly analyzed situations involving interacting stress concentration factors is the case of an infinite plate with two closely spaced holes loaded in tension, as shown in Figure 1.10. The direction of loading is perpendicular to the center-to-center spacing between the holes.

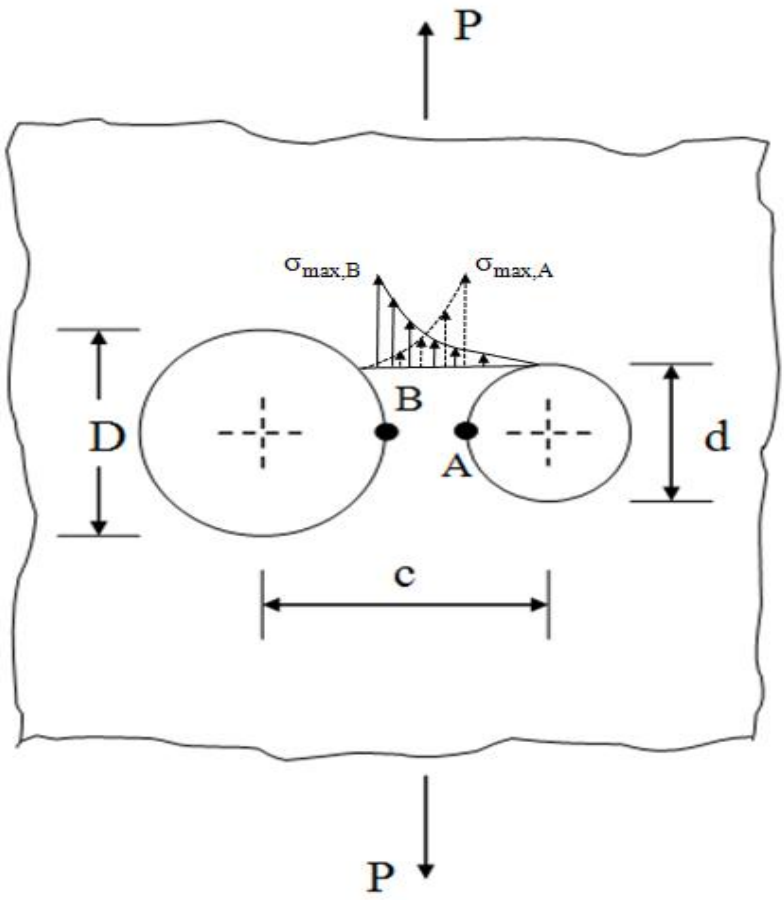

Figure 1.10. Infinite Plate with Two Circular Holes in Perpendicular Tension

In ESDU Data Item 75007 [15], *Geometric Stress Concentration Factors: Two Adjacent Unreinforced Circular Holes in Infinite Flat Plates*, it is shown that the K_t values for the small and large holes increase as d/c increases. This translates to a rise in stress concentration factors as the center-to-center spacing between holes decreases. This also holds true for two holes of equal size, where D/d = 1.0. Stress concentration factor values are shown to vary significantly for different D/d ratios.

Separate stress concentration factors are presented for both the small and large holes in [15]. The maximum stresses generally occur at points A and B for the small and large holes, respectively. All K_t values for this situation of geometry and loading approach 3 as c increases, which is the theoretical K_t of a single hole in an infinitely wide plate. This means that as the center-to-center spacing between the holes increases, the interacting K_t effects are mitigated. In practice, if $c \geq 4D$ then no combined stress concentration factors need be considered.

For an infinite plate with two circular holes in perpendicular tension, the larger stress concentration factor is associated with the smaller hole. The combined stress distribution depends upon the exact center to center distance between the holes and hole diameters. ESDU Data Item 85045 [16], *Stress Concentrations: Interaction and Stress Decay for Selected Cases*, covers this case in detail. The individual stress distributions for the small and large holes are shown in Figure 1.10.

Peterson [11] also includes stress concentration factor charts for the case of two closely spaced holes loaded in tension with a load direction perpendicular to the center-to-center spacing between holes. Similar results and comparable K_t values to those given in ESDU Data Item 75007 [15] were determined. Other studies and research by Graham, Raines, Swift and Gill [17] and Middendorf [18] on this same combination of geometry and loading have confirmed these findings.

The situation shown in Figure 1.10 is considered to be one of the most commonly occurring circumstances of interacting stress concentrations observed in aerospace applications. Closely spaced holes are seen most frequently in aerostructures when a hole is misdrilled or mislocated in close proximity to a blueprint hole.

Another similar and common occurrence of interacting stress concentration factors is presented in Figure 1.11. This case of multiple stress concentrations is identical to the one previously shown in Figure 1.10 with the exception that the direction of loading is now parallel to the center-to-center spacing between holes.

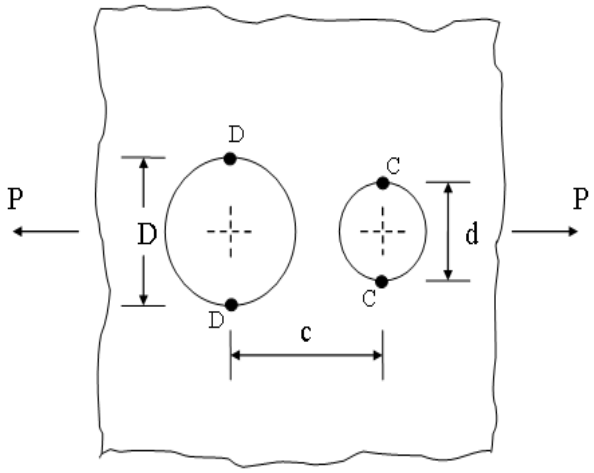

Figure 1.11. Infinite Plate with Two Circular Holes in Parallel Tension

ESDU Data Item 75007 [15] also covers this combined K_t circumstance. The data presented is somewhat unique in that as d/c increases, that is as the proximity of the holes with respect to one another increases, the stress concentration factors for the large hole and small hole tend to decrease. For most K_t interactions, the concern is that stress will go up as the critical features become closer to each other. Here the importance of load direction is illustrated. *When the load direction is parallel to the spacing between details, the stress concentration factors decrease as the proximity between features increases*.

Once again, the conclusions presented immediately above hold true for a wide range of D/d ratios, including two holes of the same size, where D/d = 1.0. The stress concentration factor values are shown to vary according to the ratio of D/d. For the small and large holes, the maximum stresses will generally occur at points C and D, respectively. As d/c goes to zero, or as the proximity of the holes with respect to one another decreases, the K_t values presented for the small and large holes in ESDU Data Item 75007 [15] approach 3 which is the stress concentration factor of a single hole in an infinite plate loaded in tension. It should also be noted that the K_t of the larger hole tends to increase slightly while the K_t of the smaller hole tends to decrease as D/d increases.

Peterson [11] also presents stress concentration factors for the situation shown in Figure 1.11. The results presented by Peterson [11] for two closely spaced holes in an infinite plate in axial tension with a load direction parallel to the center-to-center-spacing between holes are taken from ESDU Data Item 75007 [15] and Haddon [19].

In practice, the case of interacting stress concentrations presented in Figure 1.11 is typically ignored. Values of $K_t = 3$ can be conservatively used for both the small and large holes. However, if a more detailed or accurate assessment of the stresses at the holes is required, analysts and engineers may use the stress concentration factors determined considering the effects of interaction. Again if $c \geq 4D$, then no combined K_t effects should be taken in to account.

Now consider the case of two circular holes in an infinite plate subjected to biaxial loading, as shown in Figure 1.12. This example of stress concentration interaction exists as a combined case of the previous two circumstances of circular holes in an

infinite plate, where the loads shown in Figure 1.10 and Figure 1.11 have been superimposed.

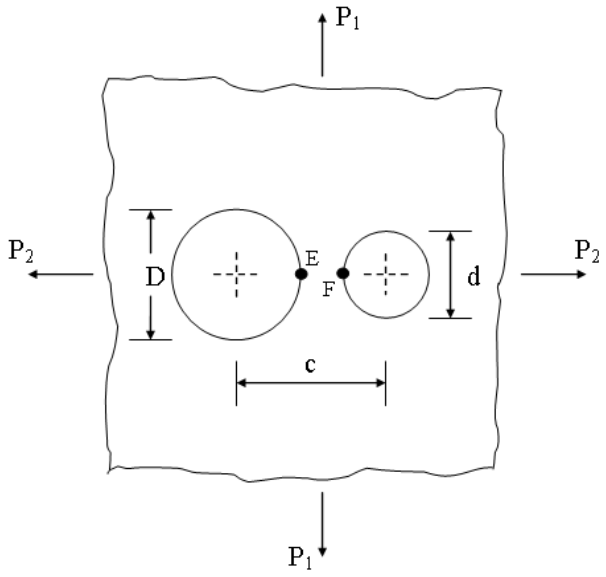

Figure 1.12. Infinite Plate with Two Circular Holes in Biaxial Tension

A K_t chart for this combination of geometry and loading is presented in the NASA Astronautic Structures Manual, Volume 1 [20]. It is shown that for various ratios of d/D, the stress concentration factors for the small and large holes increase as c/2d increases. It can therefore be concluded that the case of an infinite plate with two holes in biaxial tension behaves similar to the case of an infinite plate with two holes in perpendicular tension with stress concentration factors rising as the holes become closer to one another. The maximum stresses occur at the points labeled E and F in Figure 1.12 for the large and small holes, respectively.

Peterson [11] also presents a stress concentration factor chart for two closely spaced holes in biaxial tension with data taken from Haddon [19] and Salerno and

Mahoney [21]. The graph of K_t values in Peterson [11] for an infinite plate with two holes in biaxial tension is somewhat limited in that only three D/d ratios are considered and P1 is assumed to be equal to P2. Further, it also only provides one K_t to be used for both the small and large holes. The stress concentration values shown in Peterson [11] confirm the findings presented by NASA in [20] for this interacting stress concentration case in that these values increase with a decreasing c/d ratio as the center-to-center spacing between holes becomes smaller.

Peterson [11] gives stress concentration factors for different ratios of P1/P2, assuming that the holes in biaxial tension are aligned perpendicular and parallel with the P1 and P2 load directions, respectively.

It may sometimes be necessary to consider shear loading with respect to K_t interaction. An infinite plate with two closely spaced holes loaded in shear is presented in Figure 1.13. Situations involving shear loading for closely spaced holes may be seen in aerostructures when holes are misdrilled or mislocated in shear webs. These webs typically have a smaller thickness when compared with other parts or details loaded in tension, therefore, the higher stresses caused by interaction of closely spaced geometric features should be accounted for.

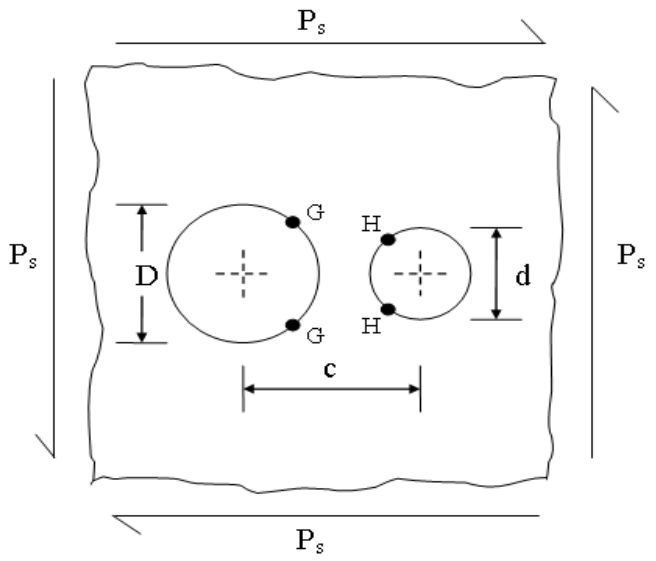

Figure 1.13. Infinite Plate with Two Circular Holes in Shear

A graph of stress concentration factors for this case of shear loading is given in ESDU Data Item 75007 [15]. For the various D/d values presented, the separate SCFs for both the small and large holes tend to increase slightly with a decrease in the center-to-center spacing between holes. The maximum stresses at the large and small holes occur at points G and H, as shown in Figure 1.13. Whether the maximum stresses are found at the upper G or H points, as opposed to the lower G or H points, is dependent upon the direction of shear loading.

Equations (15) and (16), presented by ESDU in [15], show the relationship between the stress concentration factors for both the small and large holes, $K_{t,d}$ and $K_{t,D}$, the maximum stresses found at the holes, f_d and f_D, and the value of the applied shear stress, q.

$$f_d = K_{t,d}\sqrt{3q^2} \tag{15}$$

$$f_D = K_{t,D}\sqrt{3q^2} \tag{16}$$

Peterson [11] also presents stress concentration factors for interaction between two holes in an infinite plate in shear. Similar results are shown for various D/d ratios in terms of stress concentrations when compared to ESDU Data Item 75007 [15]. For this case involving shear loading, both Peterson [11] and ESDU [15] present results using data taken from Haddon [19].

1.3.3. Closely Spaced Notches. Combined stress concentrations are not limited strictly to circular holes. K_t interaction effects may also be present when notches are placed in close proximity to one another. Figure 1.14 shows two closely spaced notches in a plate of finite width. The critical geometric features are aligned parallel to the primary direction of loading.

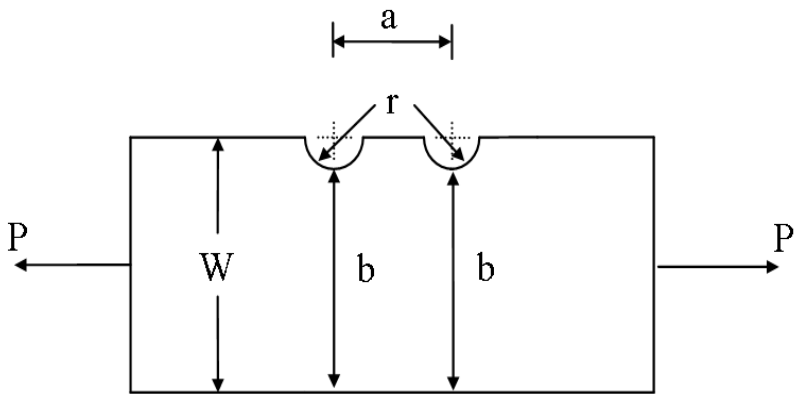

Figure 1.14. Two Closely Spaced Notches in a Finite Width Plate

ESDU Data Item 85045 [16] contains graphical data for close proximity notches in a finite width plate. Multiple notches with equal radii are considered. K_t values are presented for two, three, four, and five notches aligned parallel with an applied tension load. The length of the plate is assumed to be infinite. SCF values are plotted versus a ratio of a/r. The K_t chart presented by ESDU in [16] shows that the stress concentration factors decrease from a maximum value at a/r = 0 to a minimum value between a/r = 2 and a/r = 8, depending upon the number of notches placed in close proximity. The stress concentration factors then increase back up to a maximum as a/r increases. This case illustrates the complex nature of stress concentrations involving the effects of both stress decay and stress increases due to interaction. Data presented in ESDU Data Item 85045 [16] is said to be taken from Durelli, Lake, and Phillips [22,23].

The information in ESDU Data Item 85045 [16] for closely spaced notches is somewhat limited in that the requirement of W/r = 18 must be met for true accuracy. However, it is typically considered acceptable for these stress concentration factor values to be used for analysis in situations where the width of the plate, W, is much greater than

the radii of the notches, r. Another requirement is that the notches must be semi-circular in shape.

Peterson [11] also gives K_t values for various combinations of closely spaced notches in finite width plates. All of these charts are for notches positioned in line with the direction of loading. Peterson [11] actually contains identical data to that presented by Ling [24] for the particular case of close proximity notches. Other data presented in [11] for this combined K_t occurrence is derived from Atsumi [25], Isida [26], Hetenyi [27]. The Peterson [11] charts for closely spaced notches tend to show that the stress concentration factors decrease as the width of the plate, W, increases. These K_t values decrease as the spacing between the notches, a, decreases, exhibiting properties of stress decay.

Closely spaced notches usually exist in aerostructures as a design feature. Placing the notches in close proximity to each other with respect to the primary load direction can help to reduce stress concentrations in certain pieces of structure. Multiple notches may also be introduced during repairs of aerospace parts. Discrepancies including damage, gouges, and misdrilled pilot holes may be trimmed out by creating a notch or multiple notches. Fatigue and stress analysts can assist in designing proper repairs for these cases by taking in to account the stress concentration factors that would result from placing notches in locations where none previously existed.

1.3.4. K_t Interaction of Different Geometric Feature Types. Up to this point, this discussion of combined stress concentrations has been limited to interaction between multiple features of the same type. However, some occurrences of interacting stress risers involve two or more types of geometric details. For instance, a hole may intersect a

radius, or the stress concentration at a hole may be affected by a nearby notch, etc. Consider the specific case of a hole in a radius as shown in Figure 1.15.

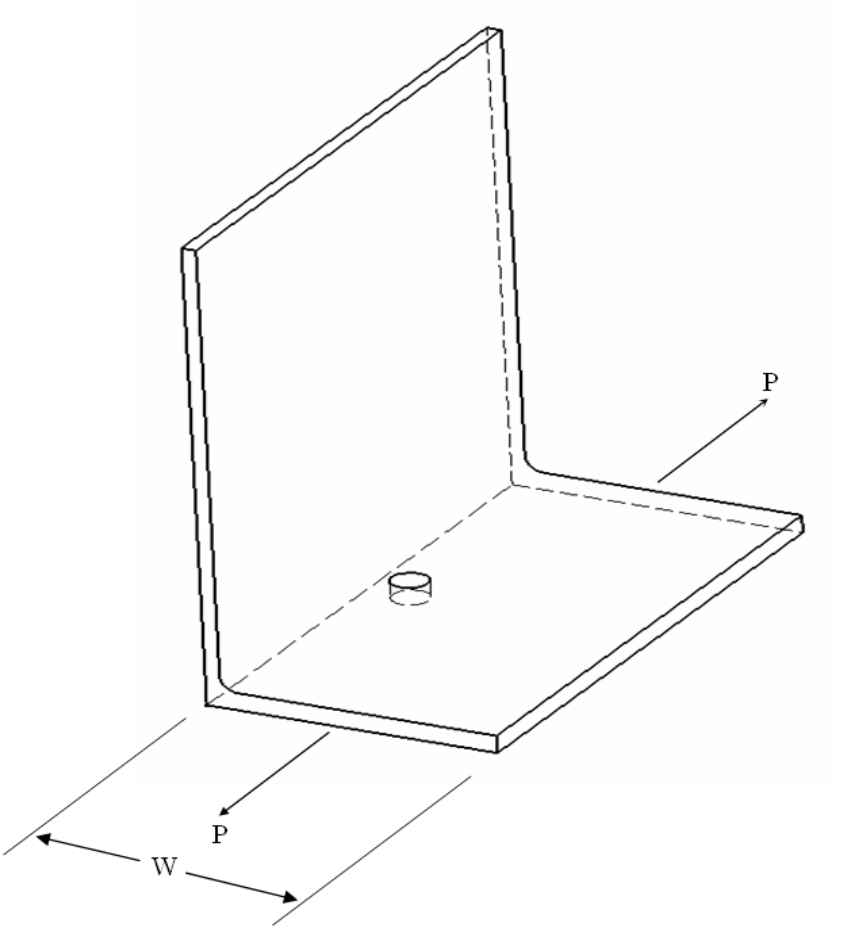

Figure 1.15. Hole in a Radius in Axial Tension

Graham, Raines, Swift and Gill [17] and Graham [28] develop stress concentration factors for the situation of combined SCFs illustrated in Figure 1.15. These factors are dependent upon several variables including the diameter of the hole, the width of the plate, and the distance from the center of the hole to the root of the radius.

Holes drilled at or near a radius occur frequently in aerostructures and are the result of mistakes made by manufacturing in mislocating holes during the drilling operation. Radius blocks are typically used to ensure proper installation of the fastener in the mislocated hole, however adjustments to the stress concentration factor at the hole may be required based on the amount of interference that exists between the hole and radius.

Now consider another case of stress concentration interaction between features with different geometry types, as displayed in Figure 1.16. A hole placed between two fillets is shown, with an axial tension load applied.

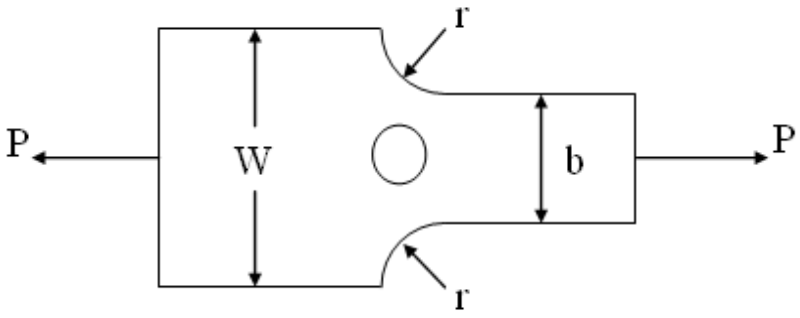

Figure 1.16. Hole Between Two Fillets in Axial Tension

Graham [28] presents a stress concentration factor chart for this instance of combined SCFs. This chart identifies a complex relationship between all of the dimensions involved in the problem, including the width of the plate, W, the distance between fillets, b, the radius of the fillets, r, as well as the diameter of the hole and its position with respect to the fillets. Changing any one of these variables can alter the

value of the stress concentration factor. The data presented by Graham [28] highlights the added complexity of calculating stress concentration factors for interaction between two or more types of geometric features over those cases involving just one type of geometry.

Stress concentration factor data and charts for other instances of multiple feature types placed in close proximity are presented in Graham, Raines, Swift and Gill [17] and Graham [28]. K_t values for a hole located between opposites notches in a finite width plate are given. It is shown by Graham [28] that for a given ratio of notch radius to plate width, the stress concentration factors tend to rise sharply as the ratio of the hole diameter to the width of the plate increases. This means that as the notches and hole get closer to one another, the K_t values increase.

Considering the relatively high frequency with which multiple geometric detail types are placed in close proximity in aerostructures, the amount of previous research that has been conducted with regards to these specific cases of K_t interaction is somewhat limited. Major stress concentration factor references like ESDU [10] and Peterson [11] predominantly present data strictly for $K_t$interaction involving single geometric feature types. Analysts and engineers in the aerospace world need K_t charts that provide accurate values for various instances of multiple features placed in proximity.

1.3.5. Other Cases of Stress Concentration Interaction. There exist many other K_t combinations found in aerostructures that have not already been discussed in this paper. Previous research has been conducted and unique stress concentration factors have been developed for many of these unique cases. Stress concentration interaction

effects are often very complex and can involve consideration of a large number of different geometric features and loading combinations at one time.

Information has been formerly presented in this paper relating to two closely spaced holes in an *infinite* plate. However, there has been a considerable amount of previous research conducted on two closely spaced holes in *finite* width plates as well. In aerostructure applications, K_t interactions tend to exist in finite width plates just as often as they do in plates categorized as having infinite widths. Figure 1.17 displays a diagram of two closely spaced holes in a finite width plate with a load direction perpendicular to the center-to-center spacing between holes.

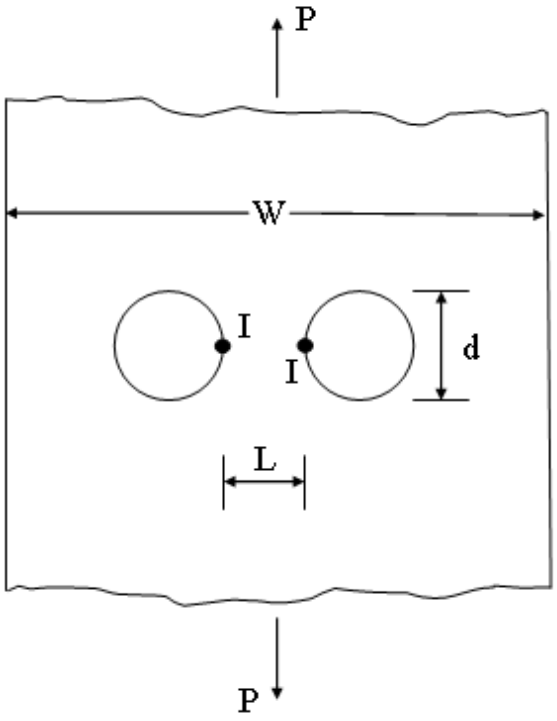

Figure 1.17. Two Closely Spaced Holes in a Finite Width Plate

ESDU Data Item 85045 [16] contains a stress concentration factor graph for this case of combined SCFs. K_t values are given at various d/W ratios. The stress concentration factors are shown to generally decrease as L/W increases. This indicates that the maximum stresses located at the points labeled I in Figure 1.17 decrease as the spacing between the holes increases with respect to the width of the plate. This instance of combined stress concentrations for a finite width plate behaves much like the same combination of geometry and loading in an infinite width plate. The data presented by ESDU in [16] is somewhat limited in that it is only valid for two holes with equal diameters.

Peterson [11] also shows similar stress concentration factor data for closely spaced holes in a plate of finite width. K_t values are provided considering a load direction parallel to the spacing between holes. For various ratios of d/W, the stress concentrations factors tend to decrease as the d/L ratio increases. Data derived from Schulz [29] was used to obtain these SCF values. Again, these factor derivations are limited to closely spaced holes of equal diameters.

Stress concentration factors for a pinned or riveted joint with multiple holes spaced perpendicular to load direction with respect to one another are given by Peterson [11]. For these pinned joints, the edge distance, or distance between the center of the holes and the edge of the plate, is taken in to account. It is shown that for various edge margins, which is the ratio of the edge distance over the diameter of the holes, K_t values increase with an increase in the ratio of hole diameter to the spacing between holes. The associated data presented by Peterson [11] is derived from Mori [30]. The stress concentrations are also shown to be higher for lower edge margins. Holes drilled near an

edge occur frequently in aerostructures and consideration should be given by engineers and analysts alike to the high stress concentration factors that may potentially result from this condition.

Various configurations of patterns of holes in a plate have also traditionally received considerable attention in previous research on K_t interactions. An example of one of these configurations is illustrated in Figure 1.18. This diagram shows a pattern of closely spaced holes in an infinite plate, subjected to tension loading in the axial and transverse directions.

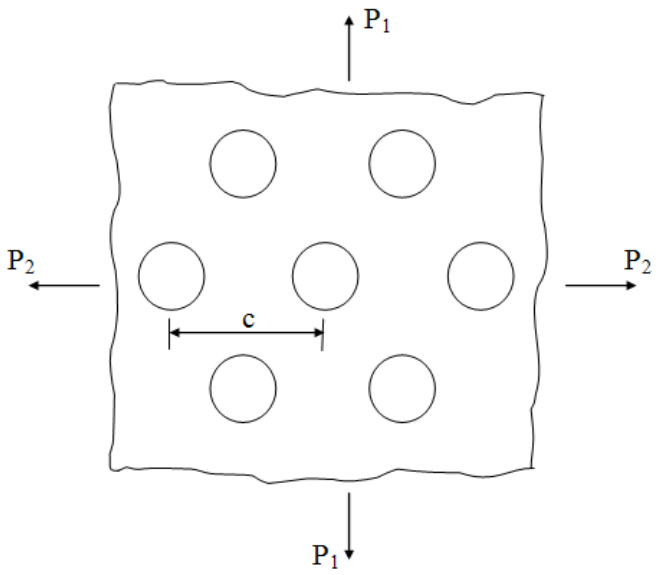

Figure 1.18. Pattern of Closely Spaced Holes in Biaxial Tension

The NASA Astronautic Structures Manual, Volume 1 [20] contains stress concentration factor charts for a number of different combinations of hole arrays subjected to a variety of loading conditions. Peterson [11] is again a good source for SCF

values involving patterns of closely spaced holes. These K_t charts provided by Peterson [11] are derived from data presented by Schulz [29], Sampson [31], Meijers [32], Horvay [33], Nishida [34], Bailey and Hicks [35], Hulbert [36], Hulbert and Niedenfuhr[37], Kraus [38] and Kraus, Rotondo and Haddon [39]. These references generally tend to provide data for arrays of holes of equal diameters which is typically how these hole patterns exist in metallic structures.

Stress concentration factor values for arrays of holes placed in close proximity tend to be dependent upon variables such as hole diameter, load direction, center to center spacing between holes, and the angle of positioning of the holes with respect to one another. The holes may be arranged in rectangular, diagonal, square, triangular, or even occasionally, circular type patterns. As is typical of most K_t interactions, stress concentrations tend to rise as the spacing between the features decreases.

Patterns of holes are seen in aerostructures most frequently in repair doublers that are added to parts by in order to maintain structural stability. These repair plates often contain large numbers of fastener holes that may be placed in close proximity. Arrays of holes can also sometimes exist as a part of the initial design of the structure. In any event, aerospace engineers must have access to accurate stress concentration factors in order to complete a fatigue or stress analysis of critical sections that may contain arrays of holes.

Cutouts are another geometric feature that have historically been analyzed for stress concentrations. Rectangular cutouts are sometimes placed in close proximity to each other or to nearby holes. Consider the simple instance of stress concentration interaction for two closely spaced cutouts shown in Figure 1.19.

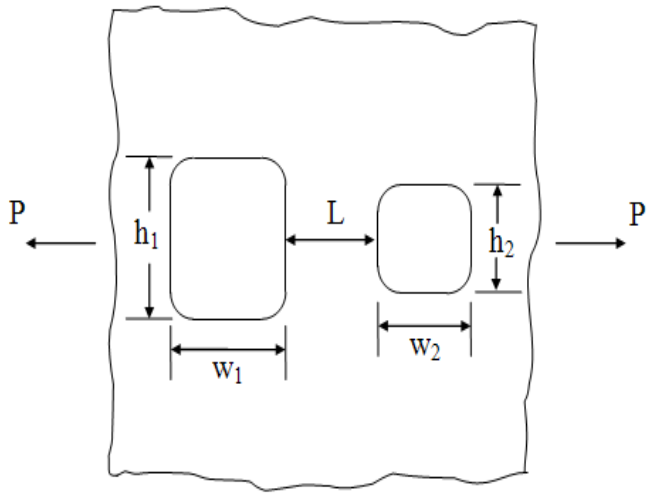

Figure 1.19. Closely Spaced Cutouts in Tension

Sikora [40] presents perhaps the best collection of K_t charts for cutouts of various sizes. Many of the stress concentration factor plots in [40] involve K_t interaction for two or more cutouts placed in close proximity. This study was published by the U.S. Navy where no doubt the stress concentration effects of cutouts receive considerable attention as these types of details are common to naval structures.

Cutouts are also seen frequently in aerostructures. The Comet I disasters discussed in in the Federal Aviation AdministrationDamage Tolerance Assessment Handbook [4] were determined to be caused by high stress concentrations at rectangular window cutouts. This highlights the importance and criticality of developing accurate stress concentration factors for these types of geometric features.

Circular cutouts are used in aerospace applications and are sometimes referred to as "lightening holes". These "lightening holes" are employed as a weight saving measure

in certain structural components. These circular holes may be rather large when compared to typical fastener holes. Stress concentration factor charts that cover circular holes may not necessarily contain data that would provide K_t values for large circular cutouts especially in cases of interaction. Therefore, other K_t charts that cover these types of details must be used or developed as required.

The information relating to stress concentration factors presented by Sikora [40] includes various situations involving single rectangular cutouts, closely spaced rectangular cutouts, circular holes and rectangular cutouts placed in close proximity. The SCFs given are naturally dependent on the height and width of the rectangular cutouts, the spacing between cutouts, and the direction of loading.

1.4. RESEARCH OBJECTIVE

The main purpose of this research is to study the effect of stress concentrations placed in close proximity to each other and their impact on fatigue performance. Unique cases of interaction between a hole and radius are analyzed. Distinct stress concentration modification factors are developed to assist engineers conducting metal fatigue analysis for instances involving hole/radius interference. Physical testing and finite element analysis methods are used to derive these factors.

2. MOTIVATION

This section outlines the purposes and goals for the research contained in this paper that relates to interacting stress concentrations. The motivation is twofold. The two main reasons for this study relating to SCFs for geometric features placed in close proximity share equal importance. Specific details are provided relating to both an academic justification as well as an industry justification for this research. It is generally hoped that the information contained in this dissertation can be used by students, academic professionals and industry professionals alike to both provide a reference for specific situations of stress concentration factor interactions and to present K_t values that engineers and analysts can use as part of a detailed fatigue and or stress analysis of aerostructures.

2.1. ACADEMIC NEED

It is a main goal of this research that students, academic researchers, and instructors can make use of the information contained within this dissertation relating to stress concentration factor interaction. The breadth of currently available knowledge on the specific topic of combined SCFs is generally somewhat limited. It is hoped that this study will further the amount of available academic material directly related to K_t interactions. The academic related objectives for this research are listed.

- Advance existing research in the area of K_t interaction by conducting studies of some unique cases involving combined stress concentration factors that have not

been previously investigated. This would include situations involving features of different geometric types in combination that may not have been analyzed previously.

- Develop stress concentration factor data that leads to an improved understanding of the effects of positioning, dimensions, and load direction on K_t values of various geometric features placed in close proximity to one another.

- Provide a blueprint for testing procedures and methods related to a detailed study of SCF interactions. It is hoped that the empirical techniques used in this research can be replicated and used by other academics to conduct similar investigations on stress concentration factor interactions.

- Illustrate the use of the CATIA Generative Structural Analysis (GSA) Workbench [41] as part of an in-depth study of K_t interactions. The overall amount of historical research using finite element methods relating to combined stress raisers is fairly narrow in scope and size. Academic material specifically involving the use of CATIA Generative Structural Analysis to study interacting SCFs is not known to exist. It is hoped that the detailed use of this FEM/FEA software tool significantly adds to the information currently available that relates to finite element modeling and analysis involving combined K_t data.

- Present a detailed comparison between testing results and finite element analysis results for specific cases of stress concentration factor interaction. K_t values and

data developed from both the FEM/FEA and empirical studies will be analyzed and compared. Conclusions can be made with regards to the test results justifying the finite element models/analysis.

- Show the manner in which the stress concentration factor values obtained as part of this research can be used in a simplified fatigue analysis of aerostructures. It is hoped that academics studying, or specializing in, metal fatigue can utilize the information contained in this overall study to examine how fatigue relates to, or is impacted by, K_t interactions. Researches may use the stress concentration factor values presented within this paper for cases of interaction in their own fatigue analysis studies. The goal is to contribute to an improved general, theoretical and practical understanding of fatigue analysis as it relates to the phenomenon of combined SCFs.

2.2. INDUSTRY NEED

Another main objective of this research is the use of the information on combined stress concentrations, contained within, by engineering professionals working for companies and organizations that deal with problems and challenges related to K_t interactions. This study is focused on, but not necessarily restricted to, providing data for cases of stress concentration factor interaction that occur frequently in the aerospace industry. It is particularly desired that engineers at Spirit AeroSystems, Inc. will incorporate the stress concentrations factors generated as part of this research in to their fatigue and stress analysis, as needed. Analysts, scientists, and engineers working in other engineering disciplines may find the K_t data generated through this investigation

useful as well. Specific, industry related goals for the research contained within this dissertation are given.

- Generate stress concentration factors and related data for unique situations of K_t interaction. The goal is to provide accurate SCF data for these specific circumstances. Engineers working in the aerospace field are in need of stress concentration factors that would cover these distinct instances in order to conduct an accurate structural analysis.

- Add to the amount of specific knowledge available to the aerospace industry that relates to K_t interactions in order to avoid fatigue related failures. Stress concentration factors are critical to fatigue analysis and accurate SCF data is always needed in order to ensure that the fatigue life of an aircraft is being properly predicted. This research could potentially help prevent the fatigue failure of an aircraft.

- Provide Spirit AeroSystems, Inc. with its own test data related to interacting stress concentration factors. Prior to this research, Spirit did not possess company information related specifically to combined SCFs. Spirit is a large company that is responsible for the proper design and fabrication of many different types of major aerospace components. Cases of K_t interaction are seen frequently on many different aircraft programs at the company. Spirit was in need of reliable in-house data on combined stress concentration factors instead of using outdated

information supplied by other organizations, inadequate academic studies, or basic engineering judgment.

- Generate accurate stress concentration factor modification values, for cases of interaction, that can be used by Spirit AeroSystems, Inc. engineers and analysts to accurately predict fatigue lives for specific details. The K_t mod factors determined as a result of this research can be entered manually in to selected fatigue analysis software tools to account for the effects of interaction between geometric features placed in close proximity.

3. SCOPE

This research study focuses on the development of stress concentration modification factors for geometric features placed in close proximity with respect to one another. K_t modification factors are commonly applied to account for various conditions that affect the fatigue performance of critical details. Some examples of these conditions include deep countersunk holes, misdrilled holes, blending, dents, burrs, cold working and flapper peening. The applied mod factors may be either helpful or detrimental to fatigue life.

Themod factors developed through this research were determined through means of testing and finite element analysis. Testing was performed at Spirit Aerosystems, Inc. in Wichita, KS and at Missouri University of Science & Technology in Rolla, MO. All finite element modeling and analysis was conducted using the CATIA [41] three-dimensional modeling and analysis software suite. Simplified fatigue analyses were performed using data obtained from the physical testing and FEM/FEA. The fatigue analysis was completed in accordance with conventionally applied methods. The research concludes with a general summary of the results. The values obtained from the open hole testing are compared with those determined through finite element analysis as well as joint testing. A flow chart containing the general organization of this research is shown in Figure 3.1.

In situations involving interacting stress concentration factors, the peak stress values measured at critical locations are always dependent upon the specific set of geometry and loading conditions being considered. Each general instance of K_t

interaction has its own unique configuration that dictates the calculated SCF values. This study consists of an in-depth analysis of variousinstances that occur in MRB repairs related to the mislocation of certain features during the fabrication process. The goal is to provide original data and analysis with respect to these specific cases.

Test specimen drawings for the individual cases of combined stress concentration factors, for geometric features placed in close proximity, that are analyzed in this study are presented in Section 4 and Appendix A. Comprehensive summaries of the open hole fatigue testing and joint fatigue testing conducted as part of this research project are given in Section 4. The finite element modeling and analysis used to derive K_t mod factors for the open hole interaction cases are detailed in Section 5. All of the stress concentration factor interactions studied herein are examples of combinations of SCFs of different geometric feature types. The K_t of a hole is superimposed on the K_t of a radius, with primary load direction also being considered.

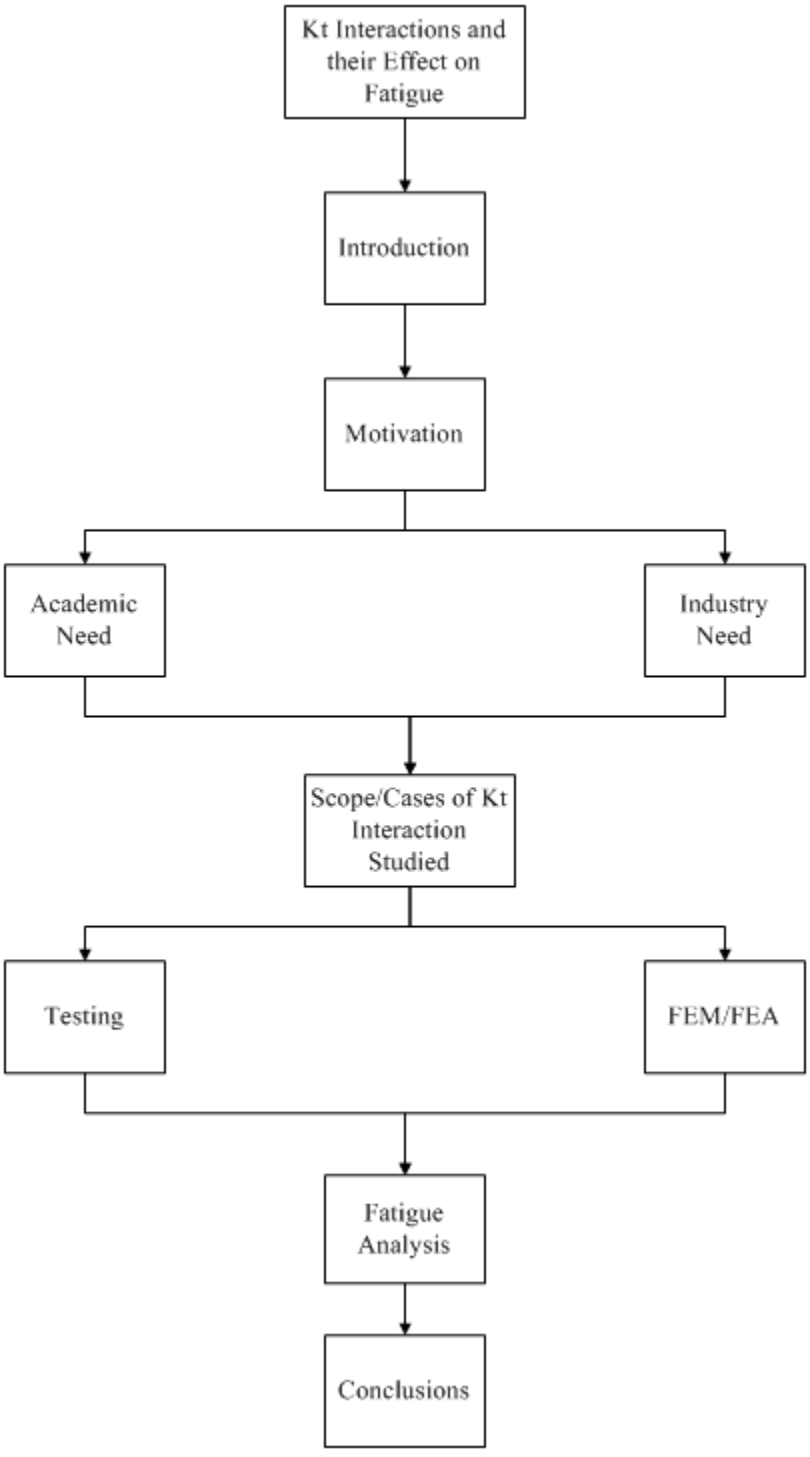

Figure 3.1. General Organization of Research

3.1. OPEN HOLE/STEP FATIGUE TESTING AND FEM/FEA

During fabrication of certain pieces of aerostructure, a situation can arise in which a hole is mislocated so that it interferes with a radius, chem-mill step, machined step, or some other similar feature. This tends to occur most frequently when the design of the part initially places the hole in close proximity to the radius or step. An isometric diagram of a typical configuration for the open hole fatigue specimens used to analyze cases of stress concentration factor interaction between holes and radii is displayed in Figure 3.2.

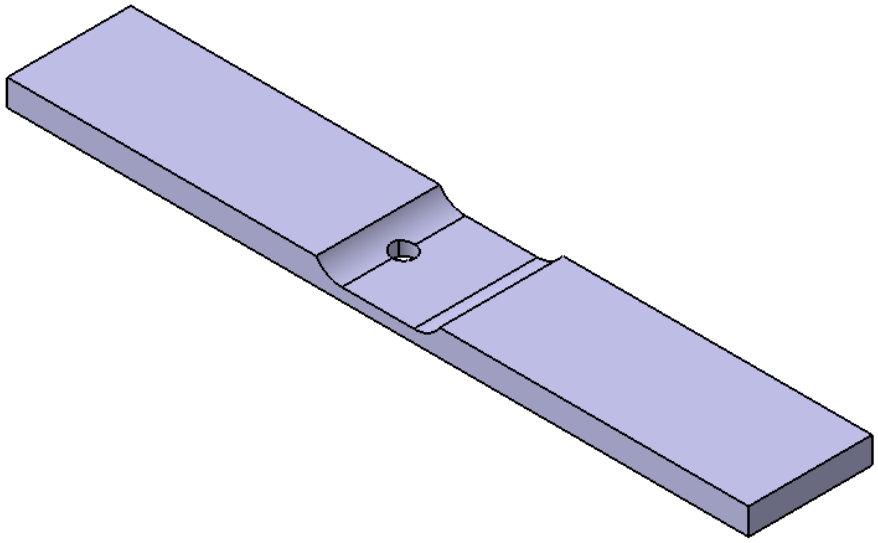

Figure 3.2. Open Hole in Radius Fatigue Test Specimen - Isometric View

The open hole research includes an in-depth study, through testing and finite element modeling/analysis, of the SCF interaction that occurs between a hole and radius,

that have a positioning, such as that shown in Figure 3.2. It is assumed that typical repair measuresinvolving the removal of material, such as spot-facing, are not possible. K_t modification factors are developed to allow engineers and analysts to properly account for the effects of hole and step interaction.

The exact geometry and dimensions for the open hole and step test specimens are provided in the Open Hole in Radius Test Specimen drawing in Figure A.1 in Appendix A. The specimen configurations are modified slightly to alter the distance between the tangent points of the radius and the centers of the nearby hole. The correlation between this distance and the K_t interaction mod factor that accounts for the interference between the step and hole is analyzed.

Detailed open hole testing information and results are presented in Section 4. All open hole finite element modeling and analysis is contained in Section 5. A summary of the open hole fatigue results along with a comparison of the testing vs. FEM/FEA data is given in Section 7.

3.2. JOINT FATIGUE TESTING

This research initially develops analysis data for open hole and step configurations. However, in typical MRB repairs of aerostructure, it is not considered desirable to leave holes open. The holes are ideally plugged with some type of rivet, bolt or other fastener installation which works to reduce the stresses in the part by improving hole fill properties. This study analyzes joints with multiple parts to account for the impact of fastener hole fill on the stress concentration factor data.

Low load transfer single row, eight fastener double shear, and stress corrosion joint testing were all performed for situations with bolts at or near radii. 3/16 inch diameter bolts with collars were used for all assembly specimens. The effect on fatigue performance of the collars riding under the steps was analyzed. Radius fillers were used for certain specimens to allow the collars to sit flat on the part surface and maintain proper fastener installation. For the corrosion testing, the goal was to determine if the residual stresses in the bolts at the step interference locations would cause part failure.

For typical cases of interference between holes and machined steps, manufacturing personnel may employ a radius filler, radius block, or spot-face to provide for proper installation of a fastener in the hole. Radius fillers and radius blocks add material to ensure a perpendicular, smooth surface for placement of the fastener. Spot-facing involves removing material from the part by blending out the radius to allow a flat, smooth surface for installation. Discrepant holes are often plugged in the parts where they were mislocated and additional holes are drilled in the same parts at the proper locations so that fasteners can be installed at the correct positions between multiple parts in the stack-up. However, many times due to access restrictions as well as other factors, it is not possible to complete these types of repairs in order to alleviate the interference and resulting K_t superposition between the hole and radius.

An isometric diagram of the Fatigue Dogbone Bolt in Radius assembly configuration, with collar installation shown, is provided in Figure 3.3. This joint assembly includes the Fatigue Dogbone Bolt in Radius Parts A and B along with the bolts used to fill the holes and connect the components in the stack-up. See Appendix A for the detailed Fatigue Dogbone Bolt in Radius part drawings.

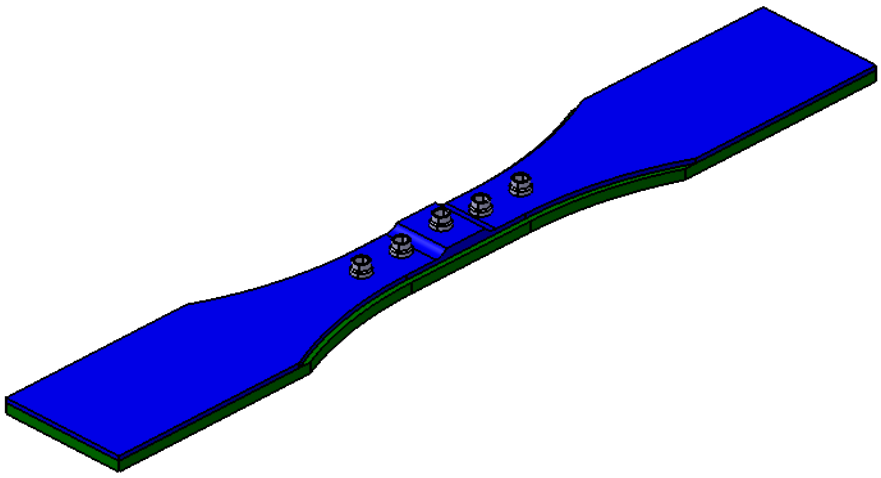

Figure 3.3. Fatigue Dogbone Bolt in Radius - Assembly - Isometric View

A diagram of the eight fastener double shear bolt in radius assembly profile is shown in Figure 3.4. This joint includes 8 Fastener Double Shear Bolt in Radius Parts A, B, C and D as detailed in the test specimen drawings in Appendix A. The bolt collar installations are also shown.

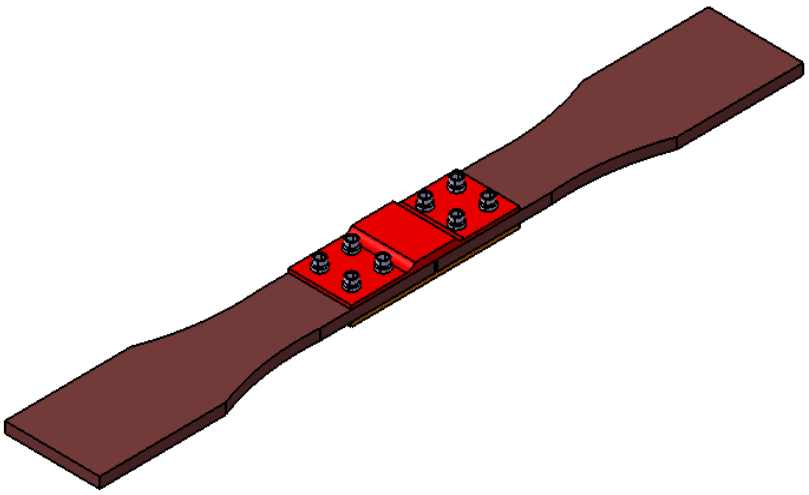

Figure 3.4. 8 Fastener Double Shear Bolt in Radius - Assembly - Isometric View

The bolt in radius sodium chloride corrosion joint test specimen configuration is presented in Figure 3.5. Collar installations at the hole locations are displayed. The specific geometry and dimensions for the corrosion specimen parts are included in the detailed testing requirements presented in Section 4.

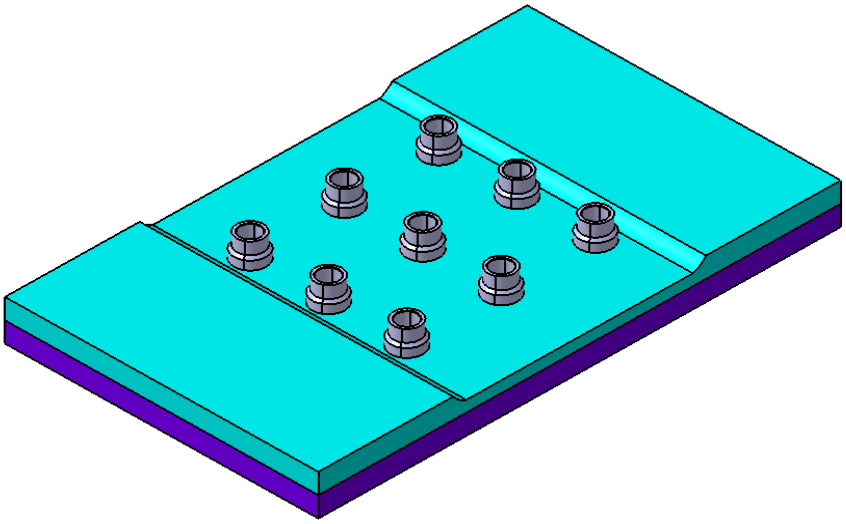

Figure 3.5. Stress Corrosion Bolt in Radius - Assembly - Isometric View

As in the case of the open-hole specimens, the profiles of the parts with radii in the joint testing stack-ups are modified to vary the distance between the hole centers and tangent points of the steps. The effect of this change in geometry on the stress concentration factors developed for the hole and radius interactions is determined. Three different distances between the holes and step tangents for each joint configuration are studied.

All details of the joint testing methods and procedures used including materials, number of specimens, fabrication techniques, hole drilling, etc. are presented in Section 4. The fatigue loading, including R values and maximum stresses, for the low load transfer and double shear specimens is also provided in the testing section of this dissertation. The joint fatigue test results are also presented in Section 4 and conclusions

with comparisons to the open hole cases are given in Section 7. All part drawings for the separate components used in the joint testing are given in the Fatigue Dogbone Bolt in Radius and 8 Fastener Double Shear Bolt in Radius drawing packages in Appendix A along with the separate part schematics shown in Section 4.

4. TESTING

4.1. TESTING OVERVIEW

4.1.1. Test Purpose. This fatigue testing analyzes the stress concentration factor interaction that occurs between a hole and radius placed in relatively close proximity to each other. Stress concentrations have a significant impact on fatigue performance. Most common stress concentrations such as a hole in a plate are relatively well known. However, the interaction of the stress concentrations between a hole and step are not well understood and the resulting impact on fatigue performance is difficult to predict. There exists a need for fatigue data that can be used to determine the MRB analysis methods for evaluation of the interaction effects between machined steps and holes. The testing is composed of both open hole and joint assembly fatigue specimens.

4.1.2. Test Materials. The materials and fasteners used in the fatigue testing are provided in Table 4.1. The open hole and step test specimens are made from 2024-T351 aluminum plate material while 7075-T7351 aluminum plate material is used to fabricate all joint test specimens. The aluminum material types used for fabrication of the test specimens are typical of those used in aerospace applications. Material availability also dictated the specific types and tempers used in this research project. All fasteners are installed in transition fit holes.

Table 4.1. Test Materials

Material	Specimen Type
2024-T351 Plate	Open Hole/Step
7075-T7351 Plate	Joint

Fastener Component	Grip Length	Nominal Diameter (in.)	Quantity
Bolt	-5	3/16	100
	-7		200
	-9		50
Collar	-		350

4.1.3. Test Matrix. Twenty-four open hole/step, sixteen fatigue low load transfer dogbone with machined step, sixteen 8 fastener double shear with machined step, and one stress corrosion test specimens were tested. The fatigue properties of open hole/step specimens and specimens with a bolt near or riding on the radius of a step were analyzed. A total of fifty-seven separate specimens were tested. This testing will be used to develop fatigue modification factors for open holes and bolts/collars that are positioned at or near a radius in aluminum. The fatigue test matrix is presented in Table 4.2.

Table 4.2. Test Matrix

Material	Specimen Type	Specimen Drawing	Quantity
2024-T351 Plate	Open Hole with Step	Open Hole in Radius Test Specimen - 1	5
		Open Hole in Radius Test Specimen - 2	3
		Open Hole in Radius Test Specimen - 3	4
		Open Hole in Radius Test Specimen - 4	4
		Open Hole in Radius Test Specimen - 5	4
		Open Hole in Radius Test Specimen - 6	4
7075-T7351 Plate	Low Load Transfer Dogbone with Step	Fatigue Dogbone Bolt in Radius-1	4
		Fatigue Dogbone Bolt in Radius-2	8
		Fatigue Dogbone Bolt in Radius-3	4
	8 Fastener Double Shear Bolt with Step	8 Fastener Double Shear Bolt in Radius-1	4
		8 Fastener Double Shear Bolt in Radius-2	8
		8 Fastener Double Shear Bolt in Radius-3	4
	Immersion in Sodium Chloride	Per Engineering Test Plan	1
		Total	57

4.1.4. Specimen Identification. Descriptions of the formulas used for all specimen identifications in this fatigue testing project are provided in Figure 4.1.

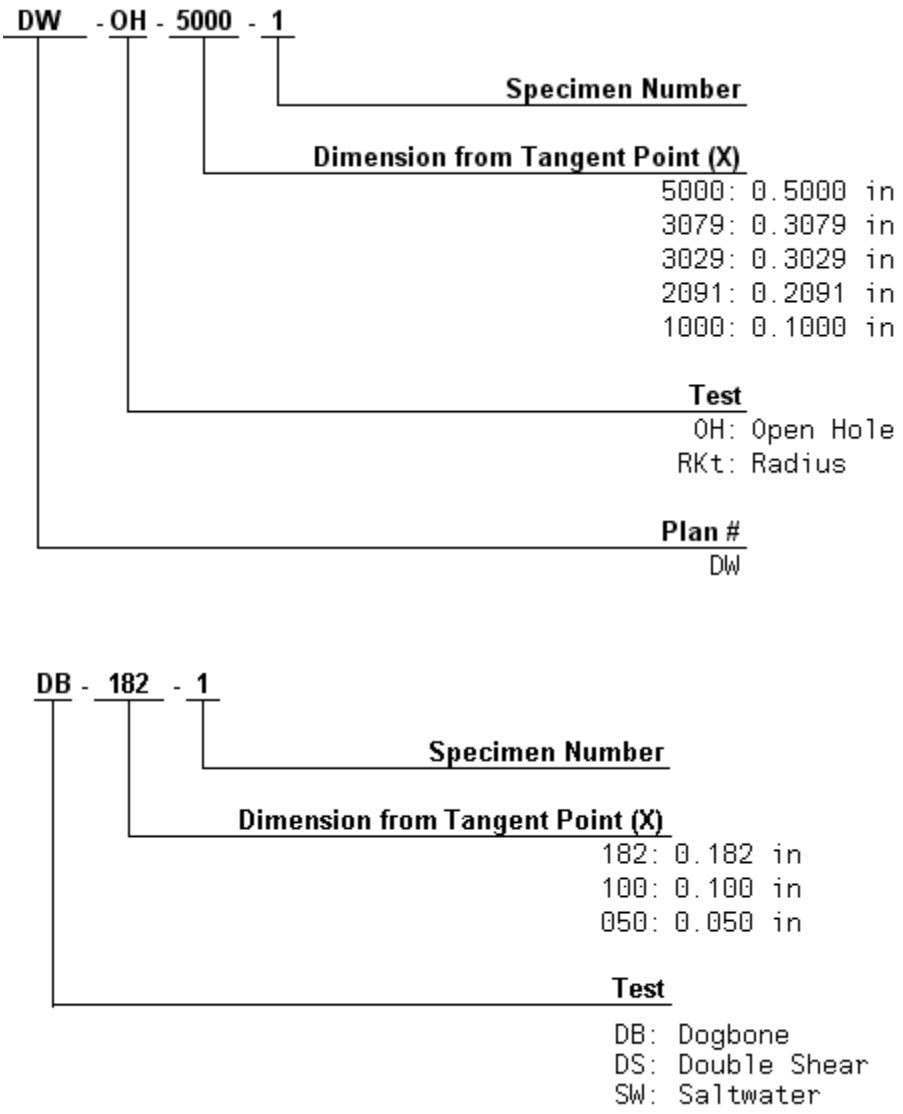

Figure 4.1. Specimen Identification

4.1.5. Test Machine. All fatigue testing was conducted using the MTS 810 hydraulic material testing system. A picture of the MTS 810 is provided in Figure 4.2. This machine uses multi-purpose axial wedge grips and cyclic fatigue TestWare® software. This test system is capable of performing constant amplitude fatigue testing in accordance with ASTM E466[42]. The MTS 810 [43] is a high-performance, high-precision device that can be used to carry out material and component tests for fatigue, fracture, static strength, temperature, etc. More information on the MTS machine including specifications and additional capabilities can be found at [43].

Figure 4.2. MTS 810 Material Testing System

4.2. OPEN HOLE/STEP TESTING

4.2.1. Test Purpose. The purpose of this fatigue testing is to analyze open hole and step specimens to investigate any degradation in fatigue life due to a hole being placed at, or in close proximity to, a nearby radius. It is determined whether or not a hole very near a radius but not necessary interfering with the radius has any negative impact on fatigue life that would be associated with K_t interaction. The holes are placed at a series of distances away from the radii in order to properly analyze these effects.

4.2.2. Fabrication Details. The open hole/step fatigue specimens were manufactured from 2024-T351 plate material. The open hole/step fatigue test matrix is shown in Table 4.3.

Table 4.3. Open Hole/Step Test Matrix

Material	Specimen Drawing	X Dimension (in.)	Specimen ID	Quantity
2024-T351 Plate	Open Hole in Radius Test Specimen - 1	-	DW-RKt-1 to 6	5
	Open Hole in Radius Test Specimen - 2	.5000	DW-OH-5000-1 to 3	3
	Open Hole in Radius Test Specimen - 3	.3079	DW-OH-3079-1 to 3	4
	Open Hole in Radius Test Specimen - 4	.3029	DW-OH-3029-1 to 4	4
	Open Hole in Radius Test Specimen - 5	.2091	DW-OH-2091-1 to 4	4
	Open Hole in Radius Test Specimen - 6	.1000	DW-OH-1000-1 to 4	4
			Total	24

Specimens were fabricated according to the dimensions and geometry shown in the Figure A.1 Open Hole in Radius Test Specimen drawing of Appendix A. Specimen identifications were permanently inscribed on the coupons as instructed in the specimen drawing. Pictures of the pre-test open hole/step specimens are displayed in Appendix B. Notice the positioning of the holes with respect to the radius location for the -2 through -6 configurations.

4.2.3. Hole Drilling. All holes were prepared in accordance with approved hole drilling specifications. Holes were reamed and deburred. No holes were drilled for the -1 step fatigue specimens.

4.2.4. Fatigue Test Stresses. The applied fatigue test stresses for the open hole and step specimens, based on total gross area in the test section, and stress ratios (R), are provided in Table 4.4. A frequency of 10 Hz was used.

Step specimen DW-RKt-1 with no holes was tested first, at a 25 ksi stress level. No fatigue failure occurred for this coupon. The test was terminated at 1,000,000 cycles. The stress was increased to 30 ksi for the next specimen, DW-RKt-2. This coupon experienced fatigue failure at a relatively high number of cycles. Therefore the stress level was further increased to 35 ksi for the remaining radius only runs in order to achieve fatigue failures at reasonable numbers of cycles.

The first baseline open hole specimen, DW-OH-5000-1, was tested at a 28 ksi stress level. The number of cycles to failure for this run was observed to be relatively low. Therefore the stress level was reduced to 26 ksi for the next baseline open hole specimen, DW-OH-5000-2. The number of cycles to failure for DW-OH-5000-2 was still somewhat low. Consequently the final baseline open hole coupon, DW-OH-5000-3, was tested at 25 ksi.

All of the remaining open hole test specimens were tested at a 25 ksi stress level with the exception of DW-OH-1000-1. Stress levels for the specimens with an X call out of 0.1000 inches are based on the average thickness of the upper and lower sections of the plate as the hole is drilled directly through the transition section of the radius. At 16

ksi, the recorded number of cycles to failure for the DW-OH-1000-1 specimen was relatively high. All remaining coupons in the -1000 group were then tested at 25 ksi.

Table 4.4. Open Hole/Step Fatigue Test Stresses

	Loading		Qty.
Specimen ID	S_{max} (ksi)	R	
DW-RKt-1	25	0.06	1
DW-RKt-2	30	0.06	1
DW-RKt-3 thru 5	35	0.06	3
DW-OH-5000-1	28	0.06	1
DW-OH-5000-2	26	0.06	1
DW-OH-5000-3	25	0.06	1
DW-OH-3079-1 thru 4	25	0.06	4
DW-OH-3029-1 thru 4	25	0.06	4
DW-OH-2091-1 thru 4	25	0.06	4
DW-OH-1000-1	16	0.06	1
DW-OH-1000-2 thru 4	25	0.06	3
		Total	24

4.3. JOINT TESTING

Physical testing was performed on joint assembly specimens with holes placed in close proximity to radii locations to determine stress concentration mod factors for use in metal fatigue analysis. Separate fatigue testing was conducted on low load transfer bolt in radius dogbone specimens, eight fastener double shear bolt in radius specimens and stress corrosion testing with sodium chloride. Detailed test methods and procedures are provided for each of the three individual experiment types.

4.3.1. Low Load Transfer Bolt in Radius Fatigue Testing

4.3.1.1. Test purpose. The goal of the low load transfer bolt in radius dogbone fatigue specimen joint testing was to develop SCF mod factors for situations of fastener holes placed at or near steps. Holes were located at a series of three distances away from the tangent point of the radii. These hole to radii distances are specified in the Fatigue Dogbone Bolt in Radius Part B specimen drawing in Appendix A. Radius fillers were used to allow the collars to sit flat on the part surface for proper installation.

4.3.1.2. Fabrication details. Low load transfer dogbone fatigue specimens were manufactured from 7075-T7531 plate material. Material lot acceptance sheets were generated prior to machining. All material was fabricated from the same material lot and has a longitudinal (L) grain direction. All fasteners of the same diameter and grip length are from the same lot. The lot numbers forthe material and the fasteners used in the testing were recorded. The low load transfer bolt in radius dogbone fatigue test matrix is shown in Table 4.5.

Table 4.5. Low Load Transfer Bolt in Radius Test Matrix

Material	Specimen Drawing	X Dimension (in.)	Specimen ID	Quantity
7075-T7351 Plate	Fatigue Dogbone Bolt in Radius - 1	0.182	DB-182-1 to 4	4
	Fatigue Dogbone Bolt in Radius - 2	0.100	DB-100-1 to 8	8
	Fatigue Dogbone Bolt in Radius - 3	0.050	DB-050-1 to 4	4
			Total	16

Specimens were fabricated according to the dimensions and geometry called out in the Fatigue Dogbone Bolt in Radiusdrawings of Appendix A. Specimen identifications were permanently inscribed on the specimens as instructed in the

specimen drawings. Edge preparation was performed by one machinist, all at the same time for consistency. The machinist broke all sharp edges with a 400 grit emery cloth. The machinist also manufactured eight radius fillers for the specimens labeled DB-100-5 through 8. The 7075-T7351 radius fillers were fabricated according to the dimensions provided in Figure 4.3.

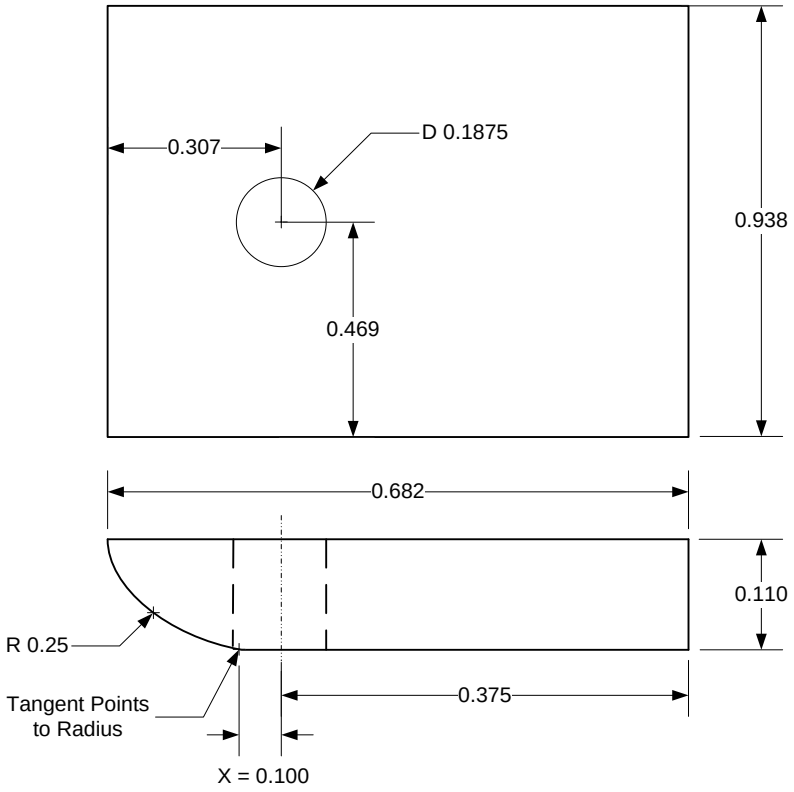

Figure 4.3. Dogbone Radius Filler

Specimen dimensions were measured and recorded. The dogbone specimen dimensions that needed quality assurance verification are: specimen thickness (T_1 and T_2), per the Fatigue Dogbone Bolt in Radius drawings of Appendix A and width in all

parts. All specimen dimensions were measured prior to assembly and before any surface treatment was applied. Chemical finish and primer were applied to all specimens.

4.3.1.3. Hole drilling and assembly. All holes were prepared in accordance with approved hole drilling specifications. The fastener shank diameters were measured and all fastener holes were drilled to allow a 0.0005 inch clearance fit (+/- 0.0005/0.0004). Holes were stack drilled and reamed. The holes in Fatigue Dogbone Bolt in Radius- Part A, where the manufacturing head of the fastener is located, were chamfer deburred, Type 3 as specified in the specimen layout drawing. All interface locations for Part A, Part B, and the radius filler were flat deburred. The exit side of the holes in Part B and the radius filler, on the side of the collar, required a deburr using a rotary tool with three rotations. The drilling parameters (speeds/feeds/lubrication/tools) used during fabrication were recorded. Hole diameters were measured and recorded by quality assurance personnel. Each hole was labeled with a permanent marking system (Hole 1 through 5 as specified in the Fatigue Dogbone Bolt in Radius drawing package).

Prior to fastener installation, all joints were fay sealed. Fay sealing is a thin layer of sealant placed between the mating surfaces of two parts in a fastened joint. The specimens were separated and fay sealed rolled on Fatigue Dogbone Bolt in Radius Part B with a thickness of 0.004 to 0.006 inches. Fasteners were installed per the following sequence (Fatigue Dogbone Bolt in Radius drawing shows hole ID's): 3-2-4-1-5. The 6/32 diameter bolts were installed with collars with an expected break-off torque range of 25 to 35 lbf-in. The torque values achieved when installing fasteners (1 fastener per group) were measured and recorded.

Two radius fillers per specimen for Holes 2 and 4 were used for specimens DB-100-5 through 8. The radius filler holes were fabricated in accordance with the requirements used for the rest of the specimens, including fay seal. Specimens were not tested until the fay seal was fully cured.

4.3.1.4. Fatigue test stresses. The test setup allows load to be transmitted within 0.005 inches of the specimen centerline passing through the centerline of the interface between the assembly parts. The applied fatigue test stresses for the low load transfer dogbone specimens, based on total gross area in the test section, and stress ratios (R), are provided in Table 4.6. A frequency of 10 Hz was used. DB-182-1 was tested first, at the S_{max} stress level shown. This specimen experienced fatigue failure at a relatively low number of cycles. Therefore the remaining dogbone tests were completed at a lower stress level of 20 ksi to achieve fatigue failures at more reasonable cycle counts.

Table 4.6. Dogbone Fatigue Test Stresses

	Loading		Qty.
Specimen ID	S_{max} (ksi)	R	
DB-182-1	25	0.06	1
DB-182-2 thru 4	20	0.06	3
DB-100-1 thru 4	20	0.06	4
DB-100-5 thru 8	20	0.06	4
DB-050-1 thru 4	20	0.06	4
		Total	16

4.3.2. Eight Fastener Double Shear Bolt in Radius Fatigue Testing

4.3.2.1. Test purpose. K_t mod factors were developed from the results of the eight fastener double shear fatigue test specimens. Holes were again located at a series of three distances away from the tangent point of the steps. For the double shear specimens,

the hole to radii distances are specified in the Figure A.7. 8 Fastener Double Shear Bolt in Radius- Part D specimen drawing in Appendix A. Radius fillers were fabricated to allow the fastener collars to sit flat on the surface of the part.

4.3.2.2. Fabrication details. The 8 Fastener Double Shear Bolt in Radius Part A, B, C and D double shear plate specimens were manufactured from 7075-T7531 aluminum material. Material lot acceptance sheets were generated prior to machining. All material was fabricated from the same material lot and had a longitudinal (L) grain direction. All fasteners of the same diameter and grip length were from the same lot. The lot numbers forthe material and the fasteners used in the testing were recorded. The eight fastener double shear bolt in radius test matrix is provided in Table 4.7.

Table 4.7. 8 Fastener Double Shear Bolt in Radius Test Matrix

Material	Specimen Drawing	X Dimension (in.)	Specimen ID	Quantity
7075-T7351 Plate	8 Fastener Double Shear Bolt in Radius - 1	0.182	DS-182-1 to 4	4
	8 Fastener Double Shear Bolt in Radius - 2	0.100	DS-100-1 to 8	8
	8 Fastener Double Shear Bolt in Radius - 3	0.050	DS-050-1 to 4	4
			Total	16

Specimens were fabricated according to the dimensions and geometry called out in the 8 Fastener Double Shear Bolt in Radiusdrawing package of Appendix A. Specimen identifications were permanently inscribed on the specimens. Edge preparation was performed by one machinist, all at the same time for consistency. The machinist broke all sharp edges with a 400 grit emery cloth. Eight 7075-T7351 radius fillers were fabricated for the specimens labeled DS-100-5 through 8. The configuration of the double shear radius filler is shown in Figure 4.4.

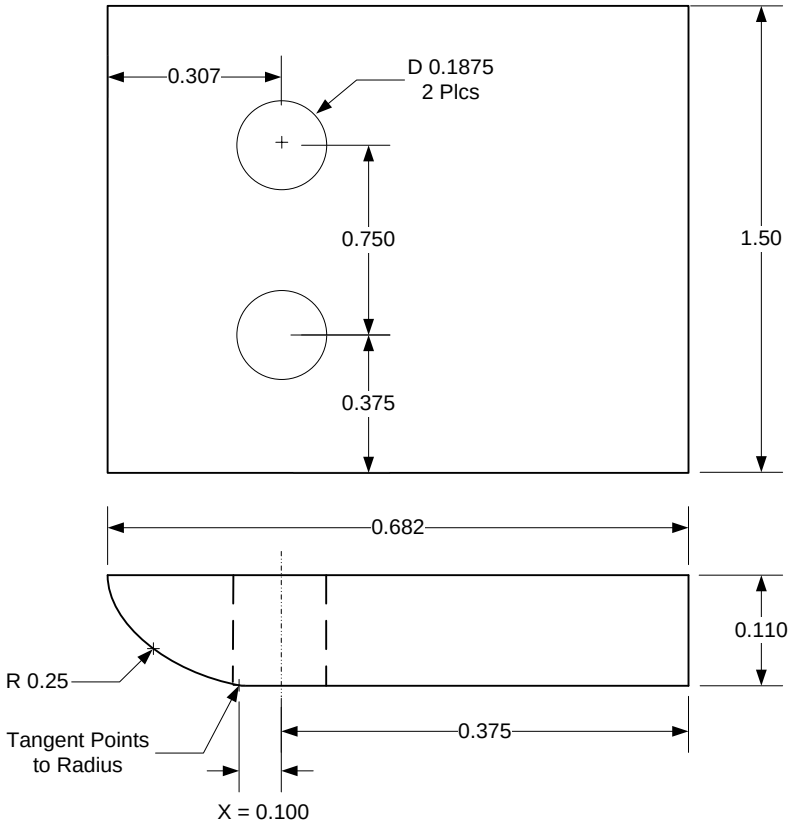

Figure 4.4. Double Shear Radius Filler

Specimen dimensions were measured and recorded. The double shear specimen dimensions that needed quality assurance verification are: specimen thickness (T_1, T_2, T_3 and T_4), per the 8 Fastener Double Shear Bolt in Radius drawings of Appendix A and width of all parts. All specimen dimensions were measured prior to assembly and any surface treatment being applied. Chemical finish and primer were applied to all specimens.

4.3.2.3. Hole drilling and assembly. All holes were to be prepared in accordance with approved hole drilling specifications. The fastener shank diameters were measured

and all fastener holes were drilled to allow a 0.0005 inch clearance fit (+/- 0.0005/0.0004). Holes were stack drilled and reamed. The holes in 8 Fastener Double Shear Bolt in Radius Part C (where the manufacturing head of the fastener is located) were chamfer deburred. All interface locations for Part A through D and the radius filler were flat deburred. The exit side of the holes in Part D and the radius filler (on the side of the collar) required a deburr using a rotary tool with three rotations. The drilling parameters (speeds/feeds/lubrication/tools) used during fabrication were recorded. Hole diameters were measured and recorded by QA. Each hole was labeled with a permanent marking system (Hole 1 through 5 as specified in the 8 Fastener Double Shear Bolt in Radius drawing package).

Prior to fastener installation, all joints were fay sealed. The specimens were separated and fay sealed rolled on 8 Fastener Double Shear Bolt in RadiusPart A and Part B with a thickness of 0.004 to 0.006 inches. Fasteners were installed per the following sequence (8 Fastener Double Shear Bolt in Radius drawings show hole ID's): 8-6-4-1-7-5-3. All bolts were installed with collars with an expected break-off torque range of 25 to 35 lbf-in. The torque values achieved when installing fasteners (1 fastener per group) were measured and recorded.

For the double shear test specimens with X call outs of 0.100 inches and 0.050 inches without radius fillers, the collars were installed slightly riding the nearby radius. A picture of a double shear test specimen showing the improper collar installation condition is shown in Figure 4.5.

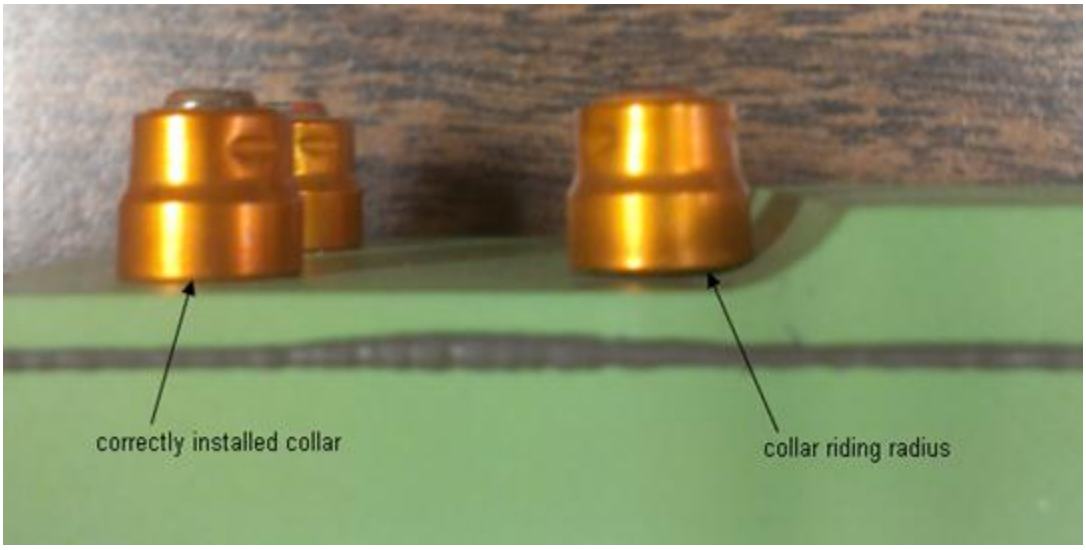

Figure 4.5. Collar Riding a Radius

Two radius fillers per specimen for Holes 2, 4, 6 and 8 were used forspecimens DS-100-5 through 8. The radius filler holes were fabricated in accordance with the requirements used for the rest of the specimens, including fay seal. Specimens were not tested until the fay seal was fully cured.

4.3.2.4. Fatigue test stresses. The test setup allows load to be transmitted through the specimen assembly centerline between the doublers. Fatigue test stress levels for the double shear specimens, based on total gross area in the test section, and stress ratios (R), are provided in Table 4.8. A frequency of 10 Hz was used. Specimen DS-182-1 was tested first, at the S_{max} stress level shown. DS-182-1 failed in fatigue at a relatively low number of cycles. The remaining double shear test specimens were therefore run at a lower S_{max} value of 18 ksi in order to obtain more realistic failure cycle counts.

Table 4.8. Eight Fastener Double Shear Fatigue Test Stresses

Specimen ID	Loading		Qty.
	S_{max} (ksi)	R	
DS-182-1	20	0.06	1
DS-182-2 thru 4	18	0.06	3
DS-100-1 thru 4	18	0.06	4
DS-100-5 thru 8	18	0.06	4
DS-050-1 thru 4	18	0.06	4
		Total	16

4.3.3. Stress Corrosion Testing

4.3.3.1. Test purpose. A sodium chloride solution was prepared to test a specimen with bolts placed at a radius for determination of residual loads in the bolts that cause failure. The specimen was immersed in a 3.5% sodium chloride solution for 20 days to determine if bolt failure was caused by the residual stresses.

4.3.3.2. Fabrication details. All part specimens used in the stress corrosion testing were fabricated from 7075-T7531 aluminum material. Material lot acceptance sheets were generated prior to machining. All material was fabricated from the same material lot and had a longitudinal grain direction. All fasteners of the same diameter and grip length were from the same lot. The lot numbers for material and the fasteners used in the testing were recorded. The geometry and dimensions of the stress corrosion test specimen are provided in Figure 4.6. The drawing shown in Figure 4.6 serves as the test specimen drawing for the corrosion testing. There is no separate drawing package for the corrosion testing provided in Appendix A.

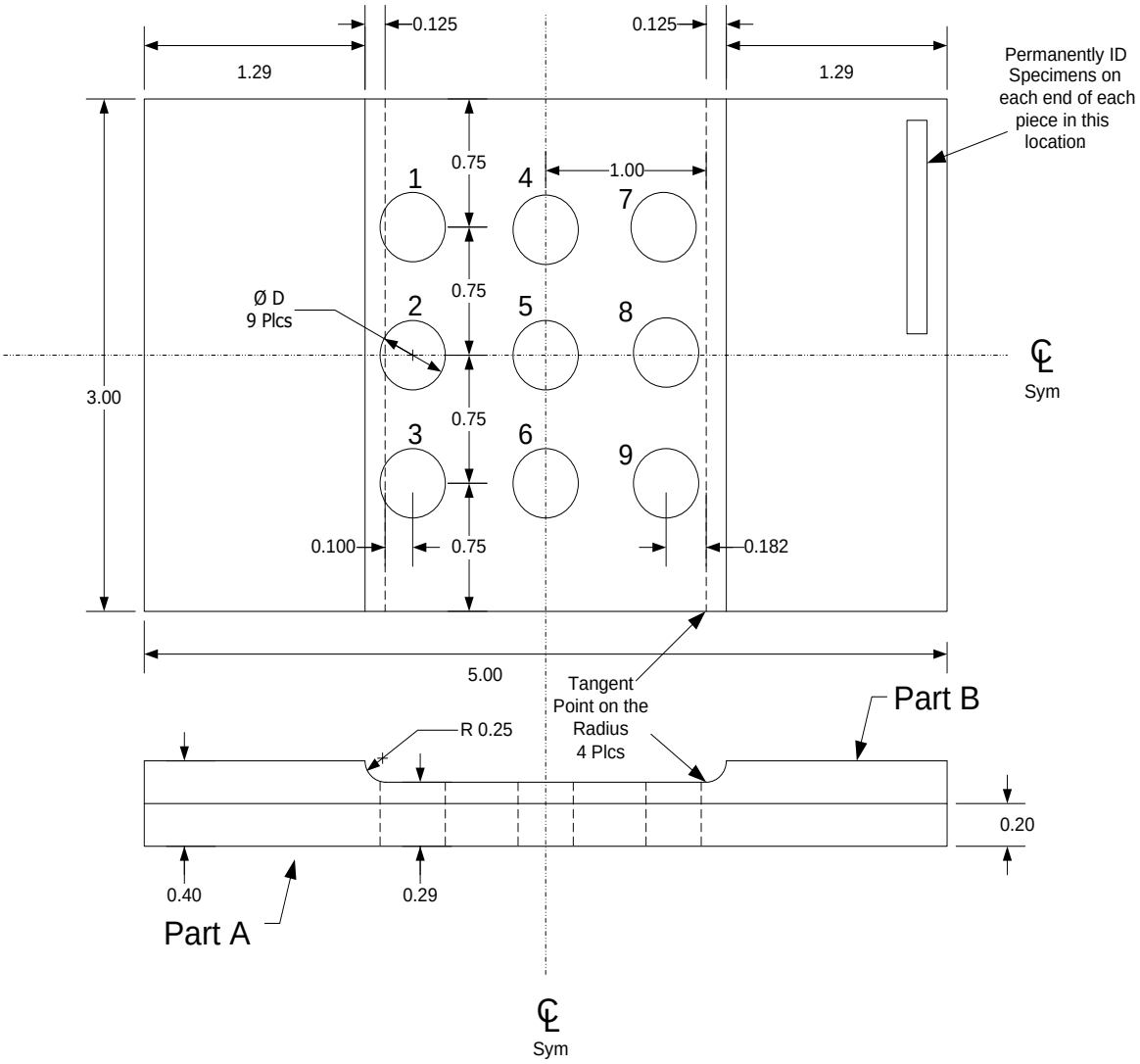

Figure 4.6. Stress Corrosion Test Specimen Drawing

The specimen was fabricated according to the dimensions and geometry called out in Figure 4.6. Edge preparation was performed by one machinist, all at the same time for consistency. The machinist broke all sharp edges with a 400 grit emery cloth. The specimen was labeled SW-1.

Specimen dimensions were measured and recorded. The stress corrosion test specimen dimensions that needed quality assurance verification are: specimen thickness

and width of all parts. All specimen dimensions were measured prior to assembly and any surface treatment being applied. Chemical finish and primer were applied to the specimen.

A picture of the assembled, pre-test corrosion specimen is provided in Figure 4.7. Note that two additional fasteners were incorrectly included in the final configuration. This fabrication error is inconsequential as it did not affect the general impact of corrosion related to bolts placed at or near a radius. These two discrepant fasteners are the lower most bolt/collar combinations shown in Figure 4.7.

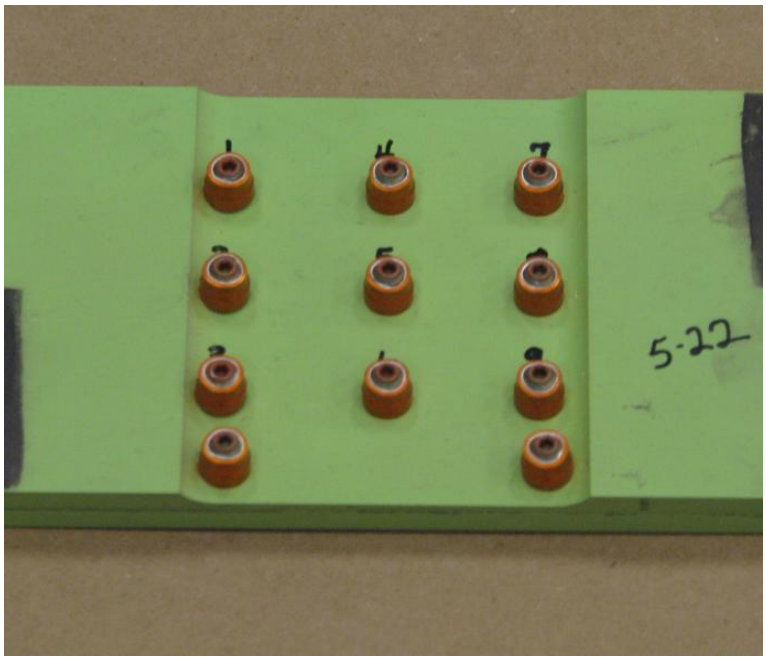

Figure 4.7. Pre-Test Stress Corrosion Test Specimen

4.3.3.3. Hole drilling and assembly. All holes were to be prepared in accordance with approved hole drilling specifications. The fastener shank diameters were measured and all fastener holes were drilled to allow a 0.0005 inch clearance fit (+/-

0.0005/0.0004). Holes were stack drilled and reamed. The holes in Part A, where the manufacturing head of the fastener is located, were chamfer deburred. All interface locations for Part A and B were flat deburred. The exit side of the holes in Part B required a deburr using a rotary tool with three rotations. The drilling parameters (speeds/feeds/lubrication/tools) used during fabrication were recorded. Hole diameters were measured and recorded by quality assurance personnel. Each hole was labeled with a permanent marking system (Hole 1 through 9 as numbered in Figure 4.6).

All joints were fay sealed prior to fastener installation. The specimens were separated and fay sealed rolled on Part B with a thickness of 0.004 to 0.006 inches. The sequence of fastener installation was: 1-2-3-4-5-6-7-8-9. The fastener number scheme is provided in Figure 4.6. Bolts were installed with collars with an expected break-off torque range of 25 to 35 lbf-in. Torque values achieved when installing fasteners were recorded.

4.3.3.4. Corrosion solution details. The test specimen was immersed in 3.5% sodium chloride solution for a minimum of 10 minutes per hour for a total of 20 days. Stress corrosion testing was conducted in accordance with ASTM G44-99 [44]. The air temperature was maintained at 80 ± 2˚F and the relative humidity was kept at 45 ± 10% through the entire test cycle.

4.4. TEST RESULTS

4.4.1. Open Hole/Step Specimen Test Results. Raw results data for the open hole/step fatigue test specimens is provided in Table 4.9. Fatigue test loads, stresses, R ratios and testing dates are given. The number of fatigue cycles to the first detectable crack and final failure are shown. Locations for the final failures are also identified.

The first step specimen with no holes, DW-RKt-1, was run at a fatigue stressof 25 ksi. No fatigue failure occurred at this maximum stress level. The test was terminated at 1,000,000 cycles. Consequently, the stress level was increased to 30 ksi for the second step specimen, DW-RKt-2. The number of cycles to failure of 523201 was still relatively high for this second run therefore the remaining three step specimens with no holes were tested at a higher stress level of 35 ksi to achieve a more reasonable cycles to failure value.

A stress level of 28 ksi was used for the first baseline open hole specimen, DW-OH-5000-1, with the hole placed at the center of the plate away from the radii. This coupon failure at 66738 cycles, a relatively low number. Therefore the stress level was decreased to 26 ksi for the DW-OH-5000-2 specimen which failed at 90803 cyles. The final baseline open hole specimen, DW-OH-5000-3, was tested at a stress level of 25 ksi. This specimen failed at a reasonable 114987 cycles.

All of the remaining open hole coupons were tested at a 25 ksi stress level with the exception of DW-OH-1000-1. The stress level for the DW-OH-1000 specimen is based on the average thickness of the upper and lower sections of the plate, as the hole is drilled directly through the transition section of the radius. Refer to the dimensions and

geometry shown in the Figure A.1 Open Hole in Radius Test Specimen drawing of Appendix A for specific details regarding hole placements.

Separate fatigue test results chartsfor the step specimens with no holes and open hole specimens are shown in Figures 4.8 and 4.9. The number of cyles to first cracking and number of cycles to failure for each coupon are displayed in a bar graph format. The stress levels for each individual run are also provided in these charts.

Fatigue results plots for the step only specimens and open hole specimens are displayed in Figures 4.10 and 4.11. These plots contain information on the plate material type, X dimension call out, stress level, stress ratio, cycles to failure for each specimen and characteristic life of each test grouping. Failure cycles were recalculated as required to allow for comparisons at the same maximum fatigue stress value within each test group. For the step only coupons, the result of the DW-RKt-1 run, which had testing terminated at 1,000,000 cycles due to no fatigue failure, is shown as a runout. The DW-RKt-2 specimen, which had a recalculated cycles to failure count of 160315 based on a 35 ksi maximum stress, was treated as an outlier based on a signficant difference in cycles to failure for this run compared to the DW-RKt-3 thru 5 tests. These runout and outlier results were not included in any characteristic life calculations.

Table 4.9. Open Hole/Step Fatigue Test Results Data

SPECIMEN NO.	Thickness	Width	C/S AREA (sq in)	MAX ksi	RATIO R	Pmax lbs	Pmin lbs	TEST START	TEST COMPLETE	CYCLES 1st CRACK	CYCLES FAILURE	Failure Location
DW-RKt-1	0.100	1.000	0.100	25.0	0.06	2,500	150	11/30/2012	12/1/2012	-	1,000,000	No Failure
DW-RKt-2	0.100	1.000	0.100	30.0	0.06	3,000	180	12/2/2012	12/2/2012	522747	523201	Lower Tangent of Radius
DW-RKt-3	0.100	1.000	0.100	35.0	0.06	3,500	210	12/3/2012	12/3/2012	364908	366702	Lower Tangent of Radius
DW-RKt-4	0.100	1.000	0.100	35.0	0.06	3,500	210	12/20/2012	12/21/2012	301115	301115	Lower Tangent of Radius
DW-RKt-5	0.100	1.000	0.100	35.0	0.06	3,500	210	12/21/2012	12/21/2012	317774	317804	Lower Tangent of Radius
DW-OH-5000-1	0.100	1.000	0.100	28.0	0.06	2,800	168	12/21/2012	12/21/2012	66638	66738	Edge of Hole
DW-OH-5000-2	0.100	1.000	0.100	26.0	0.06	2,600	156	12/21/2012	12/21/2012	79946	90803	Edge of Hole
DW-OH-5000-3	0.100	1.000	0.100	25.0	0.06	2,500	150	12/22/2012	12/22/2012	108510	114987	Edge of Hole
DW-OH-3079-1	0.100	1.000	0.100	25.0	0.06	2,500	150	12/22/2012	12/22/2012	103745	110211	Edge of Hole
DW-OH-3079-2	0.100	1.000	0.100	25.0	0.06	2,500	150	12/22/2012	12/22/2012	108905	114743	Edge of Hole
DW-OH-3079-3	0.100	1.000	0.100	25.0	0.06	2,500	150	12/22/2012	12/22/2012	107843	113461	Edge of Hole
DW-OH-3079-4	0.100	1.000	0.100	25.0	0.06	2,500	150	12/23/2012	12/23/2012	96035	103500	Edge of Hole
DW-OH-3029-1	0.100	1.000	0.100	25.0	0.06	2,500	150	12/23/2012	12/23/2012	107515	112060	Edge of Hole
DW-OH-3029-2	0.100	1.000	0.100	25.0	0.06	2,500	150	12/23/2012	12/23/2012	104640	108918	Edge of Hole
DW-OH-3029-3	0.100	1.000	0.100	25.0	0.06	2,500	150	12/23/2012	12/23/2012	94842	96291	Edge of Hole
DW-OH-3029-4	0.100	1.000	0.100	25.0	0.06	2,500	150	12/24/2012	12/24/2012	129522	133860	Edge of Hole
DW-OH-2091-1	0.100	1.000	0.100	25.0	0.06	2,500	150	12/27/2012	12/27/2012	104290	112904	Edge of Hole
DW-OH-2091-2	0.100	1.000	0.100	25.0	0.06	2,500	150	12/27/2012	12/27/2012	100094	100232	Edge of Hole
DW-OH-2091-3	0.100	1.000	0.100	25.0	0.06	2,500	150	12/27/2012	12/27/2012	92835	93418	Edge of Hole
DW-OH-2091-4	0.100	1.000	0.100	25.0	0.06	2,500	150	12/27/2012	12/28/2012	105230	105557	Edge of Hole
DW-OH-1000-1	0.157	1.000	0.157	16.0	0.06	2,500	150	12/28/2012	12/28/2012	225927	240193	Edge of Hole
DW-OH-1000-2	0.157	1.000	0.157	25.0	0.06	3,913	235	12/28/2012	12/28/2012	54333	54721	Edge of Hole
DW-OH-1000-3	0.157	1.000	0.157	25.0	0.06	3,913	235	12/28/2012	12/28/2012	58903	60974	Edge of Hole
DW-OH-1000-4	0.157	1.000	0.157	25.0	0.06	3,913	235	12/28/2012	12/28/2012	56301	59822	Edge of Hole

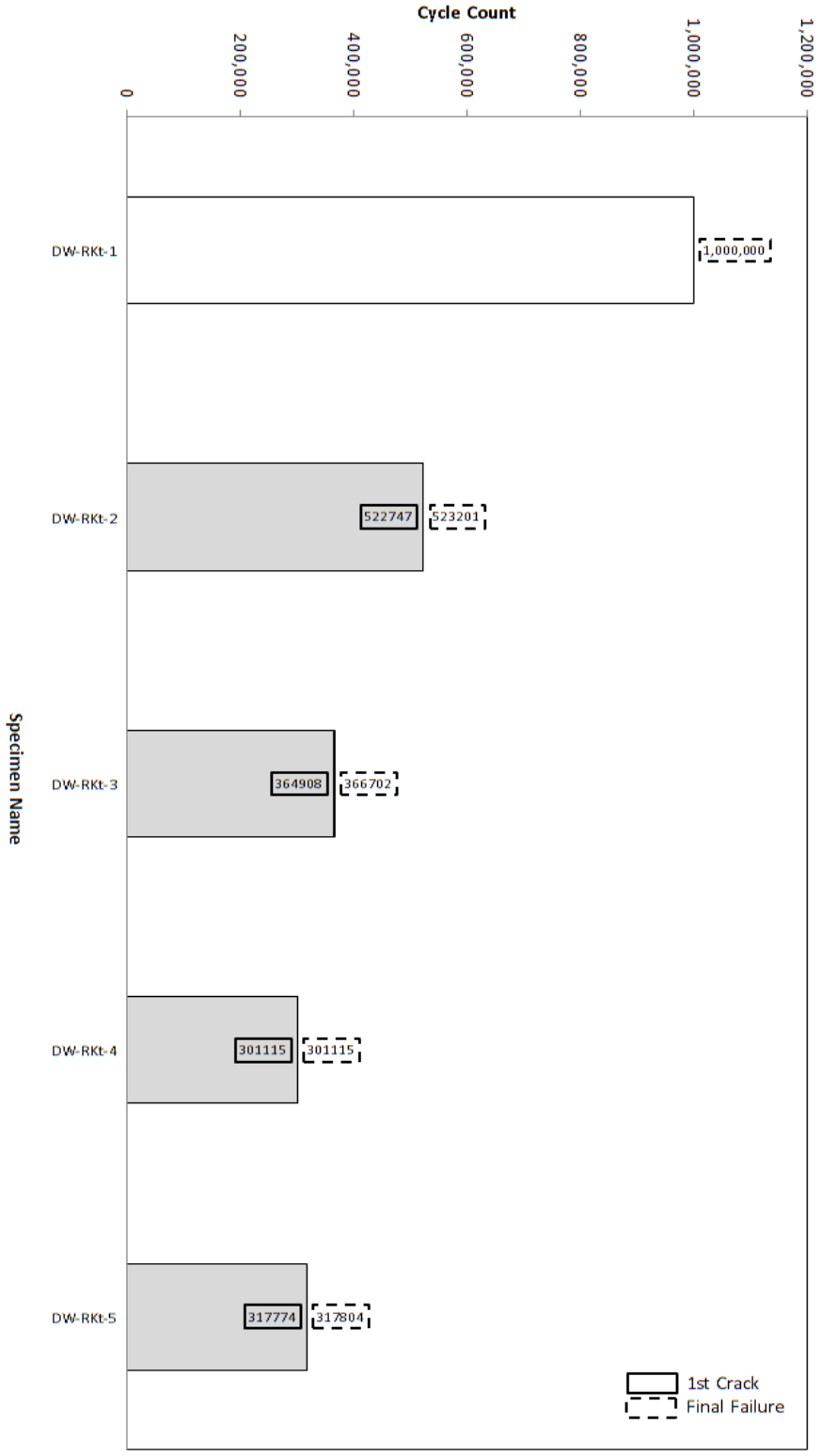

Figure 4.8. Step Specimens Fatigue Test Results Chart

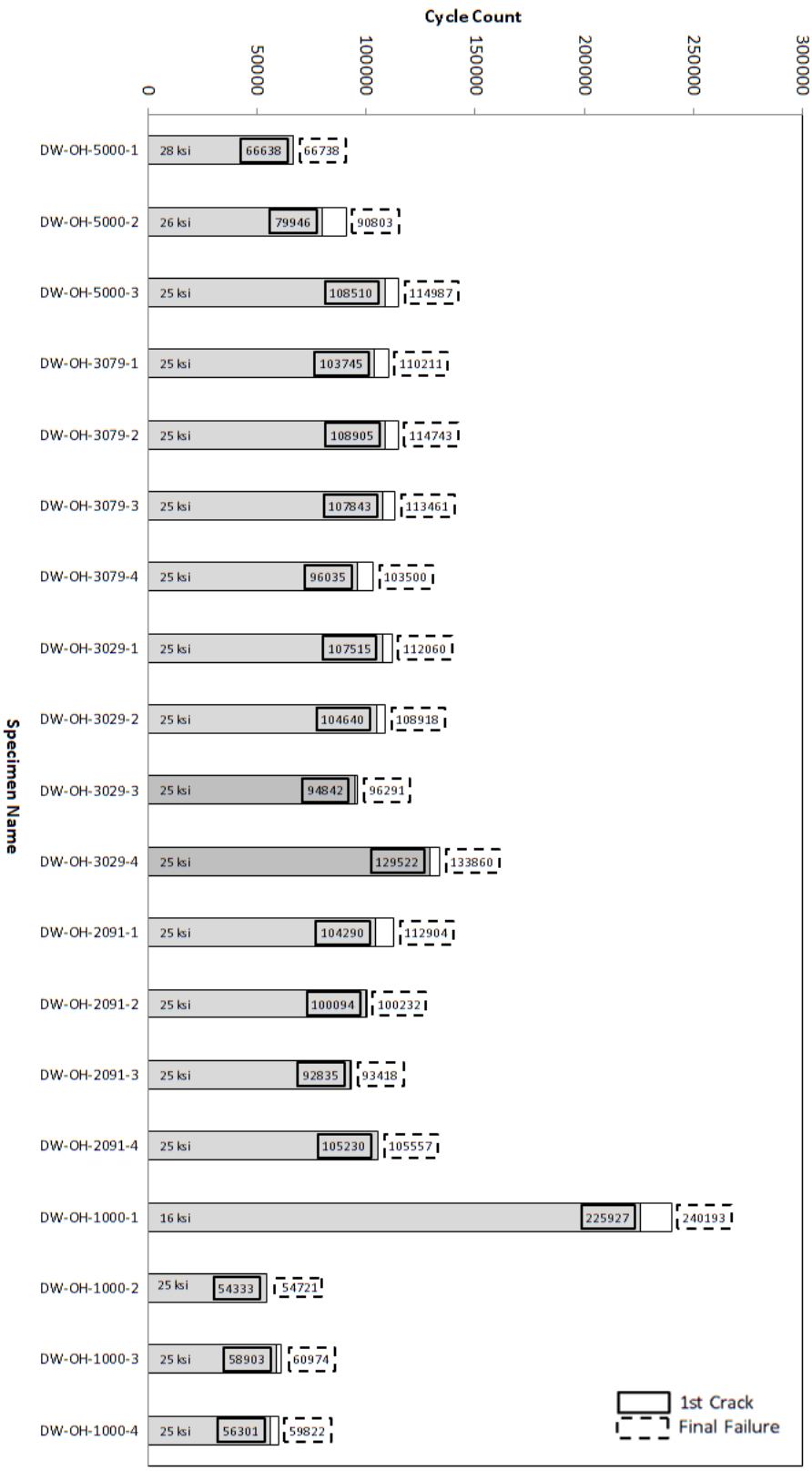

Figure 4.9. Open Hole Specimens Fatigue Test Results Chart

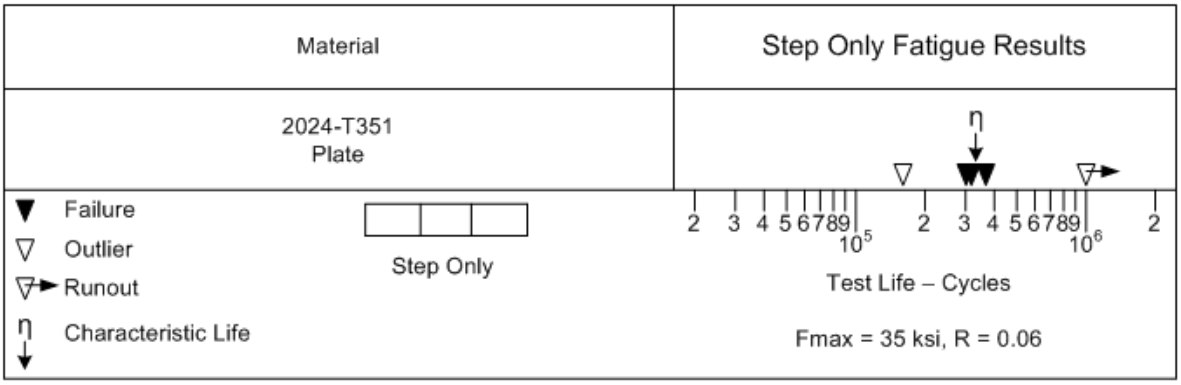

Figure 4.10. Step Only Fatigue Test Results Plot

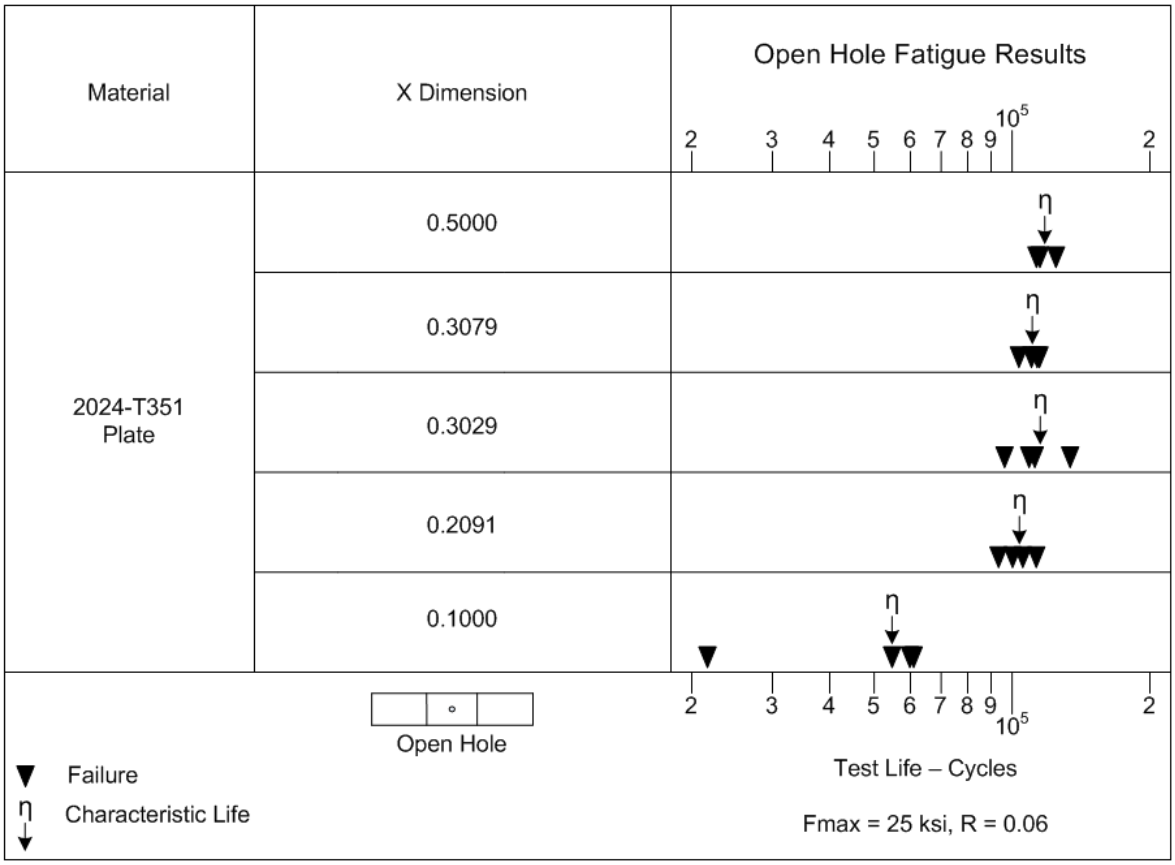

Figure 4.11. Open Hole Fatigue Test Results Plot

Pictures of the post-test, cracked open hole/step specimens are provided in Appendix B. Note that the fatigue failure for the step only runsoccurred at the lower tangent of the radius. The fatigue failures for the open hole tests were located at the edges of the holes. Each picture shows an individual cracked specimen representative of the other failed parts within that particular group. Refer to the Figure A.1 Open Hole in Radius Test Specimen drawing of Appendix A for the test group dash numbering scheme.

Figure 4.12 contains a close-up picture of the -6 post-test specimen. The -6 coupons failed at the edge of hole, slightly towards the lower tangent of the radius, indicating some stress concentration interaction between the hole and step.

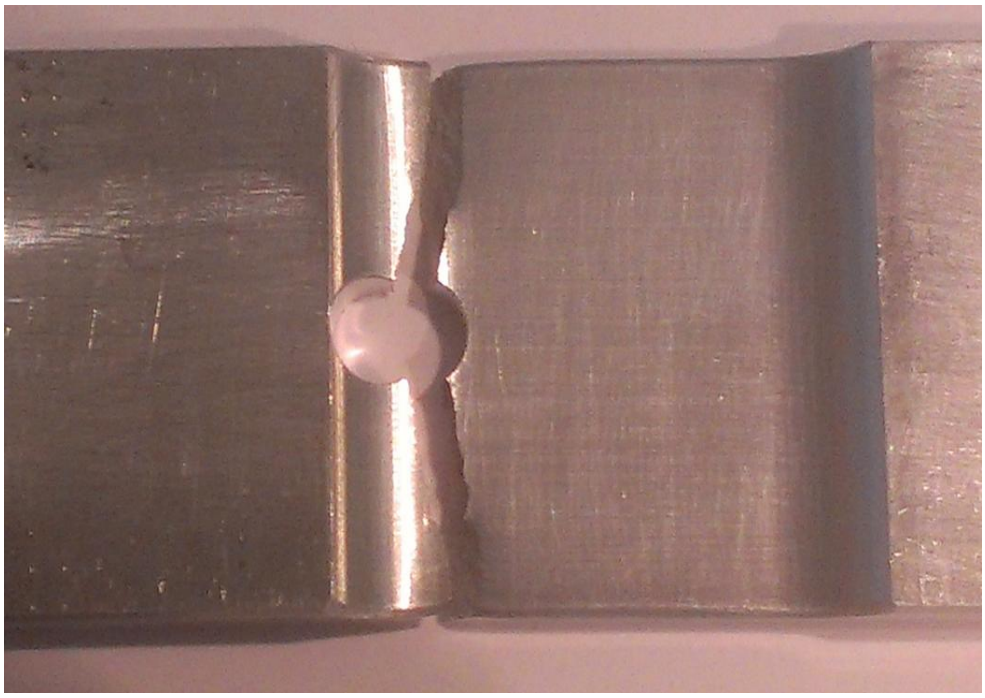

Figure 4.12. Close-Up Picture of Post-Test Open Hole in Radius Test Specimen -6

Characteristic lives for each specimen group were determined using a Weibayes analysis method [45]. The Weibayes method is a modified Weibull analysis that uses a known shape factor, β, based on previous failure data. Characteristic life plotsfound using a MLE (maximum likelihood estimate) statistical method are displayed in purple in Figures 4.13 through 4.18. Characteristic life plots determined through rank regression are shown in red. With rank regression, a curve fit of the test result data points is used considering a known shape factor.

Equation (17) is the characteristic life equation for the MLE solution. This is the relationship applied to determine the characteristic lives that are used in the calculation of all of the stress concentration modification factors presented in this study.

$$\eta = \left[\sum_{i=1}^{n} \frac{N_i^{\beta}}{r} \right]^{1/\beta} \tag{17}$$

In Equation (17), η is the characteristic life, n is the total number of specimens, N is the number of cycles to failure, r is the total number of failures and β is the shape factor. The total number of failures for each individual specimen analyzed as part of this project is 1. In this study, η is given in number of cycles.

Characteristic life plots for the open hole and step test specimens are shown in Figures 4.13 through 4.18. The occurrence CDF (cumulative distribution function) percentage shown in the plots is the probability of failure percentage. Each test result data

point is shown as a triangle. The rank regression characteristic life and MLE characteristic life for the DW-OH-1000-1 thru 4 test group are equal.

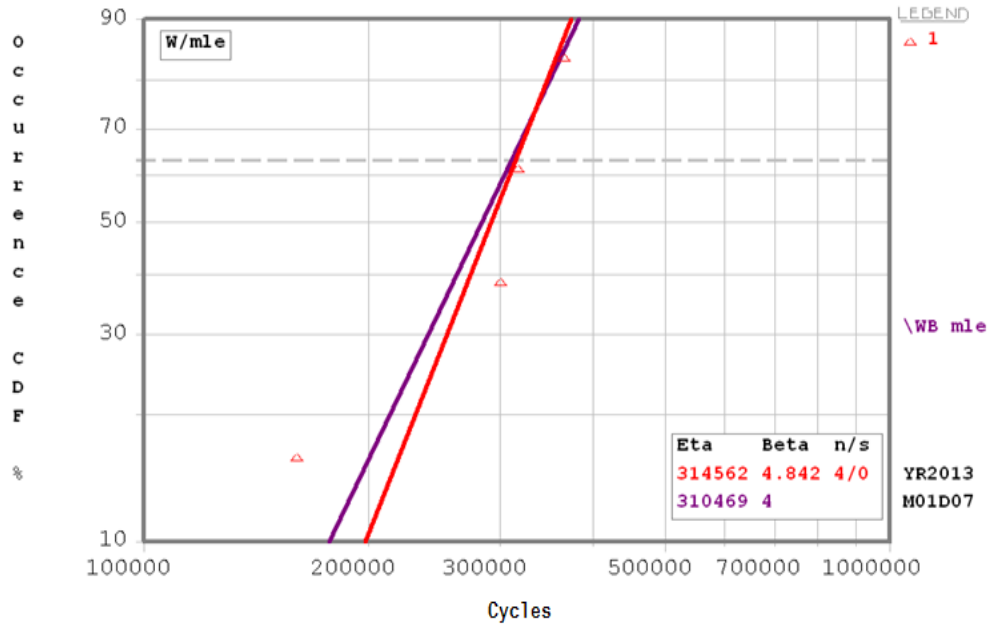

Figure 4.13. DW-RKt-1 thru 5 Characteristic Life Plot

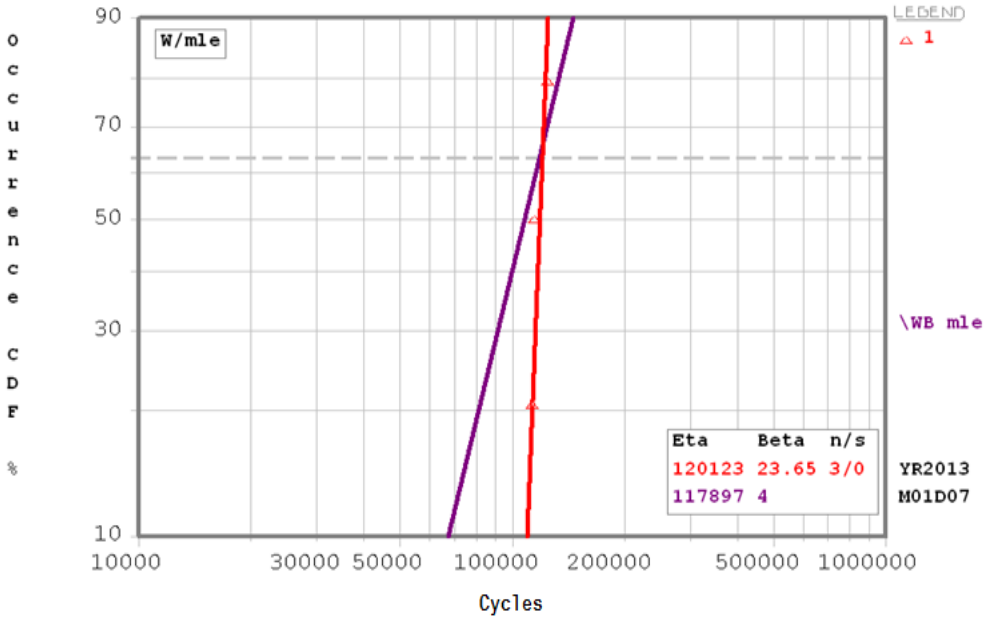

Figure 4.14. DW-OH-5000-1 thru 3 Characteristic Life Plot

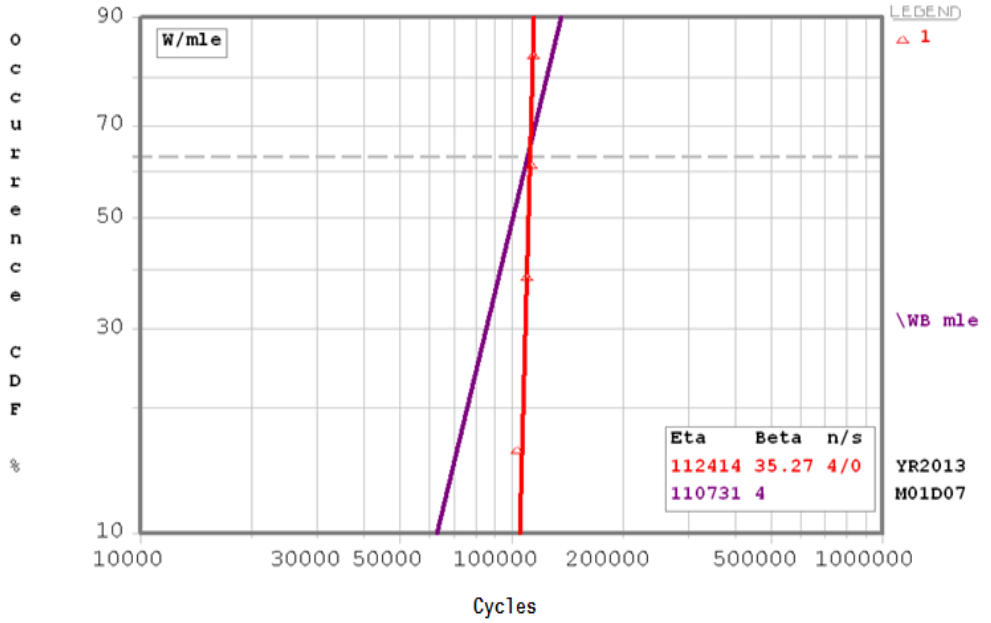

Figure 4.15. DW-OH-3079-1 thru 4 Characteristic Life Plot

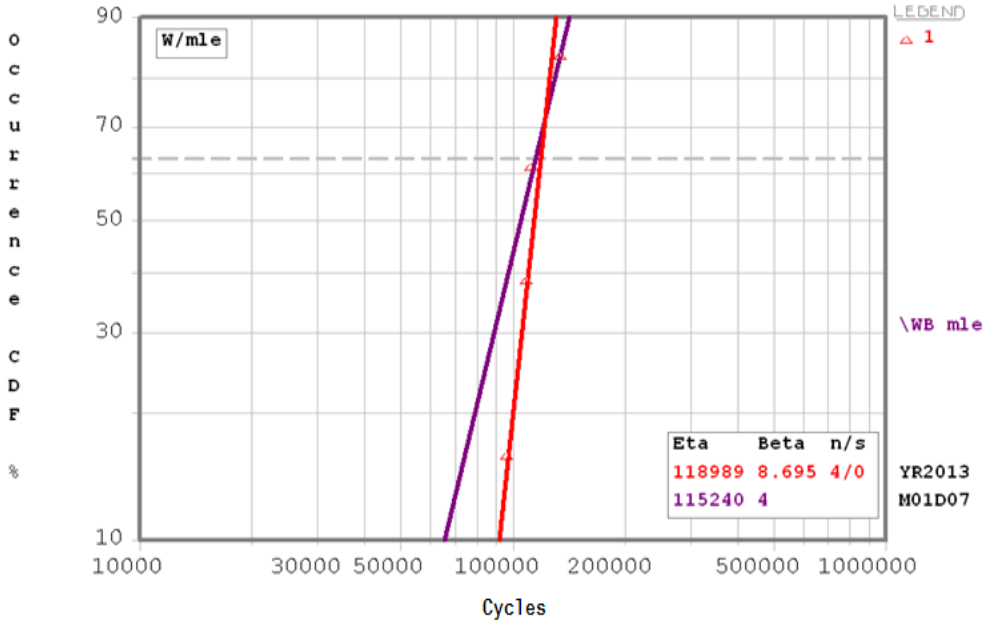

Figure 4.16. DW-OH-3029-1 thru 4 Characteristic Life Plot

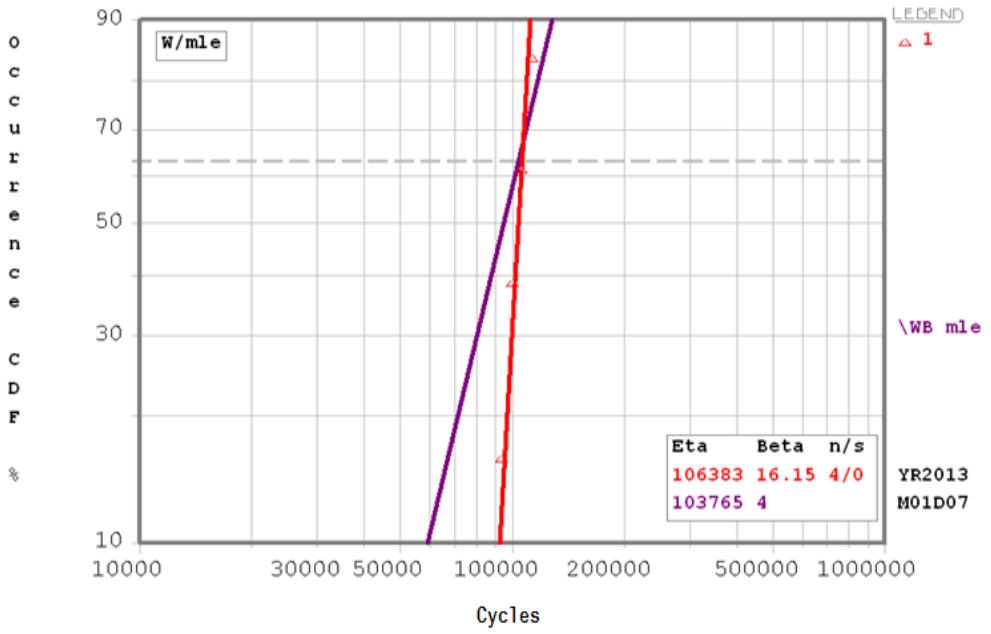

Figure 4.17. DW-OH-2091-1 thru 4 Characteristic Life Plot

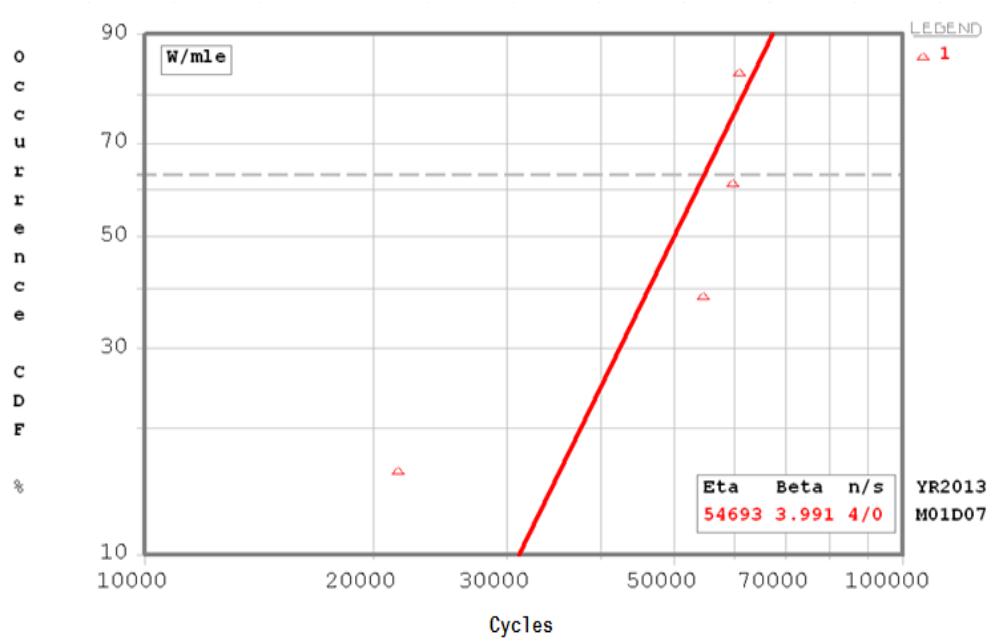

Figure 4.18. DW-OH-1000-1 thru 4 Characteristic Life Plot

The stress concentration modification factors for the open hole fatigue test specimen groups are calculated using the equivalent stress fatigue life method, as defined in MMPDS-03 [46]. This methodology is employed via application of Equations (18-22). In this set of equations, N is the MLE characteristic life of each test group, A_1,A_2, A_3 andA_4 are known coefficients based on material and K_t, $S_{eq}$is the equivalent stress, $S_{max}$is the maximum stress and R is the stress ratio. All K_t mod factors derived as part of this study are denoted with the symbol K_{tf}.

$$\log N = A_1 + A_2 \log (S_{eq} - A_4) \tag{18}$$

$$S_{eq} = S_{max}(1-R)^{A_3} \tag{19}$$

$$S_{eq,baseline} = 10^{\left(\frac{-A_1+\log N_{baseline}}{-A_2}\right)} + A_4 \tag{20}$$

$$S_{eq,interaction} = 10^{\left(\frac{-A_1+\log N_{interaction}}{-A_2}\right)} + A_4 \tag{21}$$

$$K_{tf} = \frac{S_{eq,interaction}}{S_{eq,baseline}} \tag{22}$$

Equations (18-22) were applied to the open hole/step fatigue test results to calculate stress concentration modification factors for each specimen group. All K_t mod factors for the open hole/step test groups are provided in Table 4.10. A full summary, discussion and interpretation of all mod factors derived through this research can be found in Section 7.

Table 4.10. Open Hole/Step Mod Factors

Specimen Group	Characteristic Life	K_{tf}
DW-RKt-1 thru 5	310469	NA
DW-OH-5000-1 thru 3	117897	NA
DW-OH-3079-1 thru 4	110731	1.01
DW-OH-3029-1 thru 4	115240	1.00
DW-OH-2091-1 thru 4	103765	1.02
DW-OH-1000-1 thru 4	54693	1.15

4.4.2. Low Load Transfer Dogbone Specimen Test Results. Fatigue test data was generated for the low load transfer 5 fastener dogbone specimens. The comprehensive results data for the dogbone specimen types is presented in Table 4.11. Specific part dimensions were recorded. The test machine number and testing dates are provided. Fatigue test load, stresses and R ratios are noted. The relative fatigue lives of each specimen group, compared to the baseline case, are shown. The final failure location for each specimen is identified.

The first low load transfer dogbone specimen, DB-182-1, was run at a fatigue stress of 25 ksi. A fatigue stress of 20 ksi was used for the rest of the dogbone specimens to achieve a more appropriate baseline fatigue failure in terms of number of cycles. All low load transfer dogbone test runswere used in the development of characteristic lives and K_t mod factors through application of the equivalent stress fatigue life method.

A bar chart detailing the relative fatigue lives of each five fastener low load transfer dogbone specimen group is provided in Figure 4.19. The fatigue results are presented in graphical format to allow for an easier comparison between the various test group configurations. Four individual specimens were tested for each profile type.

Running a number of samples of the same specimen type allows for the determination of a statistical average interms of number of fatigue cyles to final failure.

Table 4.11. Low Load Transfer Dogbone Fatigue Test Results Data

SPECIMEN NO.	Part A		Part B		C/S AREA (sq in)	TEST MACHINE	LOAD RANGE kip	STROKE RANGE in.	MAX ksi	RATIO R	Pmax lbs	Pmin lbs	TEST START	TEST COMPLETE	RELATIVE LIFE	Failure Location
	Thickness	Width	Thickness	Width												
DB-182-1 thru 4	0.200	1.125	0.089	0.938	0.308	5	20	5.0	25.0	0.06	7,695	462	7/18/2012	7/19/2012	1.000	FASTENER 4, TAIL SIDE
	0.200	1.125	0.089	0.939	0.307	5	20	5.0	20.0	0.06	6,150	369	7/19/2012	7/19/2012		FASTENER 5, TAIL SIDE
	0.200	1.125	0.089	0.938	0.308	5	20	5.0	20.0	0.06	6,169	370	7/23/2012	7/23/2012		FASTENER 1, TAIL SIDE
	0.200	1.125	0.088	0.940	0.307	5	20	5.0	20.0	0.06	6,140	368	7/24/2012	7/24/2012		FASTENER 1, TAIL SIDE
DB-100-1 thru 4	0.200	1.125	0.088	0.938	0.307	5	20	5.0	20.0	0.06	6,138	368	7/20/2012	7/20/2012	0.642	FASTENER 2, TAIL SIDE
	0.199	1.125	0.090	0.938	0.308	5	20	5.0	20.0	0.06	6,166	370	7/20/2012	7/20/2012		FASTENER 4, TAIL SIDE
	0.200	1.125	0.089	0.939	0.307	5	20	5.0	20.0	0.06	6,148	369	7/23/2012	7/23/2012		FASTENER 2, TAIL SIDE
	0.200	1.125	0.089	0.940	0.308	5	20	5.0	20.0	0.06	6,153	369	7/24/2012	7/25/2012		FASTENER 4, TAIL SIDE
DB-100-5 thru 8	0.199	1.125	0.091	0.938	0.309	5	20	5.0	20.0	0.06	6,175	371	7/20/2012	7/20/2012	1.274	FASTENER 1, TAIL SIDE
	0.200	1.125	0.089	0.939	0.308	5	20	5.0	20.0	0.06	6,161	370	7/20/2012	7/23/2012		FASTENER 1, TAIL SIDE
	0.200	1.125	0.089	0.939	0.307	5	20	5.0	20.0	0.06	6,150	369	7/23/2012	7/24/2012		FASTENER 5, TAIL SIDE
	0.200	1.125	0.089	0.938	0.308	5	20	5.0	20.0	0.06	6,170	370	7/25/2012	7/25/2012		FASTENER 2, TAIL SIDE
DB-050-1 thru 4	0.200	1.125	0.089	0.939	0.309	5	20	5.0	20.0	0.06	6,171	370	7/20/2012	7/20/2012	0.472	FASTENER 4, TAIL SIDE
	0.200	1.125	0.089	0.938	0.308	5	20	5.0	20.0	0.06	6,170	370	7/23/2012	7/23/2012		FASTENER 2, TAIL SIDE
	0.200	1.125	0.089	0.938	0.308	5	20	5.0	20.0	0.06	6,170	370	7/24/2012	7/24/2012		FASTENER 2, TAIL SIDE
	0.200	1.125	0.089	0.939	0.308	5	20	5.0	20.0	0.06	6,159	370	7/25/2012	7/25/2012		FASTENER 2, TAIL SIDE

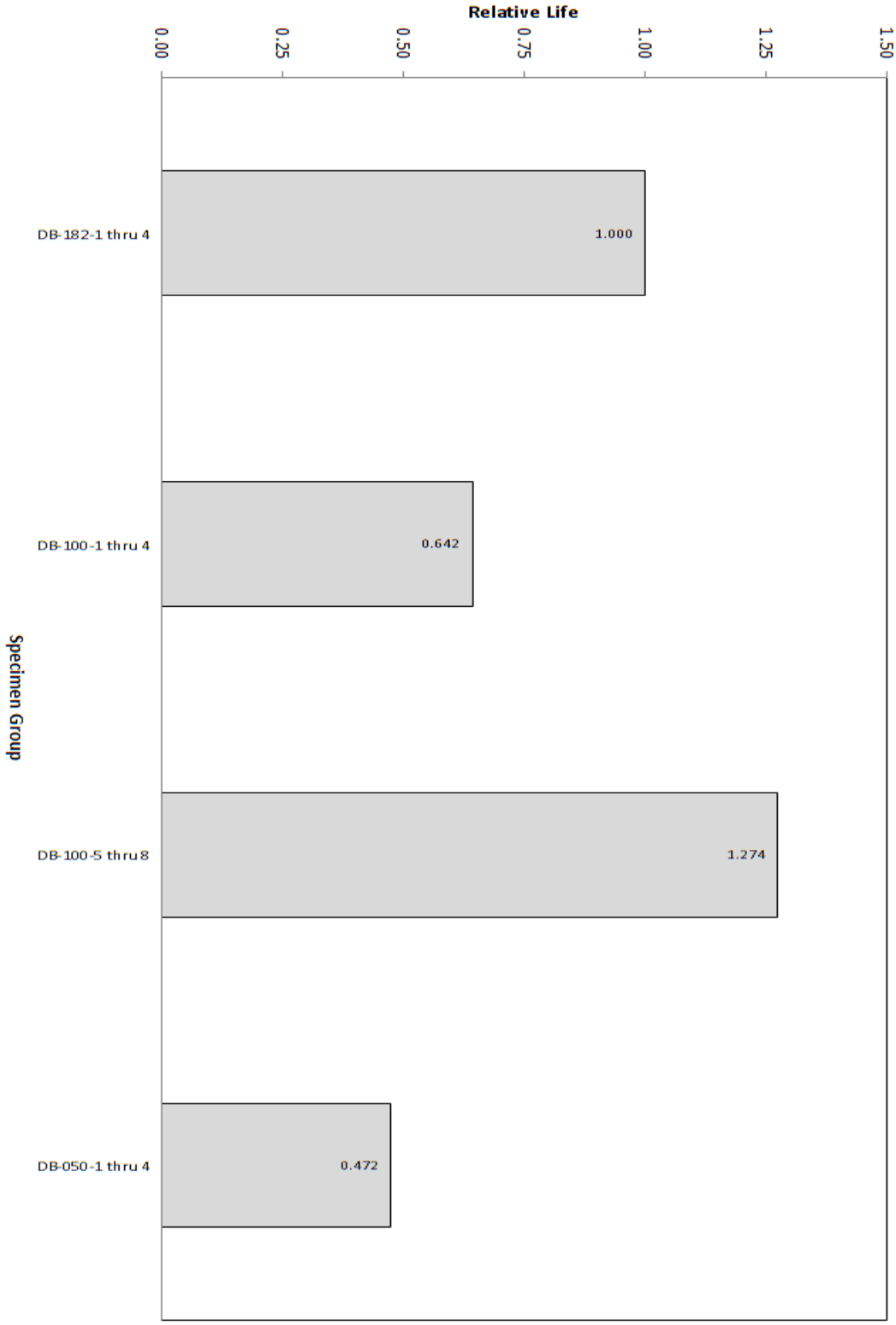

Figure 4.19. Low Load Transfer Dogbone Fatigue Test Results Chart

Stress concentration modification factors for the 5 fastener low load transfer dogbone specimen groups were calculated via application of Equations (18-22). These modification factors are presented in Table 4.12.

Table 4.12. Low Load Transfer Dogbone Mod Factors

Specimen Group	K_{tf}
DB-182-1 thru 4	NA
DB-100-1 thru 4	1.07
DB-100-5 thru 8	NA
DB-050-1 thru 4	1.12

4.4.3. Eight Fastener Hole Double Shear Specimen Test Results. Fatigue test data was generated for the eight fastener hole double shear specimens. The comprehensive results data for the double shear specimen types is presented in Table 4.13. Specific part dimensions were recorded. The test machine number and testing dates are provided. Fatigue test load, stresses and R ratios are noted for each specimen. The relative lives of each specimen group, compared to the baseline case, are shown. The specific final failure location is identified for all runs. All of the fatigue failures for the double shear test specimens with X dimensions of 0.100 in. and 0.050 in. without radius fillers occurred at hole locations at the radii.

The first eight fastener hole double shear specimen, DS-182-1, was run at a fatigue stress of 20 ksi. The number of cycles to failure for this run indicated that the stress level needed to be descreased for the remaining double shear samples. Therefore a

fatigue stress of 18 ksi was used for the rest of the DS specimens to achieve a more appropriate baseline fatigue failure in terms of number of cycles. The eight fastener double shear test results were used to calculate characteristic lives and Kt mod factors through application of Equations (18-22).

A results chart detailing the relative fatigue lives is provided in Figure 4.20. The fatigue results are presented in graphical format to allow for a visual comparison between the various eight fastener hole double shear test groups. Four individual specimens were tested for each configuration.

Table 4.13. 8 Fastener Double Shear Fatigue Test Results Data

SPECIMEN NO.	Part C		Part D		C/S AREA (sq in)	TEST MACHINE	LOAD RANGE kip	STROKE RANGE in.	MAX ksi	RATIO R	Pmax lbs	Pmin lbs	TEST START	TEST COMPLETE	RELATIVE LIFE	Failure Location
	Thickness	Width	Thickness	Width												
DS-182-1 thru 4	0.091	1.501	0.100	1.501	0.287	8	11	5.0	20.0	0.06	5,734	344	6/21/2012	6/21/2012	1.000	FASTENER 4, TAIL SIDE
	0.091	1.500	0.101	1.499	0.287	8	11	5.0	18.0	0.06	5,169	310	6/22/2012	6/22/2012		FASTENER 2, HEAD SIDE
	0.092	1.501	0.101	1.499	0.289	8	11	5.0	18.0	0.06	5,211	313	6/25/2012	6/25/2012		FASTENER 6, TAIL SIDE
	0.091	1.501	0.100	1.500	0.286	8	11	5.0	18.0	0.06	5,145	309	6/26/2012	6/26/2012		FASTENER 6, TAIL SIDE
DS-100-1 thru 4	0.091	1.502	0.101	1.500	0.288	8	11	5.0	18.0	0.06	5,187	311	6/22/2012	6/22/2012	0.611	FASTENER 6, HEAD SIDE
	0.090	1.502	0.100	1.500	0.285	8	11	5.0	18.0	0.06	5,133	308	6/23/2012	6/23/2012		FASTENER 2, TAIL SIDE
	0.091	1.502	0.101	1.500	0.287	8	11	5.0	18.0	0.06	5,173	310	6/25/2012	6/25/2012		FASTENER 6, TAIL SIDE
	0.091	1.502	0.101	1.497	0.286	8	11	5.0	18.0	0.06	5,155	309	6/26/2012	6/26/2012		FASTENER 2, TAIL SIDE
DS-100-5 thru 8	0.091	1.502	0.100	1.502	0.286	8	11	5.0	18.0	0.06	5,150	309	6/22/2012	6/23/2012	1.362	FASTENER 4, HEAD SIDE
	0.089	1.502	0.101	1.499	0.284	8	11	5.0	18.0	0.06	5,118	307	6/23/2012	6/23/2012		FASTENER 4, TAIL SIDE
	0.090	1.502	0.101	1.498	0.285	8	11	5.0	18.0	0.06	5,129	308	6/25/2012	6/25/2012		FASTENER 2, HEAD SIDE
	0.090	1.502	0.101	1.497	0.286	8	11	5.0	18.0	0.06	5,141	308	6/26/2012	6/26/2012		FASTENER 4, TAIL SIDE
DS-050-1 thru 4	0.092	1.502	0.101	1.499	0.289	8	11	5.0	18.0	0.06	5,199	312	6/23/2012	6/23/2012	0.612	FASTENER 2, TAIL SIDE
	0.089	1.503	0.101	1.499	0.284	8	11	5.0	18.0	0.06	5,119	307	6/25/2012	6/25/2012		FASTENER 8, TAIL SIDE
	0.089	1.502	0.100	1.501	0.284	8	11	5.0	18.0	0.06	5,106	306	6/25/2012	6/26/2012		FASTENER 2, TAIL SIDE
	0.090	1.502	0.101	1.498	0.286	8	11	5.0	18.0	0.06	5,157	309	6/26/2012	6/26/2012		FASTENER 4, TAIL SIDE

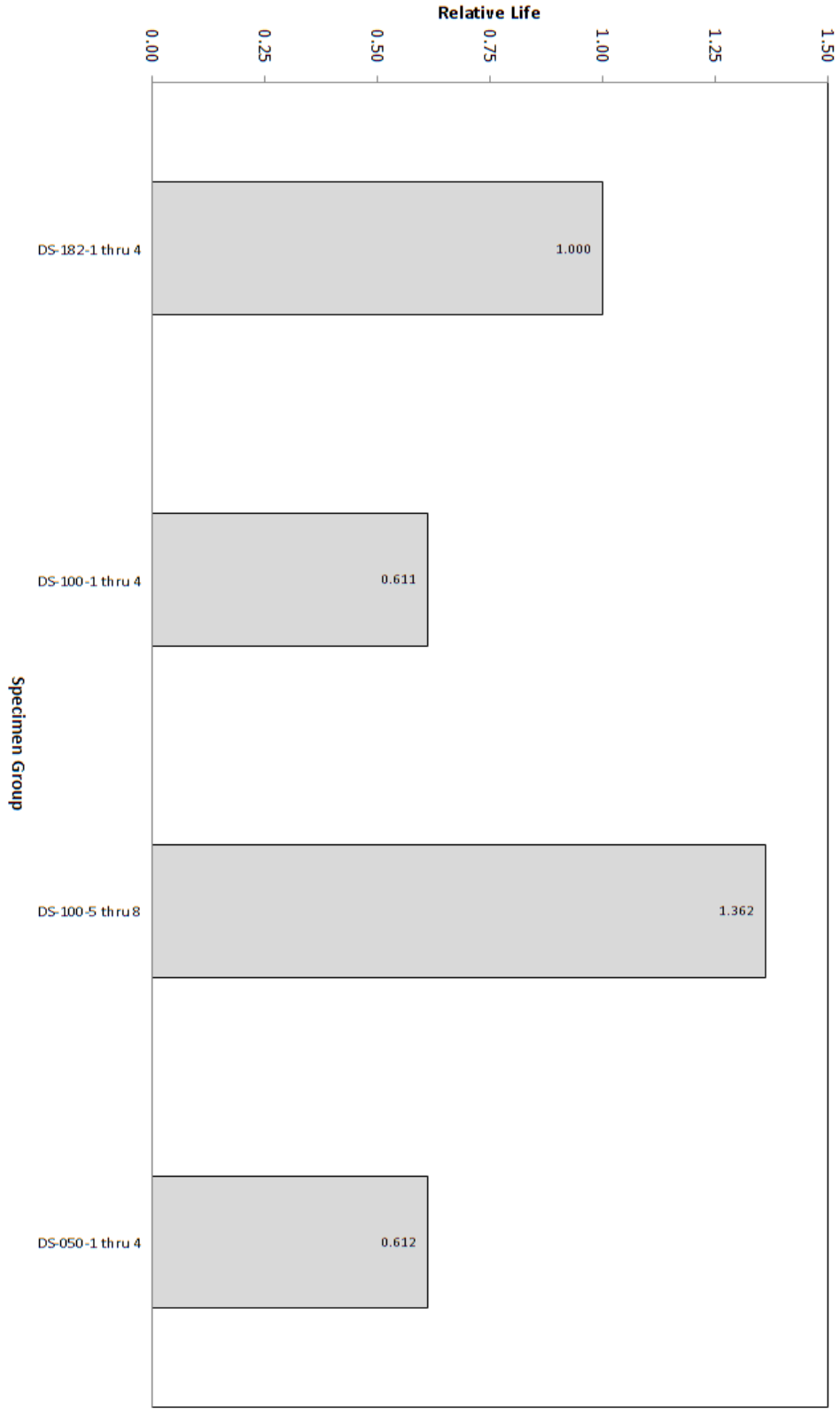

Figure 4.20. 8 Fastener Double Shear Fatigue Test Results Chart

Pictures of typical failures for the eight fastener double shear test specimens are shown in Figure 4.21. Note that the fatigue failures occurred at the holes located near the radius.

.

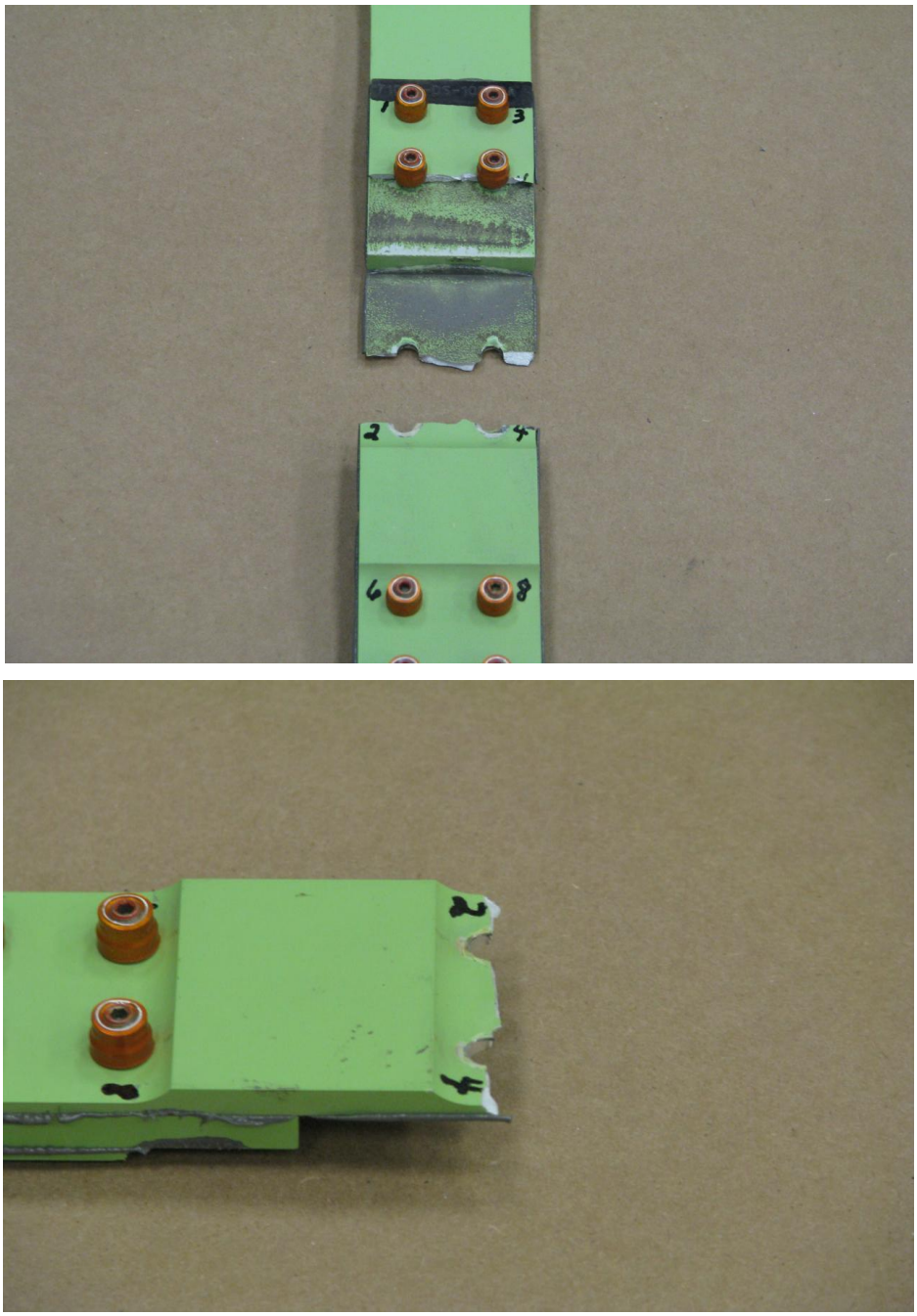

Figure 4.21. 8 Fastener Double Shear Typical Failure

K_t mod factors for the eight fastener double shear fatigue test specimen groups were calculated using Equations (18-22). These stress concentration modification factors are presented in Table 4.14.

Table 4.14. 8 Fastener Double Shear Mod Factors

Specimen Group	K_{tf}
DS-182-1 thru 4	NA
DS-100-1 thru 4	1.08
DS-100-5 thru 8	NA
DS-050-1 thru 4	1.08

4.4.4. Stress Corrosion Specimen Test Results. Upon completion of the stress corrosion test, remnants of corrosion on each fastener collar were observed. However the corrosion was minimal and no fastener or collar failures were found. The specimen was considered to have passed the test as no cracking or failures were present. Stress corrosion was not an issue for the condition of the collars riding a radius. A photo of the post-test stress corrosion specimen is shown in Figure 4.22. A close-up of the fastener 11 collar that shows indications of corrosion is presented in Figure 4.23.

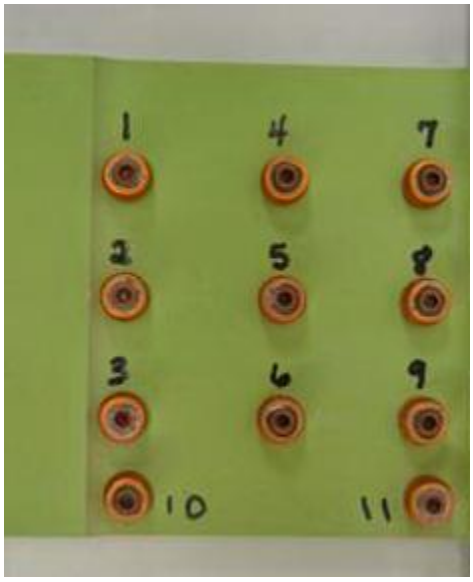

Figure 4.22. Post-Test Stress Corrosion Specimen

Figure 4.23. Post-Test Stress Corrosion Fastener 11 Collar

5. FINITE ELEMENT MODELING/ANALYSIS

The finite element method is a long-established technique for use in structural analysis. A critical structure can be broken up in to a number of elements of specified sizes in order to obtain a solution to the differential equations that govern the model. FEMs are composed of elements that are one-dimensional, two-dimensional, or three-dimensional. All of the models used in this study are composed of 3D elements. The complex geometric nature of the features being analyzed relating to the holes interacting with a step dictate the use of solid elements.

Finite element modeling and analysis has been proven as a cost-effective, time saving alternative to physical testing, which typically requires more resources and infrastructure by comparison. Consequently, FEM/FEA is used extensively in the aerospace industry where materials, test equipment, and labor can be very expensive. The precision of a proposed finite element solution to any given problem in structural mechanics can vary greatly and is dependent upon many different parameters. However, properly constructed models with correct inputs have been proven to provide incredibly accurate results when compared to empirical testing. Various outputs including displacements, loads, stresses and strains can be obtained through FEA. The finite element method can easily be applied to determine stress concentration factors for various combinations of geometry and applied loading.

The differential equations that govern finite element models are complex. A range of computer software suites are available that simplify as well as automate, to a certain extent, the process of creating and analyzing finite element problems. In this

research study, the CATIA Generative Structural Analysis finite element software tool [41] is used exclusively. CATIA (GSA) is an easy to use, comprehensive simulation tool that has full capability with respect to FEM/FEA [47]. All pre-processing and post-processing tasks are performed within the CATIA (GSA) Workbench environment.

CATIA is a computer aided drafting/computer aided engineering software suite used in the design and modeling of parts and structures. The CATIA Generative Structural Analysis module operates within the CATIA environment which automatically reads in the geometry data stored in the .CATPart file type. The CATIA (GSA) finite element analysis results are saved as .CATAnalysis files.

Finite element analysis is an extremely detailed subject. A substantial amount of reference material exists, including entire textbooks as well as academic and industry research, that provide a more comprehensive background on FEM/FEA than what is presented within this short general description.

5.1. MODEL CONSTRUCTION

For comparison purposes to the physical fatigue testing of the situations involving interacting stress concentrations between a series of holes and radii, finite element models were created to conduct a computer simulation involving the structural behavior of these details. The first step in the application of the finite element method to this study was to construct a series of models using the CATIA design software suite [41]. CATIA is a 3D modeling tool used extensively in the aerospace industry.

Models were created in CATIA for the open hole in radius and step specimens, as shown in Figure A.1 in Appendix A. The open hole models differ according to the X

distance callout between the center of the hole and the tangent point of the radius. A model was also created for the step specimen with no holes for determination of the stress concentration factor of the radius itself. The open hole and step models used in this study are shown in Figure 5.1. The dimensions of the models used in the analysis exactly match the dimensions called out in the respective dash number configurations of the Open Hole in Radius Test Specimen drawing of Appendix A. All hole diameters are 0.1875 inches and all radii are 0.25 inches.

These finite element models and the resulting analysis were created for comparison purposes to the physical open hole testing. Finite element analysis results for the open hole and step test specimens were derived. A comprehensive summary of the stress concentrations factors and K_t modiciation factors derived from the FEA results is also provided in this paper.

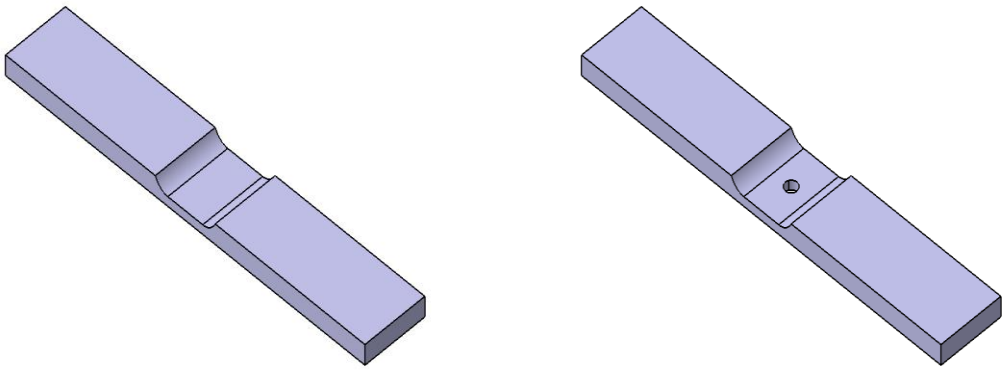

-1

-2

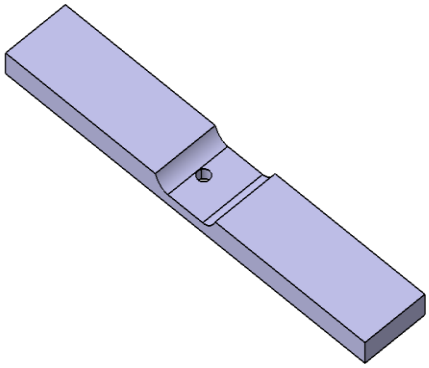

-3

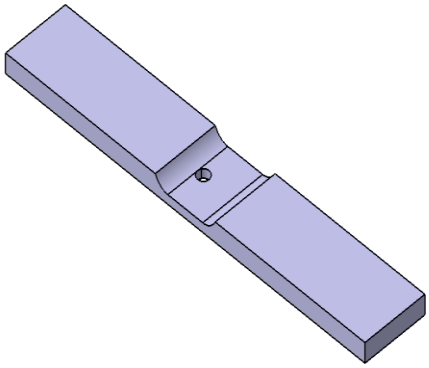

-4

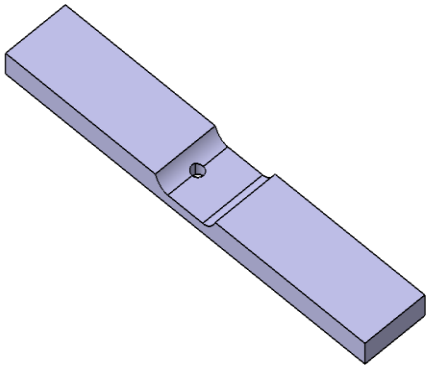

-5

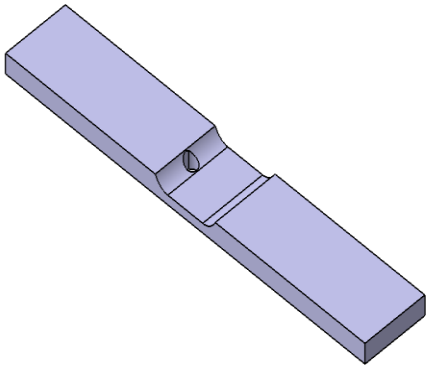

-6

Figure 5.1. Open Hole in Radius Test Specimen Models

5.2. MATERIAL PROPERTIES

A set of material properties was created in the CATIA (GSA) Workbench for the 1.000 in. thick, 2024-T351 plate material used to fabricate the open hole/step test specimens. Table 5.1 shows the specific set of material properties entered for all parts. Material property values were obtained from MMPDS-03 [46].

Table 5.1. Material Properties

Material	E (Young's Modulus) psi	ν (Poisson's Ratio)	ω (Density) lb/in^3
2024-T351, 1.000 in. thick	10700000	0.33	0.100

The plates were defined as solid, homogeneous sections in CATIA (GSA). The material properties listed above were then assigned to each plate model. The material type used in this finite element analysis study was specified as elastic, isotropic.

CATIA (GSA) requires that users enter in material properties with specified units. The CATIA Generative Structural Analysis Workbench environment is somewhat unique in that most FEM/FEA software packages do not possess a built-in system or set of defined units. English units of measurement are used exclusively in this analysis. The aerospace industry in the United States uses the English system with the preferred measurement of lengths in inches.

5.3. FINITE ELEMENT TYPE AND MESHING

All finite element analysis conducted as part of this research, using the CATIA Generative Structural Analysis module, was performed with parabolic tetrahedron type

elements. These parabolic tetrahedron elements are elastic and iso-parametric. The solid tetrahedrons have 10 nodes, with 3 degrees of freedom per node. A diagram of the element, with node locations identified, is given in Figure 5.2.

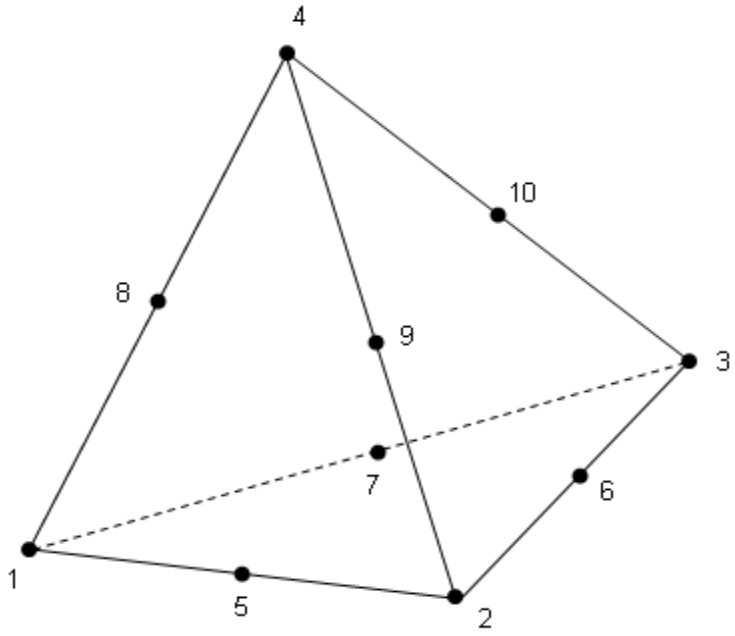

Figure 5.2. Parabolic Tetrahedron 10-Node Element

The Octree Tetrahedron Mesher tool in CATIA (GSA) was used to apply the 3D meshes to all parts. Parabolic element types were selected. A mesh size of 0.100 inches was used. The Open Hole in Radius Test Specimen -2 mesh contains a total of 12718 nodes and 7151 elements. These values are typical for all of the models studied as part of this research. A diagram of the meshed Open Hole in Radius Test Specimen -2finite element model is displayed in Figure 5.3.

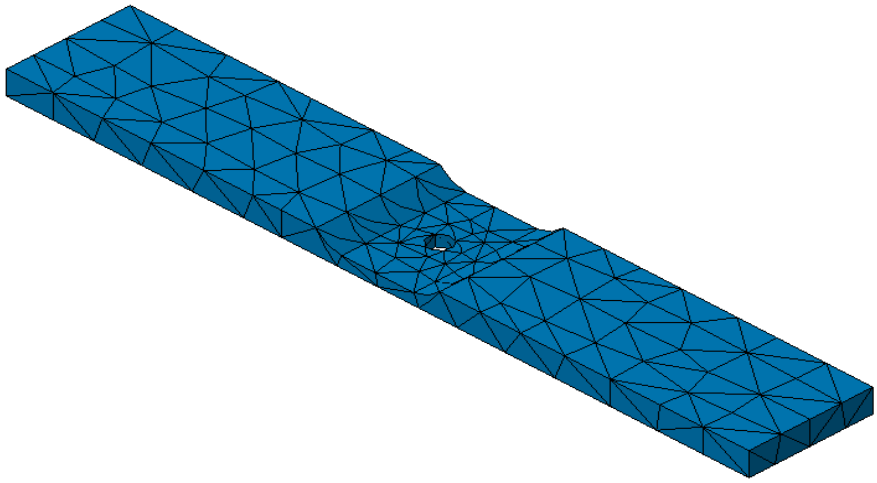

Figure 5.3. Open Hole in Radius Test Specimen -2Meshed Finite Element Model

5.4. APPLIED LOADS AND BOUNDARY CONDITIONS

A specific set of static boundary condition constraints and loads were applied to each model in this finite element analysis study. A clamped restraint was affixed to the face at one end of the plate in order to constrain all translational and rotational degrees of freedom. The lower face of the plate was constrained in the z-direction. A nominal, 1 psi surface force density was applied to the face at the opposite end of the plate. All stress concentration factors and stress concentration modification factors calculated from the finite element model runs are based solely on load direction and geometry. The application of a load with a nominal value is therefore sufficient.

An illustration of the loading and boundary conditions applied to the Open Hole in Radius Test Specimen -2 FEM is given in Figure 5.4. The loads and constraints shown

in this diagram are typical of those used for all of the finite elements models analyzed as part of this research.

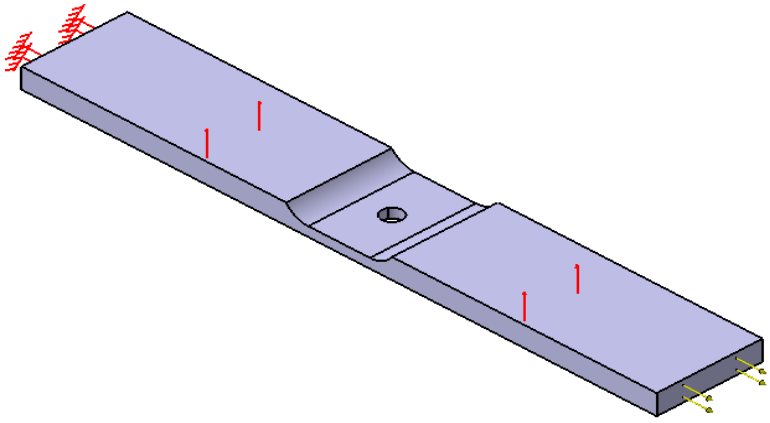

Figure 5.4. Open Hole in Radius Test Specimen -2 Loading and Boundary Conditions

5.5. STRESS CONTOUR PLOTS

The CATIA Generative Structural Analysis solver was used to compute the FEA solutions for all finite element models. The post-processor in the CATIA (GSA) module offers many different options related to the presentation of finite element analysis results. Principal stresses in the spanwise direction of primary loading were used to create all of the contour stress plots. Each stress plot wasoverlaid on the corresponding undeformed mesh. Stress concentration factors and applicable K_t mod factors were derived from this data.

Stress contour plots for the open hole/step finite element analysis are displayed in Figures 5.5-5.10. Results are presented for X call outs of 0.5000, 0.3079, 0.3029, 0.2091 and 0.1000 inches, as defined in the Open Hole in Radius Test Specimen drawing of Appendix A. The X dimension represents the distance between the hole center and tangent point of the radius.

Figure 5.5 shows the principal stress contour plot generated using the CATIA Generative Structural Analysis Workbench for the baseline Open Hole in Radius Test Specimen -1configuration with no holes. A stress concentration factor for the radius itself is obtained from the finite element results of this case. The contour plot of the Open Hole in Radius Test Specimen -1 no holes profile shows that the maximum stress value occurs at the lower tangent point of the radius.

The maximum stress value obtained from the Open Hole in Radius Test Specimen -2 contour plot, shown in Figure 5.6, is used for comparison to stress results obtained for the Open Hole in Radius Test Specimen -3 through -6 models. For a X value of 0.5000 in., the distance between the hole center and radius tangent point is large enough that no K_t interaction occurs between the hole and step. This Open Hole in Radius Test Specimen -2 analysis is therefore treated as a baseline case.

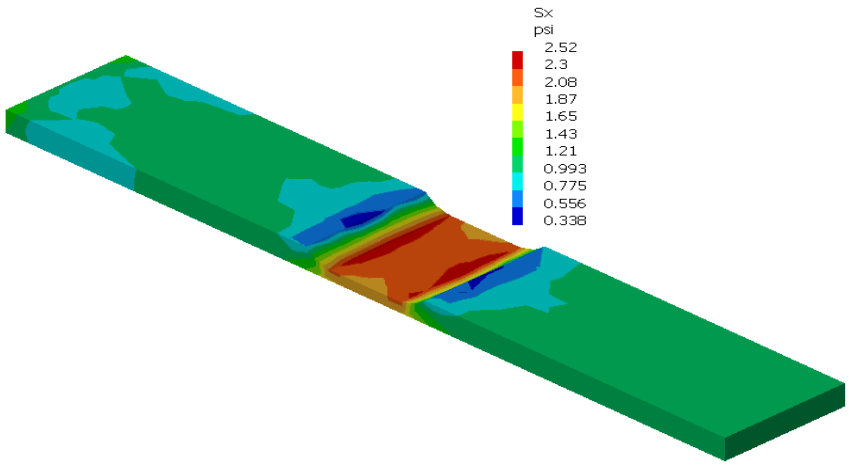

Figure 5.5. Open Hole in Radius Test Specimen -1Stress Contour Plot (No Holes)

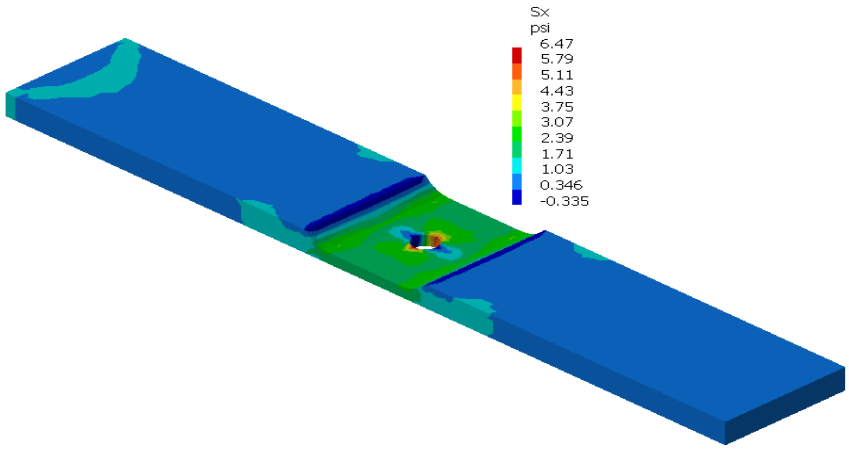

Figure 5.6. Open Hole in Radius Test Specimen -2Stress Contour Plot (X = 0.5000 in.)

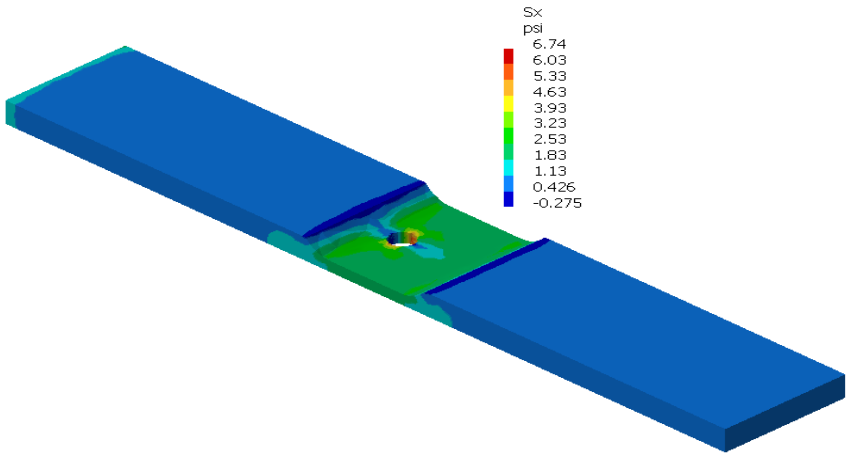

Figure 5.7. Open Hole in Radius Test Specimen -3Stress Contour Plot (X = 0.3079 in.)

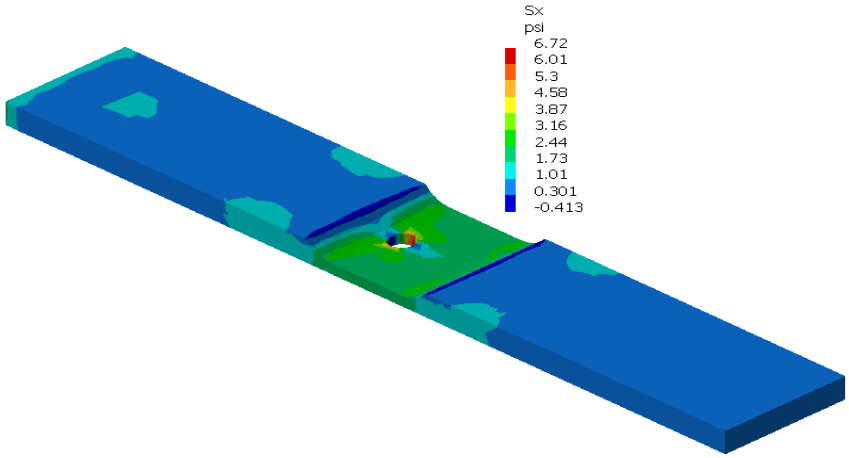

Figure 5.8. Open Hole in Radius Test Specimen -4Stress Contour Plot (X = 0.3029 in.)

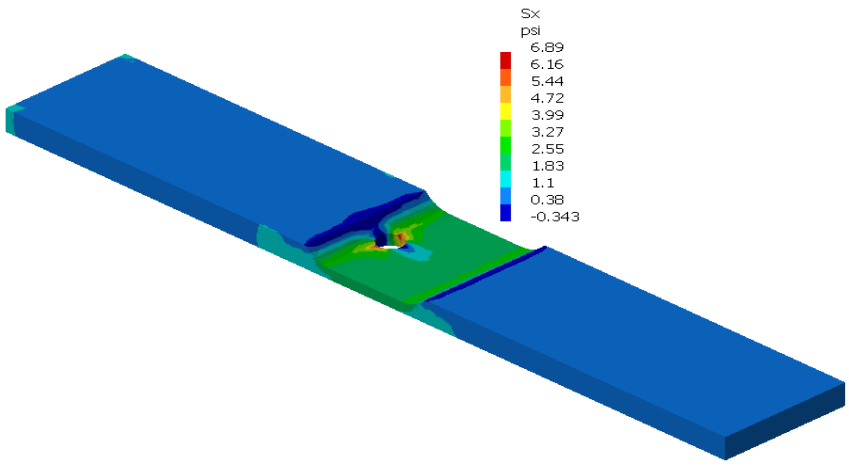

Figure 5.9. Open Hole in Radius Test Specimen -5Stress Contour Plot (X = 0.2091 in.)

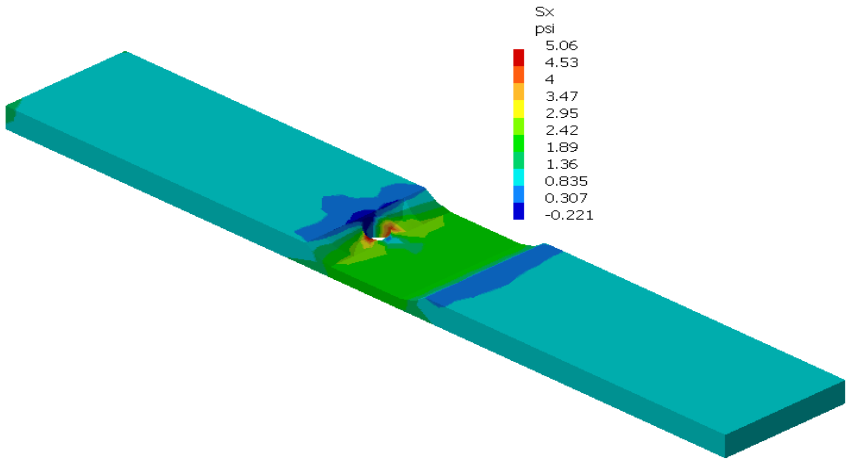

Figure 5.10. Open Hole in Radius Test Specimen -6Stress Contour Plot (X = 0.1000 in.)

A close-up view of the Open Hole in Radius Test Specimen -6stress contour plot, with the maximum stress location identified, is provided in Figure 5.11. Note that the FEA maximum stress occurs at the edge of the hole, just slightly towards the lower tangent of the radius. This indicates a stress concentration interaction between the hole and step. This specific maximum stress location appears to coincide with the fatigue failure of the corresponding test specimen as detailed in Figure 4.12.

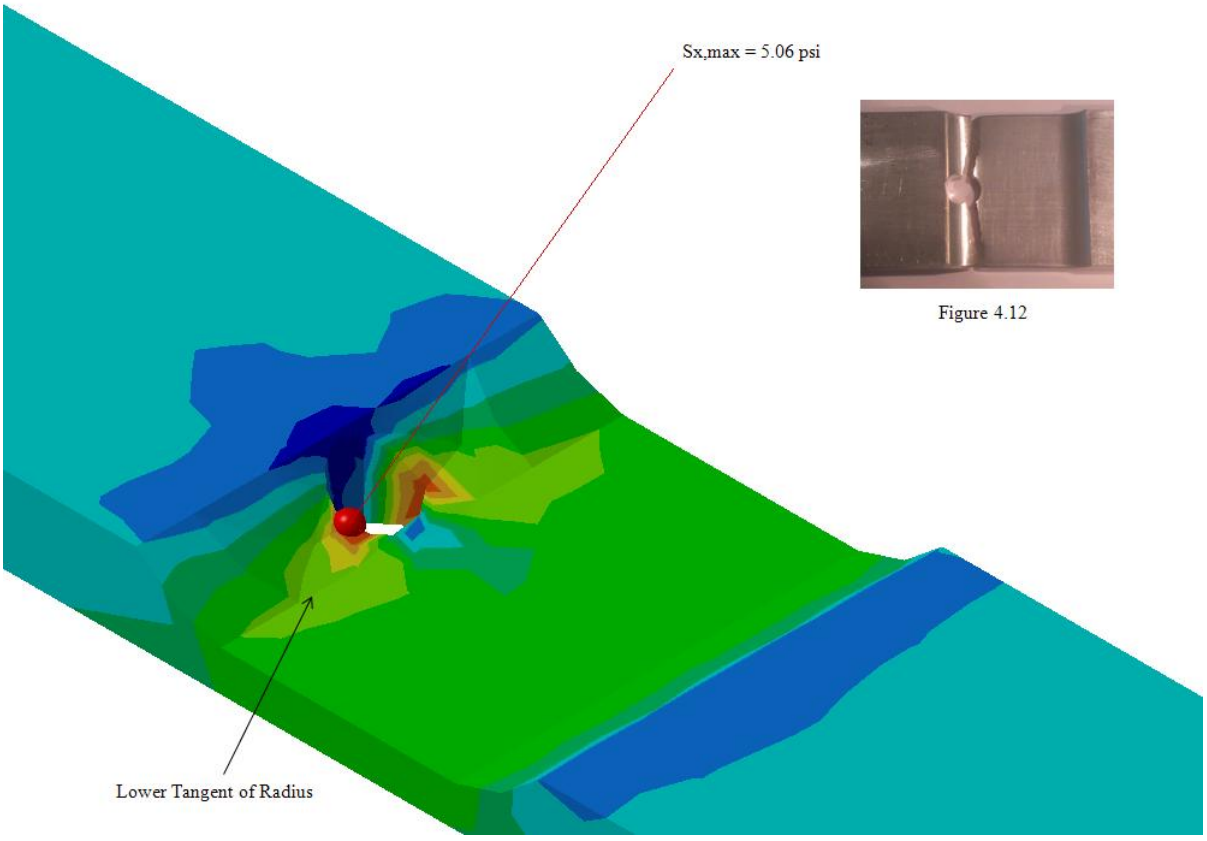

Figure 5.11. Maximum Stress Location for Open Hole in Radius Test Specimen -6

A summary of all stress concentration factors and $K_t$mod factors obtained from the FEM/FEA work is provided. Section 7 contains a comprehensive comparison between the finite element analysis and open hole/step physical fatigue test results.

5.6. ANALYSIS RESULTS INCLUDING DERIVED SCF VALUES

The maximum principal stress values obtained from the FEA results are used to calculate stress concentration factors for each open hole/step configuration. K_t values derived from the finite element analysis runs can be compared to known quantities read from reference stress concentration factor charts with matching geometries and load directions.

Consider the maximum stress value of 2.52 psi obtained from the FEA results of the Open Hole in Radius Test Specimen -1model as shown in Figure 5.5. The gross reference stress in the mid-section of the part is found by dividing the applied stress of 1 psi by the ratio of the mid-section cross-sectional area, A_m, to the end section cross-sectional area, A_e. These cross-sectional area cuts are detailed in Figure 5.12. See the Open Hole in Radius Test Specimen drawing shown in Figure A.1 in Appendix A for specific part geometry details.

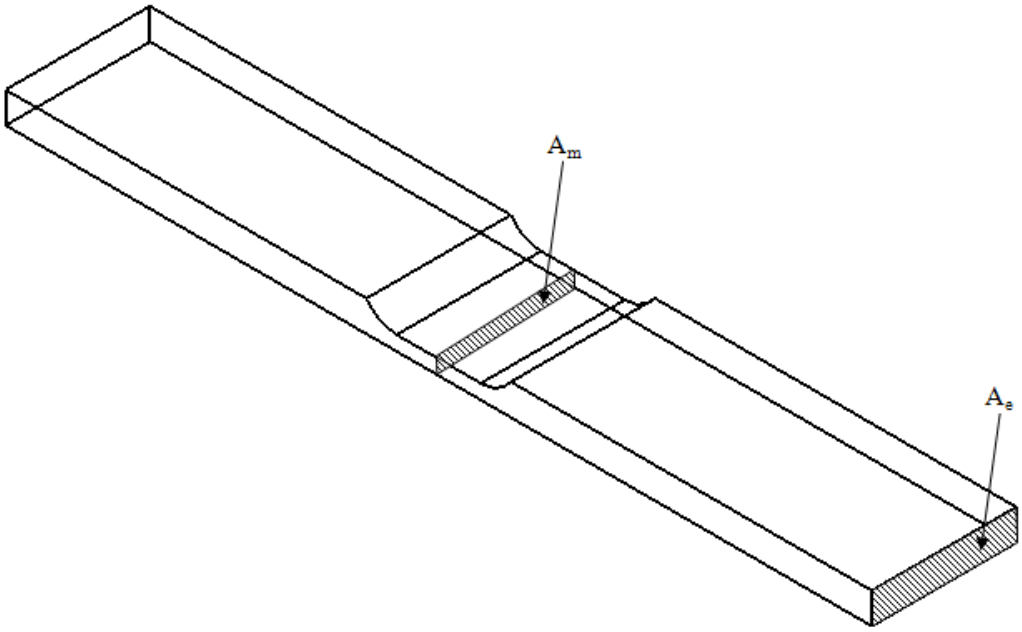

Figure 5.12. Open Hole in Radius Test Specimen -1 Cross-Sectional Area Cuts

The gross reference stress in the mid-section is calculated from Equation (23).

$$\sigma_{ref,gross} = \frac{\sigma_{applied}}{\frac{Am}{Ae}} \tag{23}$$

The stress concentration factor of the radius can be derived from the maximum stress value obtained from the Open Hole in Radius Test Specimen -1 FEA results of Figure 5.5. No net K_t exists for the step only case. The gross stress concentration factor is the only SCF needed for analysis purposes. The K_{tg} of the radius itself is calculated from Equation (10).

$$K_{tg} = \frac{\sigma_{\max}}{\sigma_{ref,gross}} \tag{10}$$

Now consider the Open Hole in Radius Test Specimen -2baseline open hole model. The net stress concentration factor, K_{tn}, which accounts for the presence of the hole, can be derived via application of Equations (10-11). The gross reference stress was previously calculated. The maximum stress for the Open Hole in Radius Test Specimen -2 is taken from the CATIA (GSA) FEA results of Figure 5.6.

$$K_{tn} = K_{tg}\frac{W-D}{W} \tag{11}$$

All of the stress concentration factor values for the open hole configurations are determined using the previously detailed method. The calculated K_{tn} value of 2.47for the Open Hole in Radius Test Specimen -2 configuration can be compared to Peterson [11] for the case of a finite-width thin plate with a circular hole loaded in tension. An equation, (24), that provides the net stress concentration factor for this situation is used to plot the K_{tn} values of in Peterson [11] for various ratios of d/H, where d is the diameter of the hole and H is the width of the plate.

$$K_{tn} = 2 + 0.284(1-\frac{d}{H}) - 0.6(1-\frac{d}{H})^2 + 1.32(1-\frac{d}{H})^3 \tag{24}$$

The net stress concentration factor of 2.47 derived from the FEA through applicationof Equations (10-11) is very close to the K_{tn} value of 2.54 calculated Equation (24). This approximate equality works to confirm and justify the results obtained from the CATIA (GSA) finite element analysis of the open hole/step specimens.

The X call out dimension of 0.5000 inches associated with the Open Hole in Radius Test Specimen -2model is large enough that no stress concentration interaction between the holes and radius exists. Therefore the K_{tn} value calculated from the Open Hole in Radius Test Specimen -2finite element analysis results is used as a baseline for comparison with the remaining open hole models.

Stress concentration factors were also developed for the Open Hole in Radius Test Specimen -3 through -6models, with X call outs of 0.3079 in., 0.3029 in., 0.2091 in. and 0.1000 in., respectively. The net SCFs for these cases, along with the calculation of the associated K_t mod factors used to account for any hole/radius interaction, are provided in Table 5.2.The gross reference stress for the Open Hole in Radius Test Specimen -6 profile is based on the average thickness of the upper and lower sections of the plate, as the hole is positioned directly through the transition section of the radius for this case.

K_t modifaction factors were calculated for the appopriate cases, with holes in close proximity to the tangent point of the radius, by appyling Equation (25). In this equation, the mod factor is found by dividing the SCF of the hole/radius interaction by the K_t value for the Open Hole in Radius Test Specimen -2baseline open hole model. These modification factors are denoted with the symbol K_{tf}.

$$K_{tf} = \frac{K_{t,\text{interaction}}}{K_{t,baseline}} \tag{25}$$

A summary of the stress concentration factors and K_t mod factors developed from the CATIA Generative Structural Analysis FEA results is provided in Table 5.2. The modification factors used to account for any stress concentration interaction between the holes and radii are denoted with the symbol K_{tf}. Results are presented for each model analyzed as part of this study on interacting SCFs.

Table 5.2. Finite Element Analysis SCFs and K_t Mod Factors

Model	K_t	K_{tf}
Open Hole in Radius Test Specimen -1	1.18	NA
Open Hole in Radius Test Specimen -2	2.47	NA
Open Hole in Radius Test Specimen -3	2.57	1.04
Open Hole in Radius Test Specimen -4	2.56	1.04
Open Hole in Radius Test Specimen -5	2.63	1.07
Open Hole in Radius Test Specimen -6	3.02	1.22

Section 7 contains a comprehensive discussion and interpretation of all mod factors derived from the FEA results. The stress concentration modification factors originating from the finite element analysis work are compared to those of the open hole

testing, as presented in Table 4.10. Examples of how these K_{tf} values can be applied in a detailed fatigue analysis are provided in Section 6.

6. FATIGUE ANALYSIS

The main purpose of the development of the K_t mod factors, by means of the physical fatigue testing detailed in Section 4 and the finite element modeling/analysis presented in Section 5, is the use of these factors in the fatigue analysis of metallic aerostructure components. Accurate stress concentration factors for any particular instance of geometry and loading studied are essential to a properly conducted fatigue analysis.

Many different methods and tools are available for use by fatigue analysts and engineers to assist with the prediction of fatigue life for an individual detail or component. Various software tools and packages which can be used to conduct a detailed fatigue analysis for a wide range of geometric features and joints are available for commercial and academic use. Many of these applications have an obvious focus on aerostructure-type components, however, a large number of different inputs are often available to the user, making some programs flexible enough to assist with an accurate assessment of non-aerospace fatigue problems as well.

A typical fatigue analysis includes selection of a detail type such as a notch, open hole, fastened joint or lug. Geometric variables associated with the particular detail type being looked at, including hole diameter, edge distance, notch radius, etc., are crucial to an accurate fatigue life prediction. A loading spectrum must be considered. This cyclical loading can be constant amplitude or variable amplitude in nature. Other parameters related to the joint type and geometry of the detail being analyzed, including part thickness, fastener fit condition and fastener type, are often used in the analysis. Analysts

performing fatigue life predictions must also account for a material with a known, accurate set of associated material properties.

Material S-N curves that allow analysts and engineers to predict fatigue lifetimes are also readily available. The equivalent stress fatigue life method, as defined in MMPDS-03 [46], can be used to calculate the fatigue life of a certain detail for a given set of material, geometric and loading parameters. Equations (18) and (19) can be used to apply the equivalent stress fatigue life method for a known stress ratio, R, and maximum stress. The equivalent stress model consolidates the S-N curves for various R values of a particular material and stress concentration factor in to the single relationship given by Equation (18). In this formula, A_1, A_2, A_3 and A_4 are known coefficients based on material type and K_t. The fatigue life, N, can easily been determined from Equation (26).

$$\log N = A_1 + A_2 \log (S_{eq} - A_4) \tag{18}$$

$$S_{eq} = S_{max} (1 - R)^{A_3} \tag{19}$$

$$N = 10^{\left(A_1 + A_2 \log(S_{eq} - A_4)\right)} \tag{26}$$

The A_1, A_2, A_3 and A_4 coefficients for each MMPDS-03 [46] equivalent stress life equation used in the fatigue analysis conducted as part of this research are summarized in Table 6.1.

Table 6.1. Equivalent Stress Life Equation Coefficents

S-N Curve [87]	A_1	A_2	A_3	A_4
2024-T3, sheet, $K_t = 2.0$	9.20	-3.33	0.68	12.3
7075-T6, sheet, $K_t = 2.0$	7.50	-2.46	0.54	18.6
7075-T6, sheet, $K_t = 1.5$	10.2	-4.63	0.51	5.30

A fatigue margin of safety can be computed by comparing the allowable stress level for a defined number of cyclesto theequivalent stress value for an applied fatigue spectrum. Thepre-set number of cycles is derived from a design service objective (DSO). DSO is also sometimes referred to as DSG, design service goal, or DLG, design life goal. This design goal is defined in the aerospace industry as a service period in which the primary structure of the aircraft is designed to be free of detectable fatigue cracking. The DSO is normally divided by a safety factor, also called a scatter factor (SF), that accounts for the standard deviation in fatigue test data used to build the S-N curve. In practice, a scatter factor with a value between 3 and 8 is commonly used. The fatigue safety margin (MS) can be calculated by applying Equations (27-29).

$$N_{allowable} = \frac{DSO}{SF} \tag{27}$$

$$S_{allowable} = 10^{\left(\frac{-A_1 + \log N_{allowable}}{A_2}\right)} + A_4 \tag{28}$$

$$MS = \frac{S_{allowable}}{S_{eq}} - 1 \tag{29}$$

Equations (27-29) were used to calculate fatigue safety margins, considering a pre-defined design service objective and scatter factor, for the open hole and joint assembly specimens analyzed as part of this study.

6.1. APPLICATION OF SCFs AND K_t MOD FACTORS

The stress concentration factors and SCF modification factors derived from the open hole/step and joint test results of Section 4 as well as the FEM/FEA results of Section 5 can be used in a detailed fatigue analysis of holes placed at or near a radius. Fatigue lifetimes and corresponding fatigue margins of safety are calculated using the relationships of Equations (18-19) and (26-29).

Solutions found using the K_t interaction formulas of Equations (12-14) are compared in order to illustrate the level of conservatism and accuracy of these methods with respect to one another. The fatigue analysis results derived from the interaction equations are also compared to the results of the testing and finite element analysis.

It is generally determined what direct effect the applied stress concentration modification factors have on the fatigue lives and fatigue safety margins of critical hole/step interaction details. The method of analysis used here can be adopted by fatigue engineers to correctly account for K_t mod factors, not only for cases of holes placed at or near a radius, but for any typical instance of combined stress concentration factors.

6.1.1. Open Hole/Step Fatigue Analysis. For the Open Hole in Radius Test Specimen -2 configuration, with an X callout of 0.5000 inches that serves as a baseline for the remaining open hole profile types, a constant amplitude spectrum is applied. The maximum spectrum stress of 25 ksi and stress ratio of 0.06 are taken from Table 4.4 for the DW-OH-5000-3 specimen.

Using the net stress concentration factor of 2.47 calculated from the finite element analysis results for the Open Hole in Radius Test Specimen -2 , a baseline fatigue life can be determined from Equations (19) and (26). The equivalent stress equation for 2024-T3 aluminum sheet with a K_t of 2.0 from MMPDS-03 [46] is used in this determination. The maximum stress is increased by a ratio equal to the SCF of the -2 specimen divided by a stress concentration factor of 2.0.

The calculated fatigue life of 119483 cycles for the Open Hole in Radius Test Specimen -2 profile, found using the equivalent stress equation of the 2024-T3 S-N curve, is very close to the characteristic life of 117897 for the DW-OH-5000-1 thru 3 test specimens as presented in Table 4.10.

The equivalent stress fatigue life can be used to determine a fatigue margin of safety via application of Equations (27-29). A typical design service objective (DSO) of 40,000 flight cycles is considered. In the aerospace industry, the DSO is a pre-defined value associated with a particular aircraft that is usually specified in units of flight cycles, flight hours or flights.

A scatter factor (SF) of 4 is used in the fatigue MS calculation. This is a value commonly applied in the aerospace industry for fatigue analysis. A scatter factor is needed to account for the inherent scatter in the testing used to generate S-N data. In

practice, this factor can be influenced by many different factors including, but not necessarily limited to, material type, part production, fatigue loading and environment. Proper fatigue testing should make every effort to manage, reduce or eliminate scatter in any form. Engineering judgment and experience can play a critical role in the selection of an appropriate scatter factor.

The fatigue margin of safety for the DW-OH-5000 baseline case can be used as a comparison point for fatigue margins calculated from the interacting stress concentration factor relationships of Equations (12-14).

The open hole/step fatigue analysis results, found by applying the three K_t interaction relationships of Equations (12-14), are presented in Table 6.2. Recall the DSO was set at 40,000 flight cycles and the scatter factor at 4. Results for the open hole/step profiles are based on a constant amplitude applied spectrum with a maximum stress of 25 ksi and stress ratio of 0.06. A full discussion of the open hole/step fatigue analysis results for all interaction methods is contained in Section 7.

Table 6.2. Open Hole/Step Fatigue Analysis Results

S-N Curve [87]	Equation	S_{eq} (ksi)	N (cycles)	MS
2024-T3, sheet $K_t = 2.0$	Baseline K_t	29.6	119483	0.65
	$K_{t1,2} = K_{t1} \cdot K_{t2}$ (12)	34.9	49242	0.40
	$K_{t1,2} = \sqrt{K_{t1}^{\ 2} + K_{t2}^{\ 2}}$ (13)	32.8	67472	0.48
	$K_{t1,2} = K_{t1}\sqrt{K_{t2}}$, where $K_{t1} \geq K_{t2}$ (14)	32.1	75974	0.52

6.1.2. Joint Fatigue Analysis

6.1.2.1. Low load transfer bolt in radius fatigue analysis . A detailed fatigue analysis was performed for the low load transfer bolt in radius specimens. The stress concentration modification factors developedfrom the joint assembly testing in Section 4 were used in the analysis. Equivalent stresses, fatigue lifetimes and corresponding margins of safety were determined.

The DB-182 profile type acts as a baseline for the remaining low load transfer dogbone specimen configurations. The distance of 0.182 inches between the hole center and lower tangent point of the radius for the DB-182 specimen configuration is large enough that no K_t interaction between the hole and radius occurs. The collar installation is per design with the collar sitting flat upon the part surface. A constant amplitude spectrum is again applied in the fatigue analysis. The maximum spectrum stress of 20 ksi and stress ratio of 0.06 are taken from fatigue test stresses for the low load transfer dogbone specimens, as shown in Table 4.6.

The Peterson [11] chart for the case of a finite-width thin plate with a circular hole loaded in tension is used to determine the net stress concentration factor for the holes of the DB-182 specimen. Equation (24) is applied to the geometry of the Fatigue Dogbone Bolt in Radius - Part B drawing shown in Figure A.4 of Appendix A in order to calculate the baseline K_{tn} for the low load transfer dogbone configurations. Figure A.4 gives a hole diameter, d, of 0.1875 inches and a plate width, H, of 0.938 inches.

$$K_{tn} = 2 + 0.284(1 - \frac{d}{H}) - 0.6(1 - \frac{d}{H})^2 + 1.32(1 - \frac{d}{H})^3 \quad (24)$$

Additional factors used to account for the hole and fit condition for the joint specimen are applied to the baseline net stress concentration factor found using the Peterson [11] chart. From the Severity Factor (SF) method presented in Niu [48], a reamed hole condition factor of 0.9 and conservative bolt hole filling factor of 0.9 are used in the calculation of a modified, fastened joint SCF.

A baseline fatigue life for the low load transfer specimen types can now be derived from Equations (19) and (26). 7075 aluminum plate material was used to fabricate the parts for all of the joint assembly testing. Therefore, the equivalent stress equation for 7075-T6 aluminum sheet with a K_t of 2.0 from MMPDS-03 [46] is used to calculate the predicted fatigue life from the spectrum stress values. The maximum stress of 20 ksi is increased by a ratio equal to the K_{tn} value for the DB-182 low load transfer dogbone specimen type divided by a stress concentration factor of 2.0.

A fatigue margin of safety for the DB-182 baseline case was determined from Equations (27-29). In this instance, the design service objective is set at 75,000 flight cycles while a scatter factor of 4 is again used.

The fatigue safety margin for the DB-182 profile is used for comparison to fatigue margins for the DB-100 and DB-050 specimen types with holes near radii. Recall from the testing information of Section 4 that proper collar installation is not possible for the DB-100 and DB-050 specimens due to the close proximity of the holes and nearby steps.

The SCF mod factors from Table 4.12 are applied using the K_t interaction method of Equation (12). This is the method customarily chosen for application of K_{tf} modication factors. For the DB-100 fatigue analysis, the baseline stress concentration factor of 2.04 is multiplied by a SCF mod factor of 1.07.

This DB-100 stress concentration factor can be used to calculate a corresponding equivalent stress and fatigue life from the equivalent stress equation of MMPDS-03 [46] for 7075-T6 aluminum sheet with a K_t of 2.0. A significant reduction in fatigue life was observed, from 23,429,629 cycles for the baseline analysis to 3,373,519 cycles for the DB-100 fatigue analysis, with the SCF mod factor applied.

The DB-100 equivalent stress is used to determine a resulting fatigue margin of safety. The DSO of 75,000 cycles and scatter factor of 4 are used throughout the joint fatigue analysis. It was determined that this design service objective and scatter factor correspond to an allowable stress of 39.1 ksi the 7075 aluminum material.

A fatigue analysis was also performed on the DB-050 configuration, using a K_{tf} value of 1.12 from Table 4.12. Thefastened joint SCF from the severity factor method for the low load transfer dogbone specimen is multiplied by the modification factor in order to find a combined $K_{t1,2}$ value.An equivalent stress level and fatigue life for the DB-050 case were calculated using this combined stress concentration factor in the equivalent stress model.A DS-050 fatigue safety margin wascalculated using the previously determined equivalent stress and allowable stress in Equation (29).

Fatigue analysis results for the five fastener low load transfer dogbone specimen types are provided in Table 6.3. The equivalent stresses, predicted cycles to failure and fatigue margins shown are valid for a design service objective of 75,000 flight cycles with a scatter factor of 4. A constant amplitudespectrum with a maximum stress of 20 ksi and R value of 0.06 was applied.

Table 6.3. Low Load Transfer Dogbone Fatigue Analysis Results

S-N Curve [87]	Specimen Type	K_{tf}	S_{eq} (ksi)	N (cycles)	MS
7075-T6, sheet $K_t = 2.0$	DB-182	NA	19.7	23429629	0.98
	DB-100	1.07	21.1	3373519	0.85
	DB-050	1.12	22.1	1453610	0.77

6.1.2.2. Eight fastener double shear bolt in radius fatigue analysis. Fatigue analysis was performed for the eight fastener double shear bolt in radius configuration. Stress concentration modification factors developedfrom the joint testing of Section 4 were applied. The effects of these mod factors on equivalent stress levels, cycles to failure and fatigue safety margins are shown.

The DS-182 specimen type serves as a baseline for the othereight fastener double shear profile types. A constant amplitude spectrum with a maximum stress of 18 ksi and stress ratio of 0.06 is used in the analysis. These values match the fatigue test stress valuesfor the eight fastener double shear specimens givenin Table 4.8.

Equation (24) is again used to determine the baseline stress concentration factor for the double shear bolt in radius specimens. Due to the row symmetry of this configuration, half of the plate width from the Figure A.7. 8 Fastener Double Shear Bolt in Radius -Part D drawing of Appendix A is considered in this calculation. A hole diameter, d, of 0.1875 inches is used for all holes drilled as part of this research.

The same reamed hole and bolt fit condition factors applied for the low load transfer dogbone joint fatigue analysis are utilized for the double shear case. An additional bearing distribution correction factor of 0.95 is considered to account for the

double shear joint type. Given the same loading and geometry conditions, a double shear joint will typically have a lower effective SCF compared to a single shear assembly such as the five fastener low load transfer specimens. These extra factors are applied to the baseline DS-182 net stress concentration factor derived from Equation (24) to determine a severity factor method, fastened joint SCF.

Equations (19) and (26) can be used to derive a fatigue life for the baseline DS-182 specimen type. The equivalent stress equation for 7075-T6 aluminum sheet with a K_t of 1.5 from MMPDS-03 [46] is needed to calculate this double shear joint fatigue life. The maximum spectrum stress of 18 ksi and stress ratio of 0.06 from Table 4.8 are applied. The double shear, fastened joint severity factor method SCF of 1.87wasused in the equivalent stress equation.

A baseline fatigue safety margin for the double shear joint type was determined from Equations (27-29). A design service objective (DSO)of 75,000 flight cycles with a scatter factor of 4was considered.

Equation (12) was used to apply the SCF mod factor for the DS-100 and DS-050 interaction cases from from Table 4.14. Both interaction specimen groups for the double shear profile types were found to have the same K_{tf} value of 1.08. The baseline, double shear stress concentration factor of 1.87 was multiplied by K_{tf}.

The equivalent stress equation from MMPDS-03 [46] for 7075-T6 aluminum sheet with a K_t of 1.5was applied in order to determine an equivalent stress and fatigue life for the DS-100 and DS-050 bolt in radius, interaction cases.

A fatigue safety margin for the double shear interaction cases was determined from the corresponding equivalent stress value and allowable stress level. Recall that the

allowable stress of 50.1 ksi for the double shear specimen types is based on 7075 material S-N data and a design service objective of 75,000 cycles with a scatter factor of 4.

The results of the eight fastener double shear joint fatigue analysis are shown in Table 6.4. The values given in this table correspond to pre-defined design service objective of 75,000 flight cycles with a scatter factor of 4. A constant amplitude spectrum with a maximum stress of 18 ksi and R value of 0.06 was considered in the analysis.

Table 6.4. Eight Fastener Double Shear Fatigue Analysis Results

S-N Curve [87]	Specimen Type	K_{tf}	S_{eq} (ksi)	N (cycles)	MS
7075-T6, sheet $K_t = 1.5$	DS-182	NA	21.8	66887661	1.30
	DS-100/DS-050	1.08	23.5	13706054	1.13

6.2. FRACTURE SURFACES

High resolution pictures were taken under a microscope of the fatigue fracture surfaces for the representative DS-050-1 and DS-100-2 broken test specimens. The fracture surfaces observed for these particular samples are typical of all of the cracked low load transfer dogbone and eight fastener double shear specimens. Images of the fracture surfaces at 30 times magnification are shown in Figures 6.1 and 6.3, while pictures at 50 times magnification are provided in Figures 6.2 and 6.4. A dimensional scale of 0.100 inches is given in the upper right hand corner of the photos.

All of the fracture surfaces tested as a part of this study exhibited signs of classic fatigue failure, with successive crack front propagation from cyclical loading. When examining the cracked test specimens, it is important to be able to distinguish between the characteristics that define the fatigue surfaces and those traits that are indicative of the portion of the surface face broken after the testing was completed in order to separate the part.

It is evident that the fatigue cracks propagated from the edges of the holes at the locations of the peak stresses. The banding outward from the hole edges can be easily observed in Figures 6.1 and 6.2. The fatigue cracking of the joint test specimens can be described as transgranular, while the cracking of the stress corrosion specimen is intergranular. For a typical fatigue surface, the rough region represents brittle failure, while the smooth part of the surface indicates crack propagation. Striations can be used to meausre the amount of crack growth per load cycle. Fatigue zones and rupture zones are characteristic of fatigue fracture surfaces. The striations are observered in the fatigue, or slow fracture, zone as the crack grows. Final failure occurs in the rupture, or fast fracture, zone which shows signs of brittle fracture, in most cases.

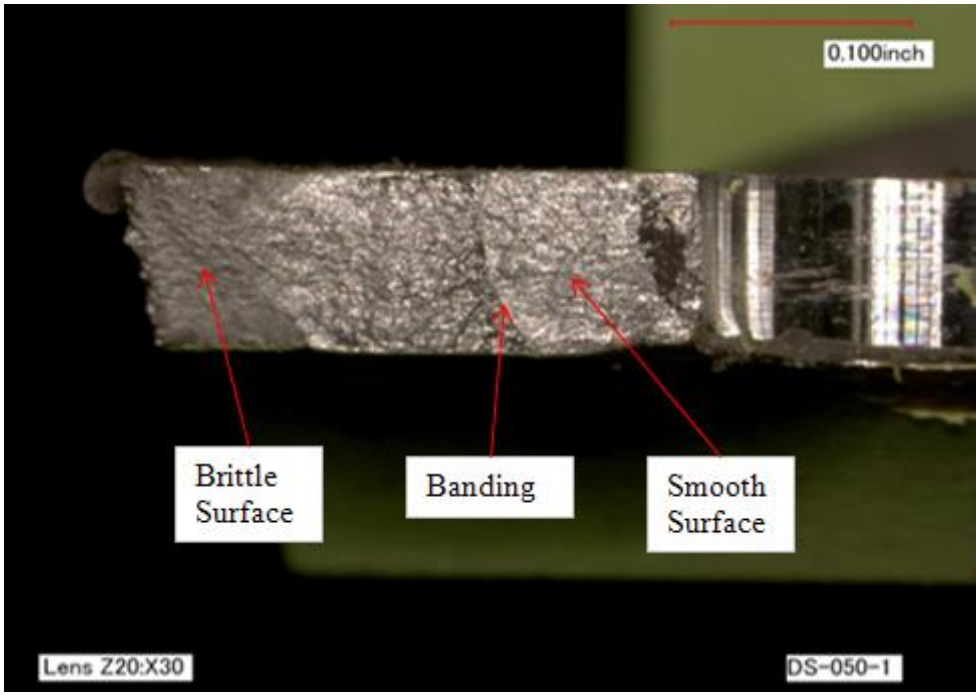

Figure 6.1. DS-050-1 Fatigue Fracture Surface (X30)

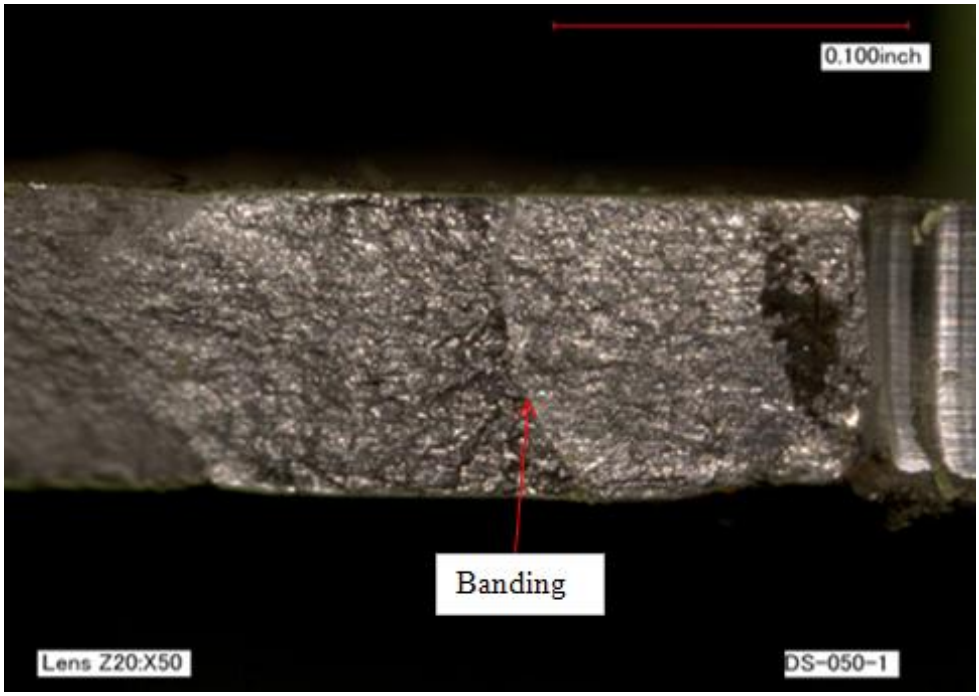

Figure 6.2. DS-050-1 Fatigue Fracture Surface (X50)

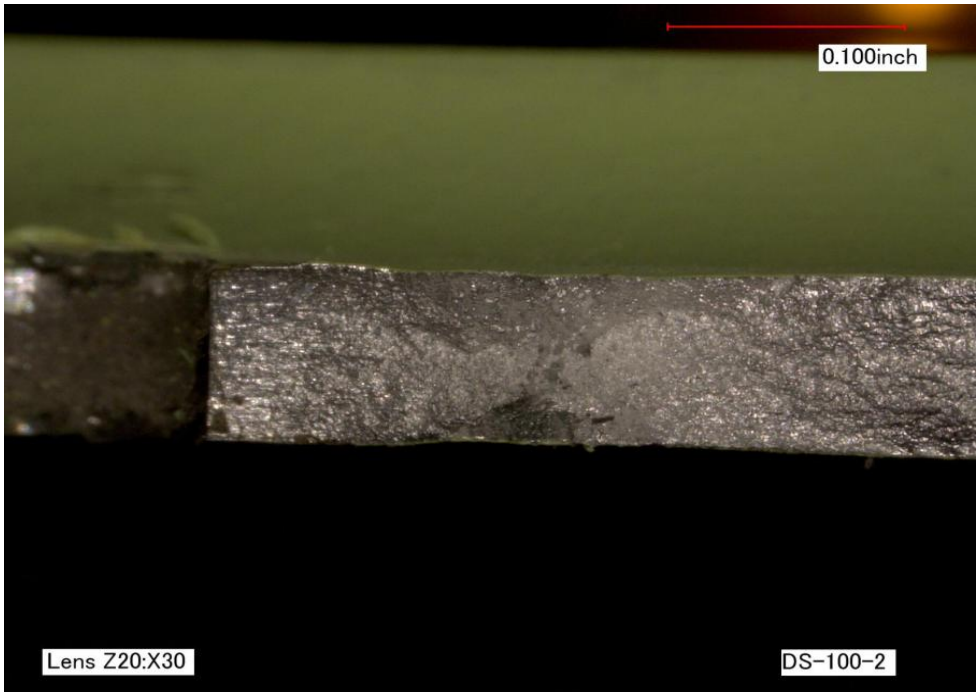

Figure 6.3. DS-100-2 Fatigue Fracture Surface (X30)

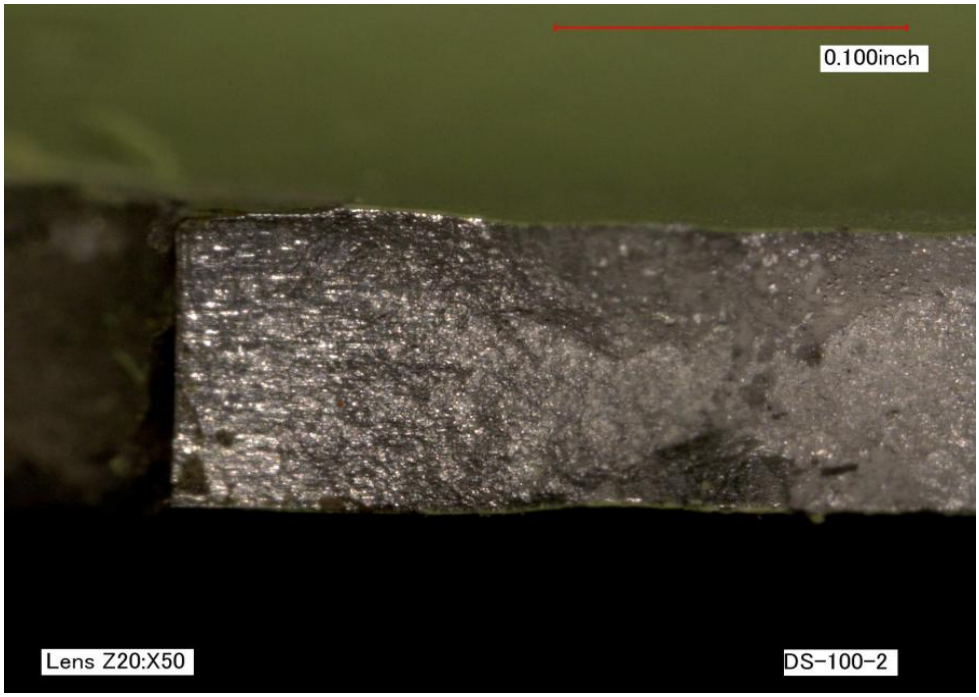

Figure 6.4. DS-100-2 Fatigue Fracture Surface (X50)

7. DISCUSSION AND CONCLUSIONS

A comprehensive summary and discussion of all conclusions drawn from this research study is provided within this section. Full interpretations of the fatigue testing results of Section 4 and finite element modeling/analysis results of Section 5 are given. The findings of the physical testing versus FEM/FEA for the open hole/step configurations are compared. The fatigue analysis results for the open hole/step and joint assembly specimens from Section 6 are explained in detail. Fatigue margins of safety derived from the multiplication, root sum squares and multiplication/square root K_t interaction relationships of Equations (12), (13) and (14) are summarized and assessed.

The overall goal of this research was the development of stress concentration modification factors for instances of hole/radius K_t interaction. The term mod factor was used primarily throughout this paper, mod being a shorthand term for modification. Other terms including, K_t correction factors, adjustment factors, fudge factors, extra factors and K_t coefficients are commonly associated with these applied values.

The mod factors derived for each analyzed instance of K_t interaction are summarized. The recommended application of these mod factors is fully explained. Tables and charts displaying the mod factor values for each specimen group are shown. Effects of the X dimension, the distance from the hole center to radius tangent, on the K_t modification factors are noted. The most conservative factors areadvised to be used in fatigue analysis for hole/radius interference cases.

A number of explicit recommendations for additional research in the area of stress concentration factor interaction of metallic structures, specifically related to hole/radius K_t interaction, are outlined.

7.1. INTERPRETATION OF TESTING AND FEM/FEA RESULTS

All stress concentration modification factors derived from the physical fatigue testing and finite element modeling/analysis results are presented in Table 7.1. An individual mod factor was determined for each open hole/step and joint assembly hole in radius specimen group. No K_{tf} is applicable for the baseline configurations.

Table 7.1. Fatigue Testing and FEA Mod Factors

	Specimen Group	K_{tf}
Testing	DW-RKt-1 thru 5	NA
	DW-OH-5000-1 thru 3	NA
	DW-OH-3079-1 thru 4	1.01
	DW-OH-3029-1 thru 4	1.00
	DW-OH-2091-1 thru 4	1.02
	DW-OH-1000-1 thru 4	1.15
	DB-182-1 thru 4	NA
	DB-100-1 thru 4	1.07
	DB-100-5 thru 8	NA
	DB-050-1 thru 4	1.12
	DS-182-1 thru 4	NA
	DS-100-1 thru 4	1.08
	DS-100-5 thru 8	NA
	DS-050-1 thru 4	1.08
FEA	Open Hole in Radius Test Specimen -1	NA
	Open Hole in Radius Test Specimen -2	NA
	Open Hole in Radius Test Specimen -3	1.04
	Open Hole in Radius Test Specimen -4	1.04
	Open Hole in Radius Test Specimen -5	1.07
	Open Hole in Radius Test Specimen -6	1.22

The SCF modification factors for the open hole and joint/assembly specimens are shown in the graphs of Figure 7.1. K_{tf} values are plotted versus a ratio equal to the hole diameter divided by the X dimension, which is the distance from the center of the hole to the radius tangent.

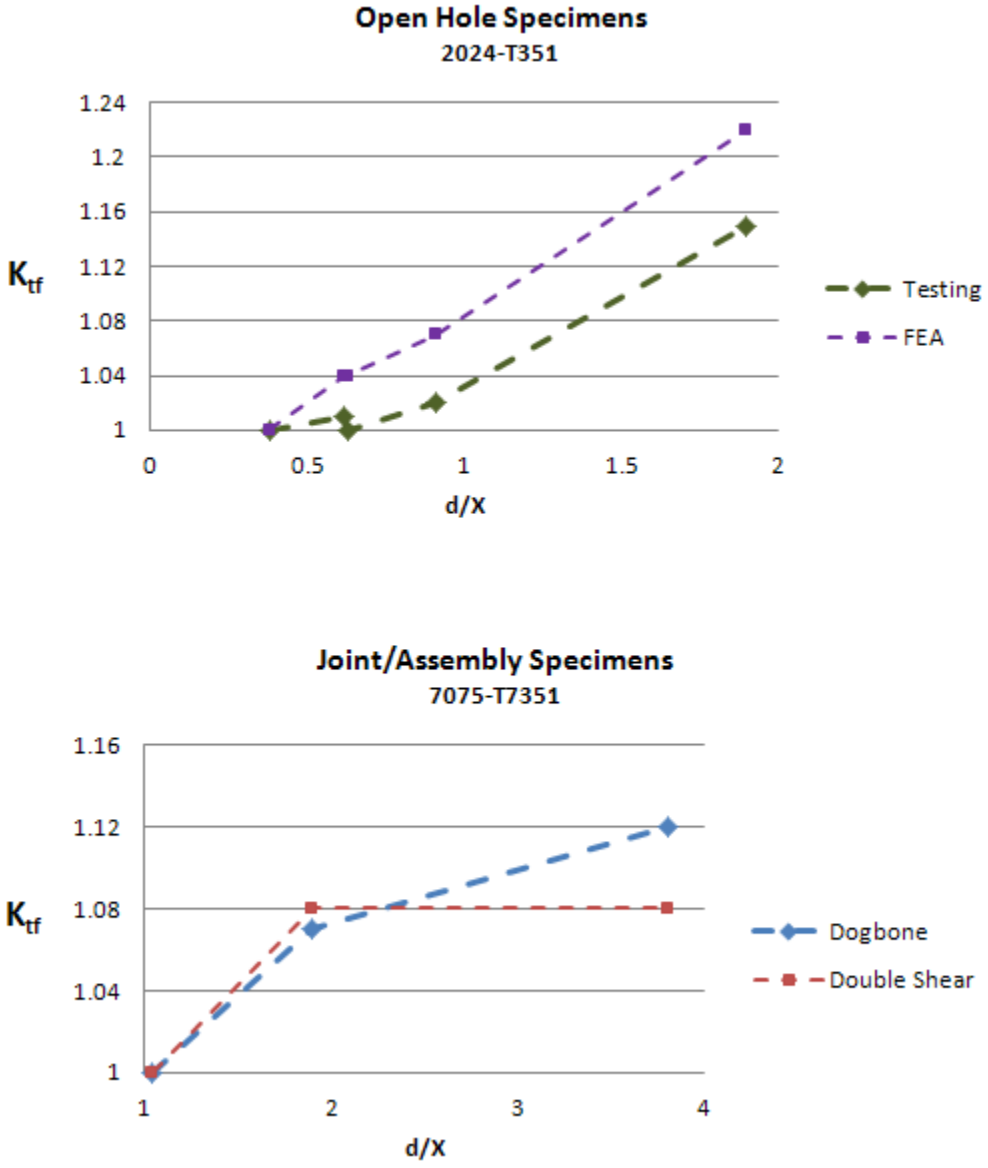

Figure 7.1. Open Hole and Joint/Assembly Mod Factor Plots

Conclusions can be drawn from the stress concentration modification factor data presented in Table 7.1 and Figure 7.1. It can be stated that for the fatigue testing, mod factors are not applicable for the step only and baseline DW-RKt-1 thru 5, DW-OH-5000-1 thru 3, DB-182-1 thru 4 and DS-182-1 thru 4 specimen groups. For the finite

element analysis, mod factors are not applicable for the step only and baseline Open Hole in Radius Test Specimen -1 and Open Hole in Radius Test Specimen -2 configurations.

It is observed from the physical test results that generally little to no interaction occurs for the DW-OH-3079-1 thru 4 and DW-OH-3029-1 thru 4 specimen groups with final K_{tf} values less than or equal to 1.01. Recall that for these two groups, the holes are placed slightly away from, or just touching, the radius tangent. Some minor interaction is indicated by the K_{tf} value of 1.02 for the DW-OH-2091-1 thru 4 coupons, with holes centered on the radius. The stress concentration modification factor of 1.15 calculated for the DW-OH-1000-1 thru 4 specimen types indicates a definite Kt interaction between the hole and radius for this particular combination of geometry and loading with the hole being drilled directly through the slope of the radius. See the test specimen drawings of Appendix A for detailed dimensional information on the individual part configurations.

The stress concentration modification factors derived from the finite element modeling/analysis of the open hole/step profiles tended to be slightly higher than those calculated from the physical testing for each corresponding specimen type. The geometric dimensions of the finite element models exactly matched the geometric dimensions for each open hole/step specimen group. The slight difference in modification factor results between the physical testing and FEM/FEA work may be partially attributed to a variance in the type of applied loading. For the testing, fatigue loading was applied while a constant stress level was used for the finite element analysis.

Mod factors are also not required for the DB-100-5 thru 8 and DS-100-5 thru 8 specimen groups that incorporated the use of radius blocks. The characteristic fatigue lives for these groups were found to be higher than the characteristic fatigue lives of the

corresponding dogbone and double shear baseline bolt in radius profiles. The joint/assembly fatigue data related to the use of the radius blocks illustrates the importance of typical repair measures for situations of bolt holes and collars at or near a radius. Proper fastener fit and installation are critical to the level of fatigue performance of any fastened joint with metallic components.

7.2. INTERPRETATION OF FATIGUE ANALYSIS RESULTS

The fatigue analysis results of Section 6 are summarized in Tables 7.2 and 7.3. The open hole fatigue margins of safety are based on a DSO of 40,000 flight cycles with a scatter factor equal to 4 while the joint assembly fatigue margins of safety are associated with a DSO of 75,000 flight cycles with a scatter factor of 4. For the open hole cases, a constant amplitude spectrum with a maximum stress of 25 ksi was considered. Maximum spectrum stresses of 20 ksi and 18 ksi were applied, respectively, in the dogbone and double shear joint assembly fatigue analysis. A stress ratio, R, of 0.06 was used in all instances.

Table 7.2. Open Hole Fatigue Analysis Results

S-N Curve [87]	Equation	S_{eq} (ksi)	N (cycles)	MS
2024-T3, sheet $K_t = 2.0$	Baseline K_t	29.6	119483	0.65
	$K_{t1,2} = K_{t1} \cdot K_{t2}$ (12)	34.9	49242	0.40
	$K_{t1,2} = \sqrt{K_{t1}^{\,2} + K_{t2}^{\,2}}$ (13)	32.8	67472	0.48
	$K_{t1,2} = K_{t1}\sqrt{K_{t2}}$, where $K_{t1} \geq K_{t2}$ (14)	32.1	75974	0.52

Table 7.3. Joint Assembly Fatigue Analysis Results

S-N Curve [87]	Specimen Type	K_{tf}	S_{eq} (ksi)	N (cycles)	MS
7075-T6, sheet $K_t = 2.0$	DB-182	NA	19.7	23429629	0.98
	DB-100	1.07	21.1	3373519	0.85
	DB-050	1.12	22.1	1453610	0.77
7075-T6, sheet $K_t = 1.5$	DS-182	NA	21.8	66887661	1.30
	DB-100/DS-050	1.08	23.5	13706054	1.13

The fatigue analysis results are shown in the graphs of Figure 7.2. For the open hole specimens, fatigue margins of safety are plotted versus the combined stress concentration factor, $K_{t1,2}$, values derived from the K_t interaction relationships of Equations (12-14). The joint assembly fatigue safety margins are plotted versus the stress concentration modification factor, K_{tf}, values.

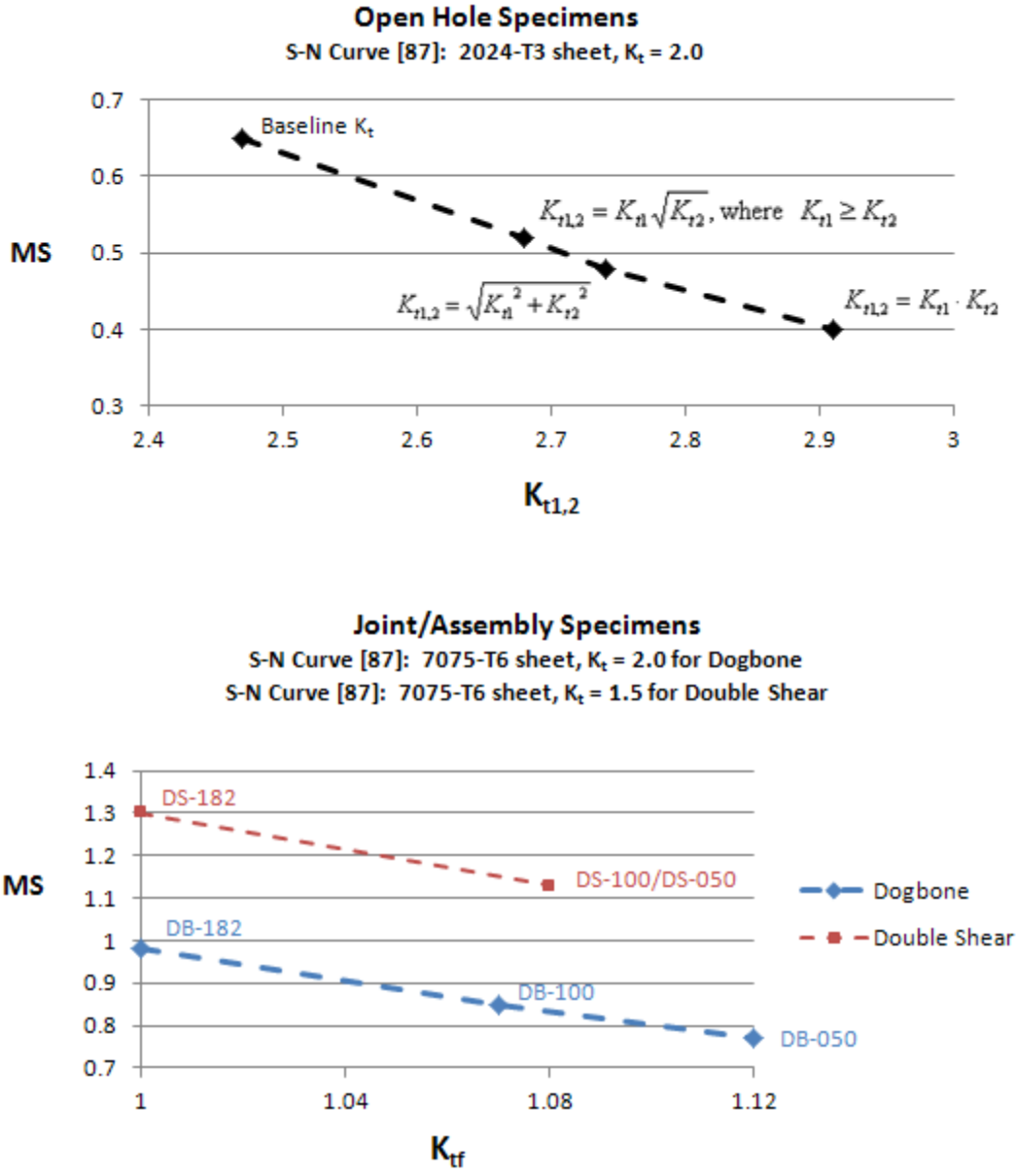

Figure 7.2. Open Hole and Joint/Assembly Fatigue Analysis Results

The fatigue analysis results indicate that the fatigue margins decrease proportionally to an increase in the combined $K_{t1,2}$ value for the open hole specimens or an increase in the applied K_{tf} stress concentration modification factor values for the joint assembly profile types.

The number of cycles to failure calculated for the baseline open hole specimen type was very close to the corresponding final failure cycle count observed in the physical fatigue testing. This approximate equality in fatigue life between the analysis and test results substantiates the calculated fatigue safety margins and fatigue lifetimes.

For the open hole specimens, the fatigue lives were derivedfrom the equivalent stress equation for 2024-T3 aluminum sheet with a K_t of 2.0 from MMPDS-03 [46]. The equivalent stress equations for 7075-T6 aluminum sheet with a K_t of 2.0 and 1.5 from MMPDS-03 [46] were used to determine the fatigue lifetimes for the joint assembly cases.

In the fatigue analysis of the open hole specimens, the three K_t interaction formulas Equations (12-14) were applied to the baseline hole in a finite width plate stress concentration factor, K_{t1}, of 2.47 and the K_{t2} of 1.18 for the step itself. The values of K_{t1} and K_{t2} were derived from the finite element analysis results of Section 5, as shown in Table 5.2. The open hole fatigue analysis results show that the multiplication/square root method of Equation (14) is the least conservative of the three proposed K_t interaction solutions. The root sum squares relationship of Equation (13) is more conservative than the multiplication/square root method but less conservative than the multiplication K_t interaction formula of Equation (12) that results in the lowest fatigue margin of safety of the three different approaches studied.

A baseline fatigue margin of safety was calculated for the DB-182 and DS-182 joint assembly specimen types. The X dimension of 0.182 inches between the hole center and lower tangent point of the radius for the baseline joint assembly configurations is large enough that no K_t interaction between the hole and radius exists. The collar is

installed correctly with no riding condition present between the collar and step. The dogbone and double shear specimens with radius blocks installed were considered to be equivalent to the baseline cases for the fatigue analysis. Fatigue lives for these radius block specimen groups were found to be higher than the fatigue lives of the corresponding DB-182 and DS-182 baseline groups in the test results of Section 4.

Baseline stress concentration factors were derived from Equation (24). Additional factors were applied to the stress concentration factors used in dogbone and double shear joint assembly fatigue analysis to account for hole and fit conditions as well as joint types. Fatigue margins were calculated for DB-100, DS-100, DB-050 and DS-050 specimens with holes placed at or near the radii. The fatigue analysis results illustrate that the fatigue margins of safety decrease as the holes are moved closer to the radii which increases the stress concentration modification factor, K_{tf}, values.

7.3. SUMMARY CONCLUSIONS

Generally, the test and FEM/FEA data indicated that the SCF mod factors tended to increase as distance between the hole and radius tangent decreased. This conclusion is illustrated in Figure 7.1. It is shown in the two plots for the joint/assembly and open hole/step specimens that the K_{tf} value is directly proportional to the d/X ratio, where d is the hole diameter and X is the distance between the center of the hole and radius tangent.

The use of the most conservative, or largest, stress concentration modification found using the derived results data is recommended. *Therefore, a K_{tf} value of 1.22 is suggested for use in fatigue analysis of these situations of holes intersecting a radius.* This applied factor is restricted for use in cases with associated geometry, loading and

materials similar to those presented within this research. It may be necessary to develop unique modification factors for specific hole in radius combinations. Engineers and analysts can apply finite element analysis and testing methods similar to those detailed within this study to derive appropriate correction factors.

The fatigue analysis results generally indicate the importance of the use of correct and accurate stress concentration factors and applicable stress concentration modification factors. These seemingly small mod factor values can have a substantial impact on the predicated fatigue performance of critical details, in-particular holes and fastened joints in metallic structures. K_t and K_{tf} values have a significant effect on fatigue lifetimes and resulting fatigue margins of safety. It is crucial that appropriate SCF values be developed through means of testing and or finite element analysis similar those detailed within this research.

The results of the stress corrosion test are not included in Table 7.1 or Figure 7.1. This was a pass/fail experiment. The corrosion specimen was said to have passed the test as no fatigue cracking failures associated with the bolt in radius condition were observed.

7.4. RECOMMENDATIONS FOR FURTHER STUDY

The research contained in this dissertation focuses on specific cases of stress concentration factor interaction involving holes placed at or near a radius or step. This study is limited in scope by design. Many other opportunities exist for closely related analysis and investigation that would broaden the overall understanding of K_t interactions and their effects on fatigue of metals.

One major recommendation for further research is the study of additional, unique cases of combined stress concentrations. The amount of general information and specific data on this topic is somewhat lacking considering the frequency with which these situations occur in the fabrication of metallic structures. K_t charts are available for common cases such as closely positioned multiple holes. However, more data is needed for distinct instances that may occur less frequently but have the potential to be just as, if not more, critical in terms of structural fatigue failure.

There is also a need for more research specifically related to holes and radii placed in close proximity with different combinations of geometry and loading considered. Holes could be placed at the top of steps to determine if the combined stress concentration factors differ from configurations that include holes located at the bottom of the steps, as presented in this study. Load direction is critical to the determination of SCFs. The effects of applied shear, biaxial, transverse, and bending stresses should all be analyzed.

Common titanium, protruding head bolts are used in this research to determine the effects of hole fill on the derived stress concentration factors. Other fasteners and plugs with different material types, geometric configurations and installation methods should also be evaluated to determine a preferable repair alternative in cases where holes are placed at or near a step and spotfacing is not a viable option. Countersunk fasteners and freeze plugs are sometimes used in aerospace applications in these instances, however these alternate installations would each have their own unique effect on stress concentration factors and additional analytical work is needed in order to determine accurate values.

All finite element modeling/analysis conducted as part of this research project wasconducted using the CATIA Generative Structural Analysis (GSA) Workbench. There are a number of other commercial FEM/FEA packages available that could be used to facilitate an in-depth study involving K_t analysis. Each program has its own unique solver that will provide slightly different results based on the exact same set of user inputs. It is recommended that finite element computer applications other than CATIA (GSA) be utilized for comparison to the results obtained from physical testing to determine the accuracy of the derived stress concentration factor values.

A specific type of element, set of analysis inputs and solution method were used in CATIA (GSA) to obtain the results presented in Section 5. Different finite element types and other variables should be studied within the CATIA Generative Structural Analysis (GSA) Workbench to determine the quantitative impact on the derived stress concentration mod factors. Minor changes to the model and solver can radically alter the resulting outputs. The accuracy of the finite element analysis is completely dependent upon the values and parameters entered in to the software.

The fatigue analysis presented in Section 6 is relatively simple and straightforward in nature. The goal was limited to detailing how a typical fatigue analysis using K_t mod factors is completed. However, it is possible to conduct a more complex and accurate fatigue study involving combined stress concentrations. It is recommended that more sophisticated fatigue analysis studies related to K_t interactions be performed and presented for the benefit of engineers and analysts working in the field of fatigue.

APPENDIX A

TEST SPECIMEN DRAWINGS

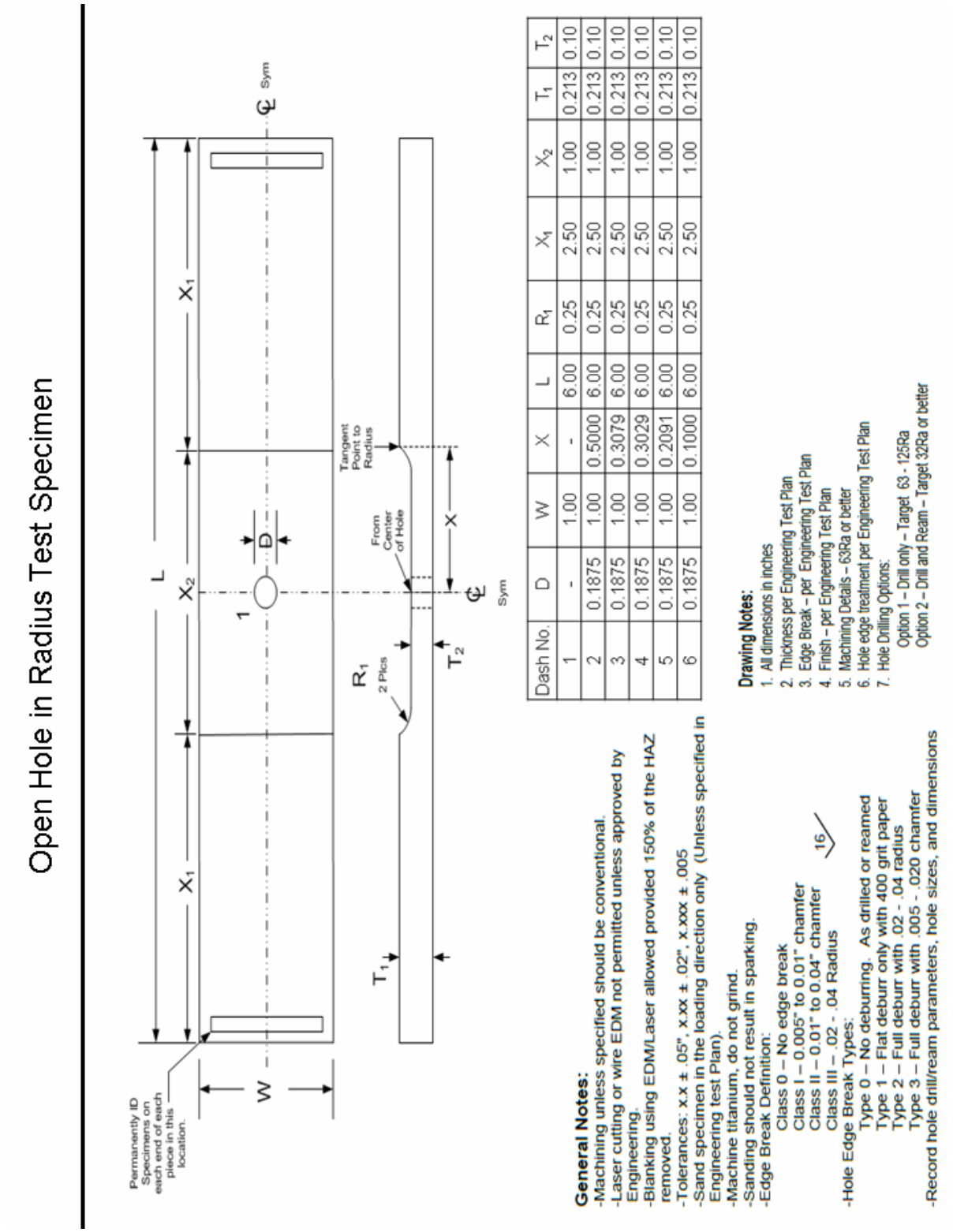

Dash No.	D	W	X	L	R_1	X_1	X_2	T_1	T_2
1	-	1.00	-	6.00	0.25	2.50	1.00	0.213	0.10
2	0.1875	1.00	0.5000	6.00	0.25	2.50	1.00	0.213	0.10
3	0.1875	1.00	0.3079	6.00	0.25	2.50	1.00	0.213	0.10
4	0.1875	1.00	0.3029	6.00	0.25	2.50	1.00	0.213	0.10
5	0.1875	1.00	0.2091	6.00	0.25	2.50	1.00	0.213	0.10
6	0.1875	1.00	0.1000	6.00	0.25	2.50	1.00	0.213	0.10

Figure A.1. Open Hole in Radius Test Specimen

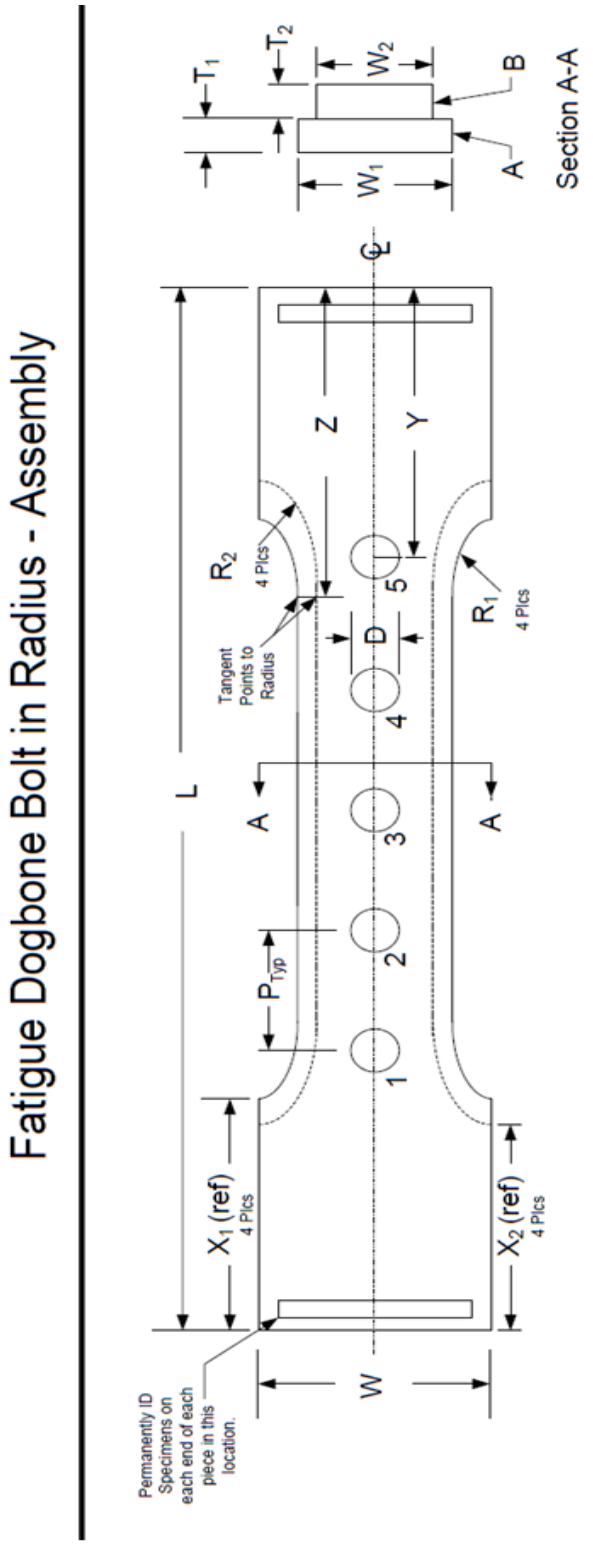

Figure A.2. Fatigue Dogbone Bolt in Radius - Assembly

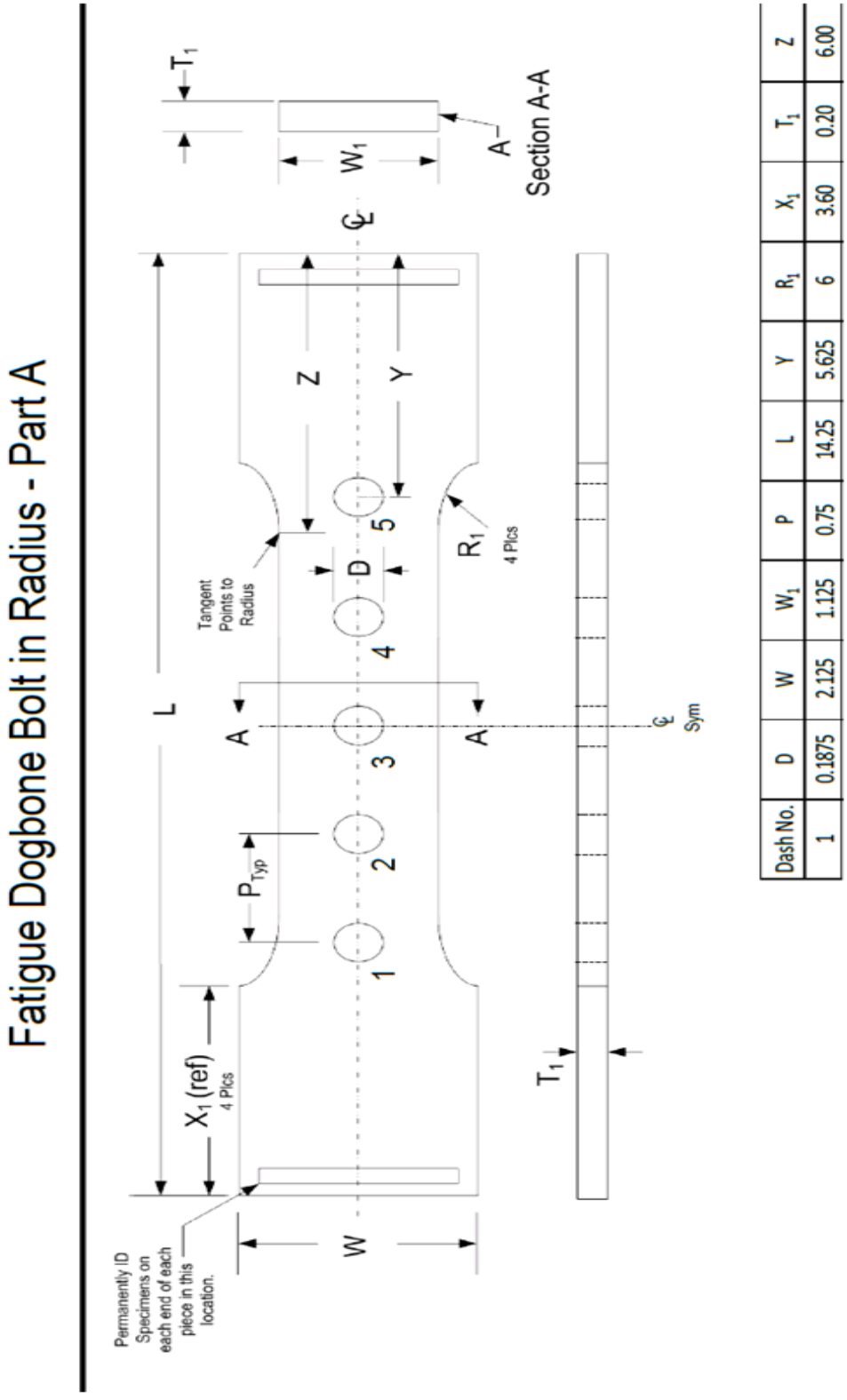

Dash No.	D	W	W_1	P	L	Y	R_1	X_1	T_1	Z
1	0.1875	2.125	1.125	0.75	14.25	5.625	6	3.60	0.20	6.00

Figure A.3. Fatigue Dogbone Bolt in Radius – Part A

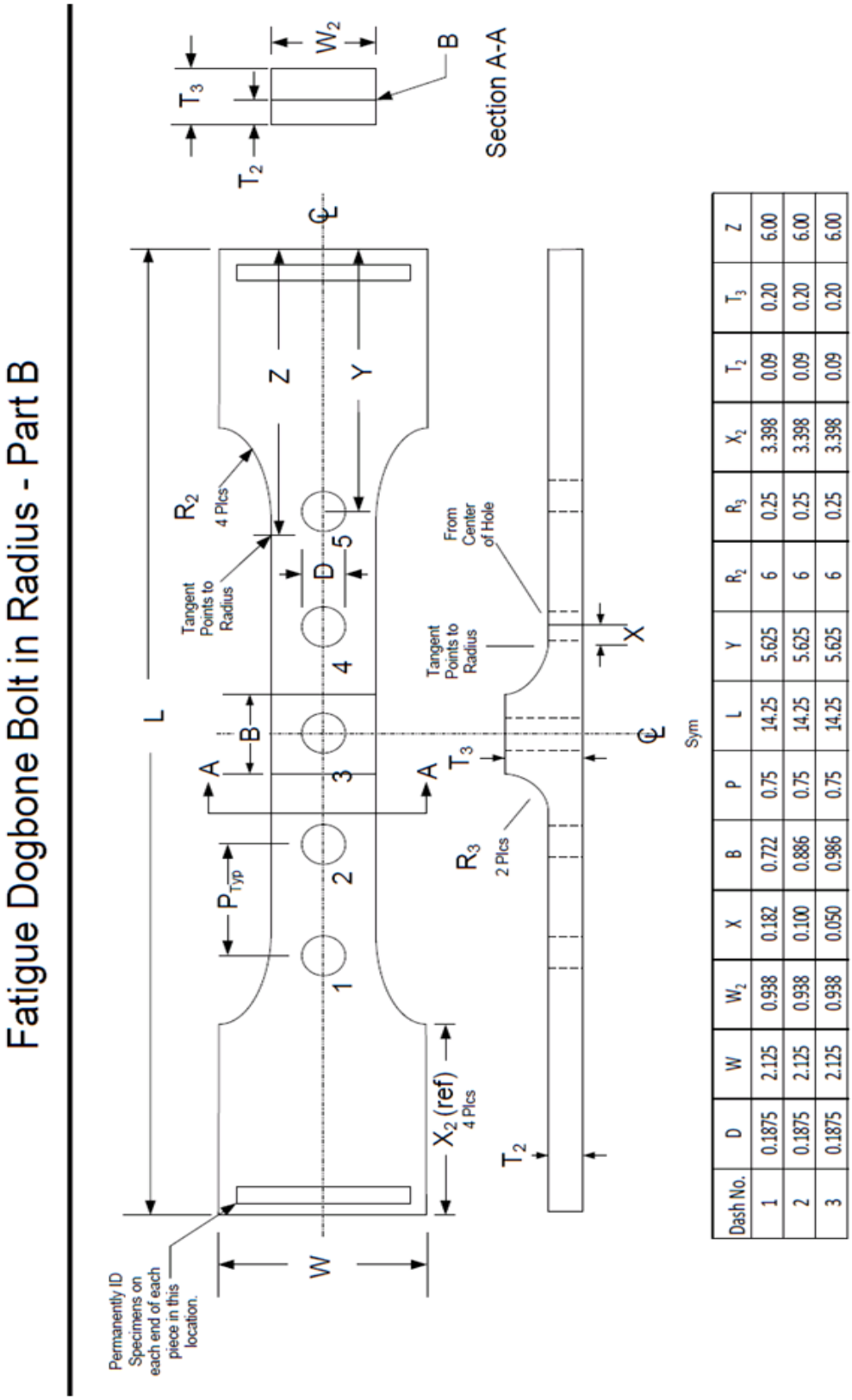

Dash No.	D	W	W_2	X	B	P	L	Y	R_2	R_3	X_2	T_2	T_3	Z
1	0.1875	2.125	0.938	0.182	0.722	0.75	14.25	5.625	6	0.25	3.398	0.09	0.20	6.00
2	0.1875	2.125	0.938	0.100	0.886	0.75	14.25	5.625	6	0.25	3.398	0.09	0.20	6.00
3	0.1875	2.125	0.938	0.050	0.986	0.75	14.25	5.625	6	0.25	3.398	0.09	0.20	6.00

Figure A.4. Fatigue Dogbone Bolt in Radius – Part B

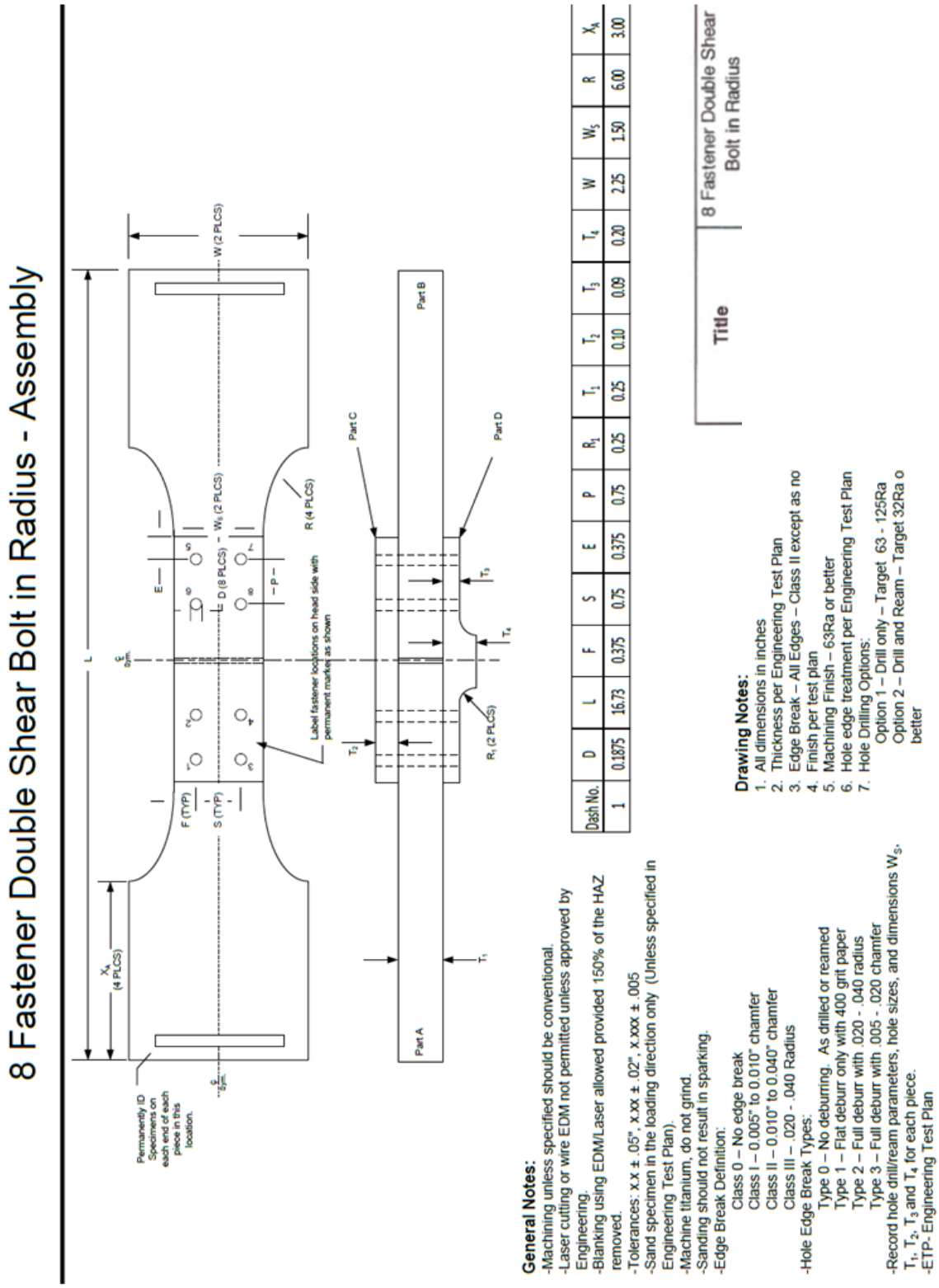

Dash No.	D	L	F	S	E	P	R_1	T_1	T_2	T_3	T_4	W	W_S	R	X_4
1	0.1875	16.73	0.375	0.75	0.375	0.75	0.25	0.25	0.10	0.09	0.20	2.25	1.50	6.00	3.00

Figure A.5. 8 Fastener Double Shear Bolt in Radius - Assembly

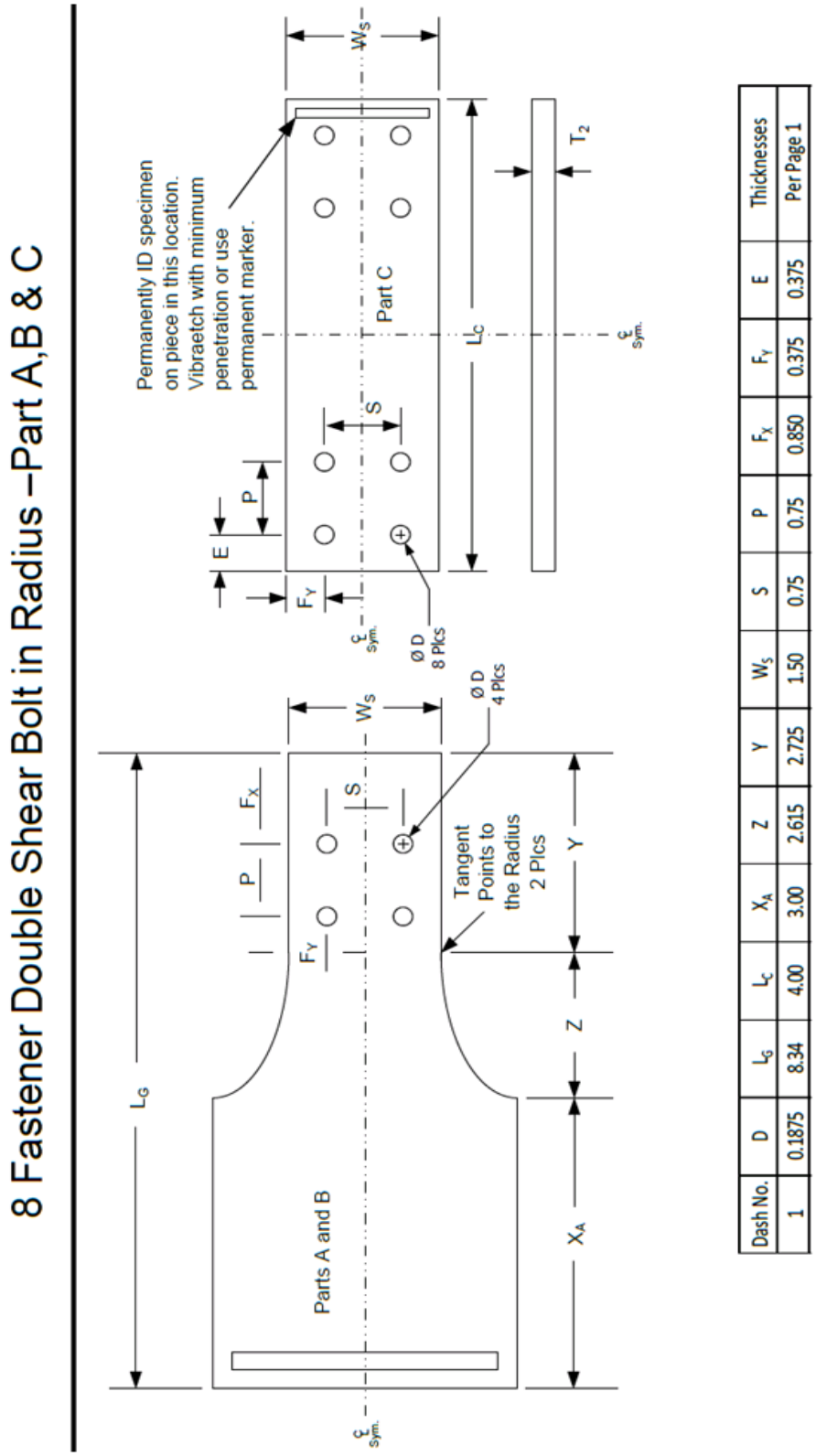

Dash No.	D	L_G	L_C	X_A	Z	Y	W_S	S	P	F_X	F_Y	E	Thicknesses
1	0.1875	8.34	4.00	3.00	2.615	2.725	1.50	0.75	0.75	0.850	0.375	0.375	Per Page 1

Figure A.6. 8 Fastener Double Shear Bolt in Radius – Part A, B & C

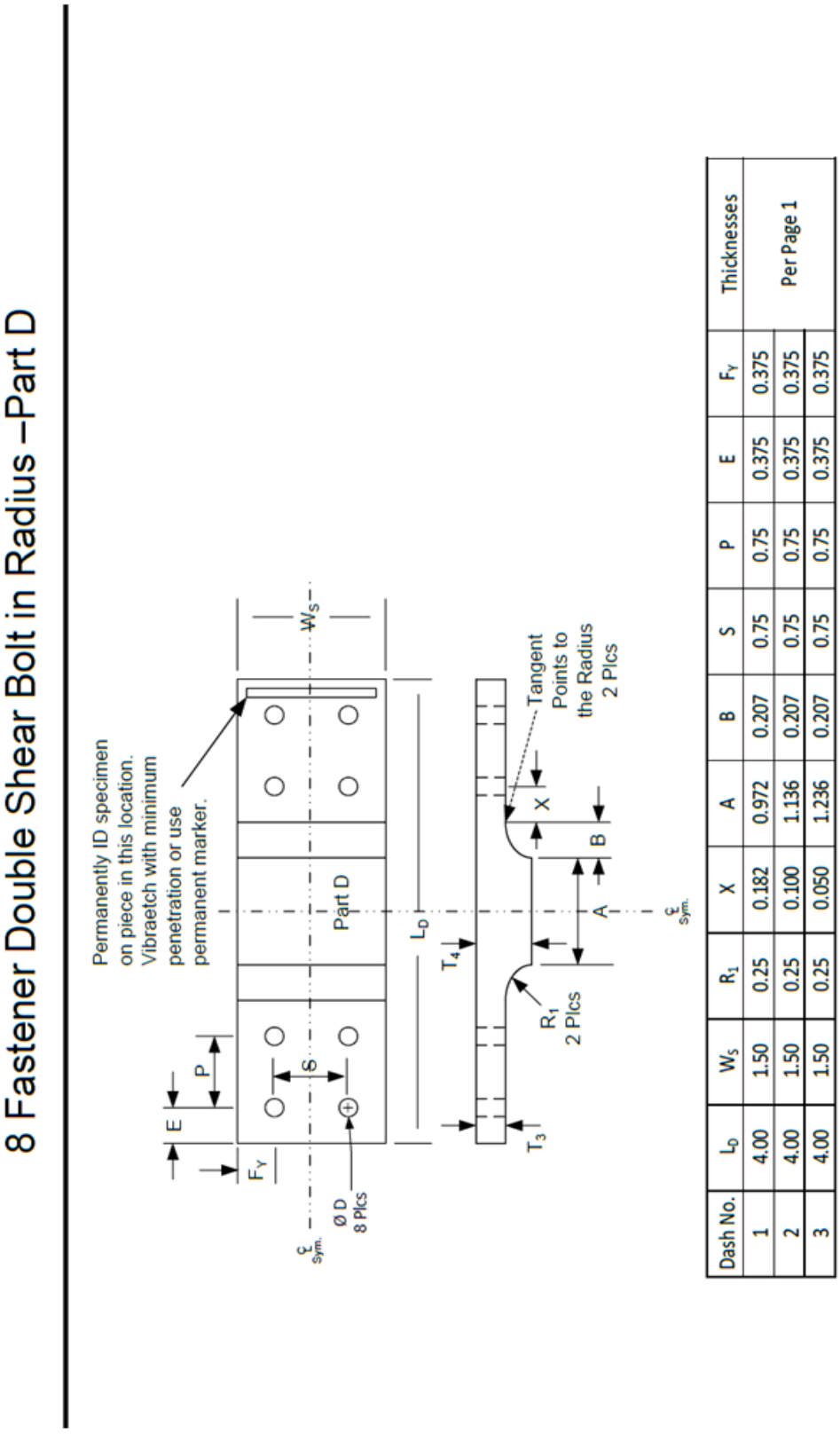

Dash No.	L_D	W_S	R_1	X	A	B	S	P	E	F_Y	Thicknesses
1	4.00	1.50	0.25	0.182	0.972	0.207	0.75	0.75	0.375	0.375	Per Page 1
2	4.00	1.50	0.25	0.100	1.136	0.207	0.75	0.75	0.375	0.375	
3	4.00	1.50	0.25	0.050	1.236	0.207	0.75	0.75	0.375	0.375	

Figure A.7. 8 Fastener Double Shear Bolt in Radius – Part D

APPENDIX B

OPEN HOLE TEST SPECIMEN PICTURES

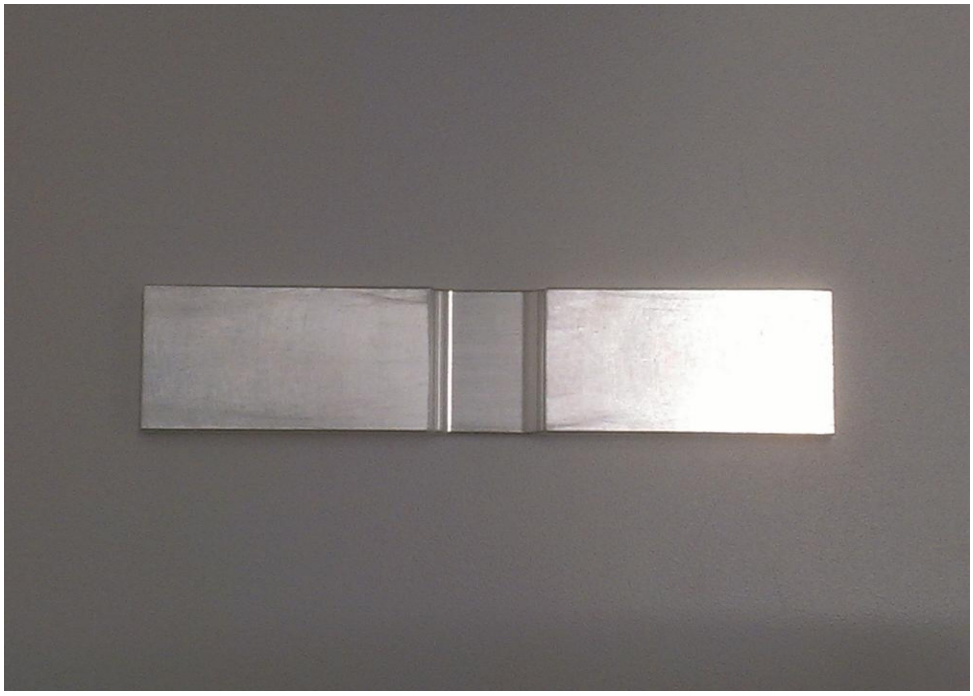

Figure B.1. Open Hole in Radius Test Specimen -1 Pre-Test Picture

Figure B.2. Open Hole in Radius Test Specimen -2 Pre-Test Picture

Figure B.3. Open Hole in Radius Test Specimen -3 Pre-Test Picture

Figure B.4. Open Hole in Radius Test Specimen -4 Pre-Test Picture

Figure B.5. Open Hole in Radius Test Specimen -5 Pre-Test Picture

Figure B.6. Open Hole in Radius Test Specimen -6 Pre-Test Picture

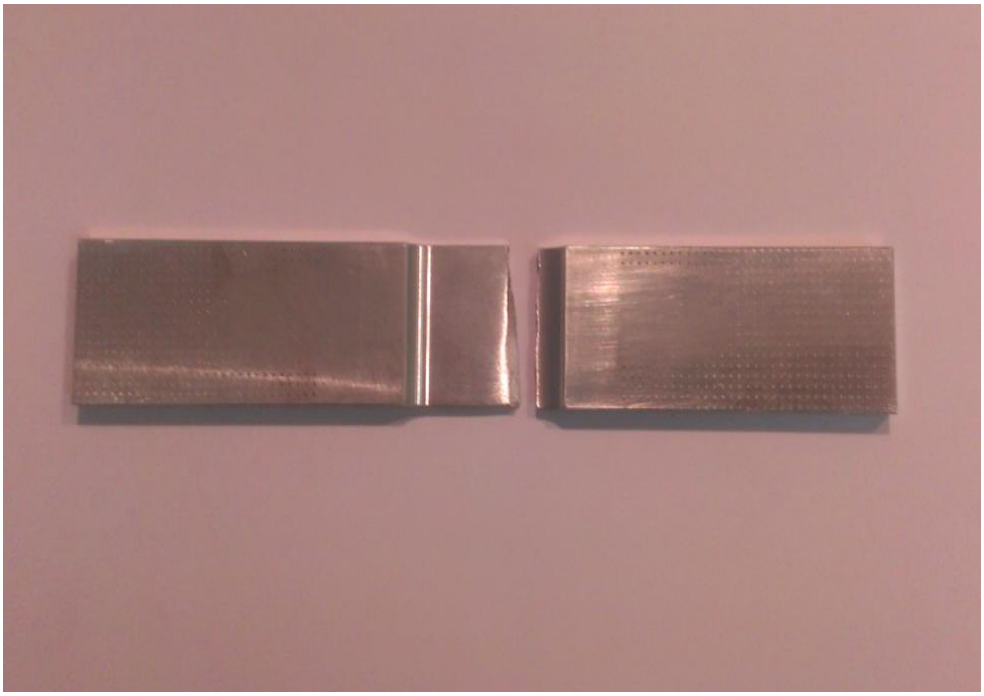

Figure B.7. Open Hole in Radius Test Specimen -1 Post-Test Picture

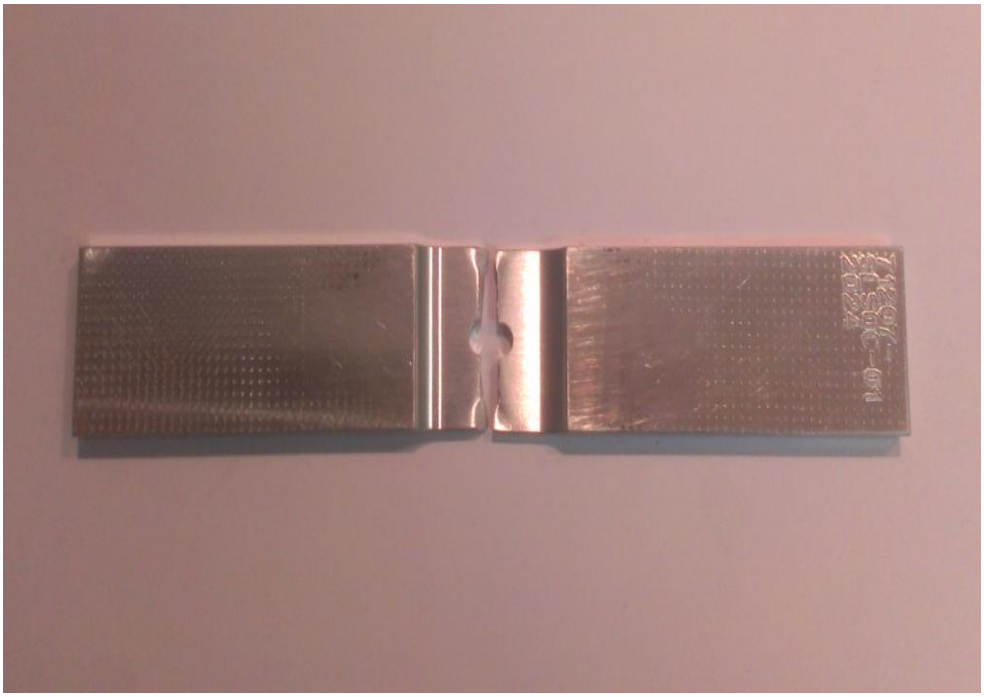

Figure B.8. Open Hole in Radius Test Specimen -2 Post-Test Picture

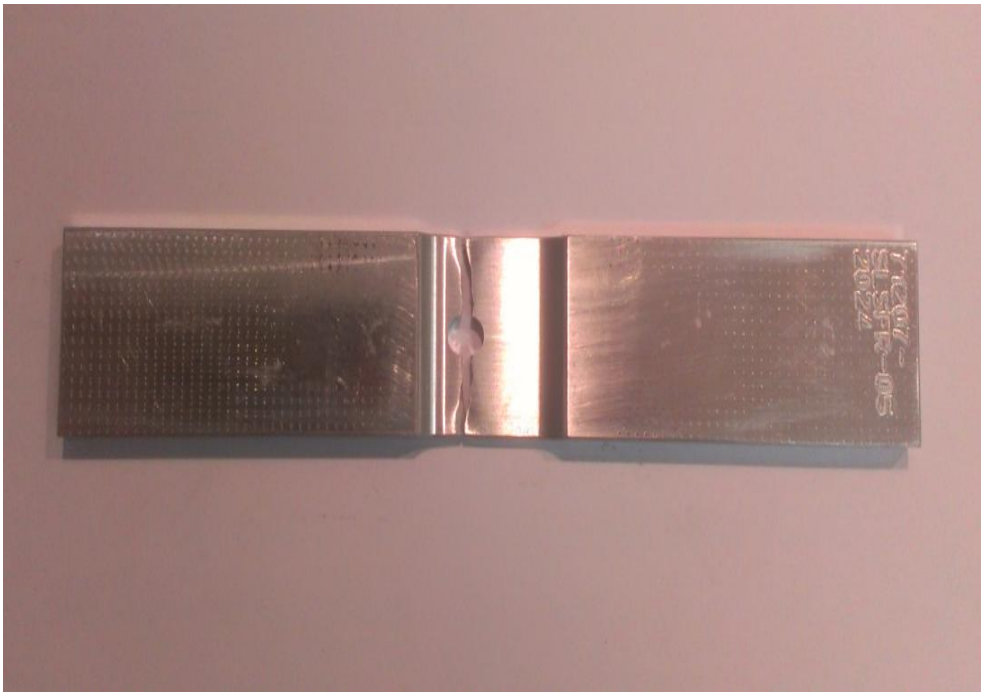

Figure B.9. Open Hole in Radius Test Specimen -3 Post-Test Picture

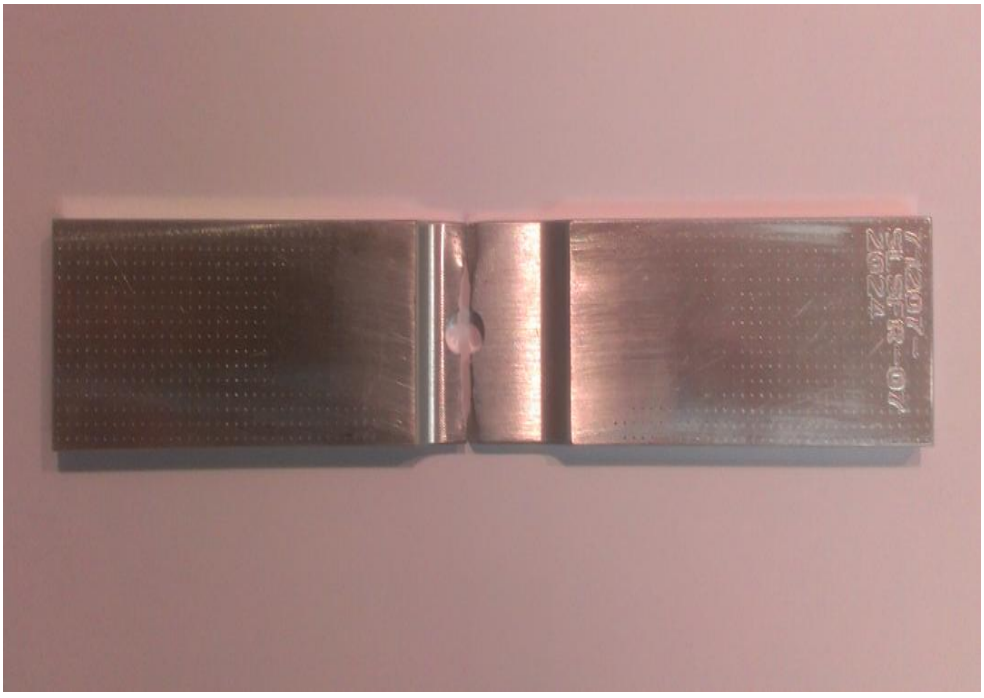

Figure B.10. Open Hole in Radius Test Specimen -4 Post-Test Picture

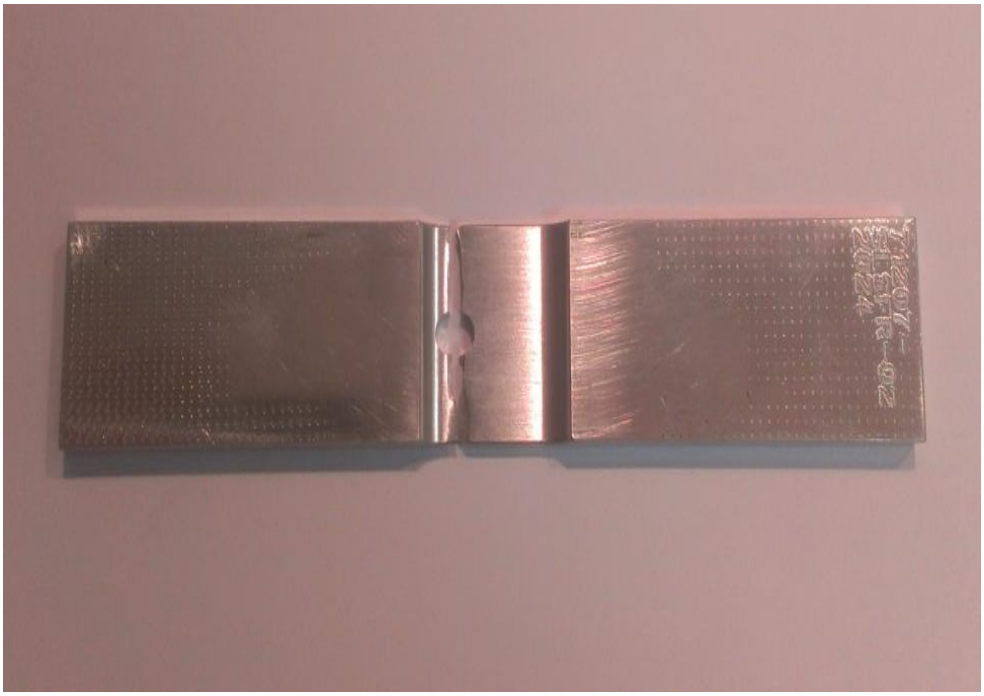

Figure B.11. Open Hole in Radius Test Specimen -5 Post-Test Picture

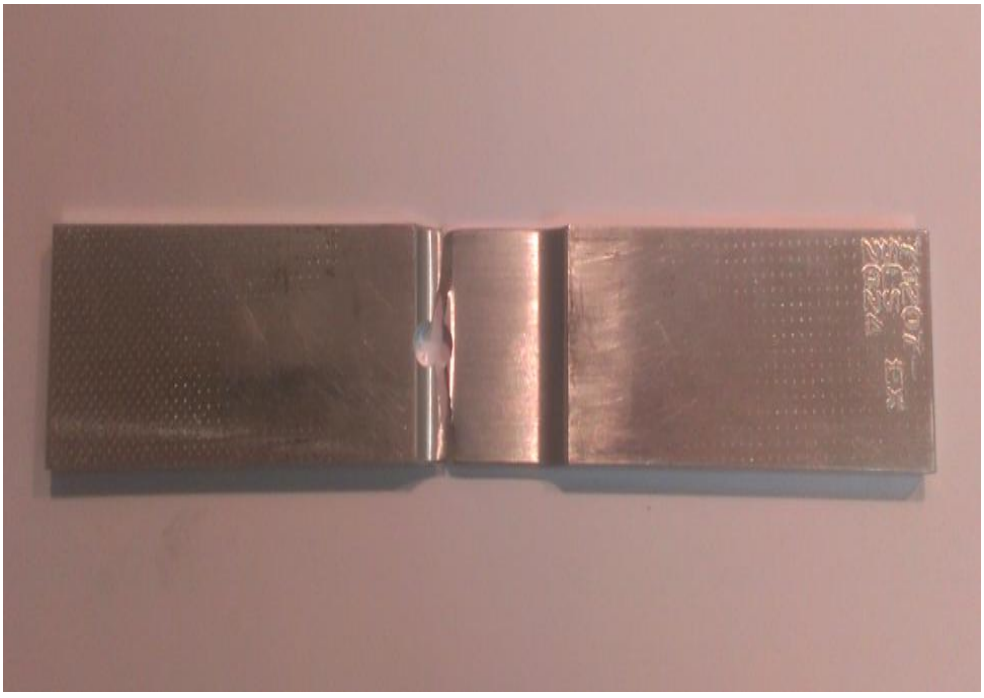

Figure B.12. Open Hole in Radius Test Specimen -6 Post-Test Picture

BIBLIOGRAPHY

[1] ASTM E1823, "Standard Terminology Relating to Fatigue and Fracture Testing," ASTM, p. 7, 2010.

[2] W.A.J. Albert "Uber Treibseile am Harz," Archive fur Mineralogie, Geognosie, Bergbau und Huttenkunde, Vol 10, (in German), pp. 215-234, 1838.

[3] A. Wöhler, "Versuche uber die Festigkeit der Eisenbahnwagenachsen," Zeitschrift fur Bauwesen, Vol 10, (in German), with English summary in *Engineering*, Vol. 4, 1867, pp. 160-161, 1860.

[4] U.S. Department of Transportation, Federal Aviation Administration, "Damage Tolerance Assessment Handbook," Vol. 1, pp. 1-3 - 1-6, 1993.

[5] National Transportation Safety Board, "Aircraft Accident Report-Aloha Airlines, Flight 243, Boeing 737-200, -N73711, near Maui, Hawaii-28 April 1988," 1989.

[6] http://www.aloha.net/~icarus/index.htm, "Aloha Airlines Flight 243 - Aircraft Accident - Maui Hawaii," May 2011.

[7] C. Rivera, http://articles.latimes.com/2011/apr/04/nation/la-na-southwest-20110404, "Fatigue cracks found in Southwest plane," Los Angeles Times, April 2011.

[8] J.A. Bannantine, J.J. Comer, J.L. Handrock, "Fundamentals of Metal Fatigue Analysis," Prentice-Hall, 1990.

[9] M.A. Miner, "Cumulative Damage in Fatigue," Journal of Applied Mechanics, Vol. 67, pp. A159-A164, 1945.

[10] ESDU, "Guide to Stress Concentration Data," Engineering Sciences Data Item 64001, 1976.

[11] W.D. Pilkey, "Peterson's Stress Concentration Factors," 2nd Edition, John Wiley & Sons, 1997.

[12] W.D. Pilkey, D.F. Pilkey "Peterson's Stress Concentration Factors," 3rd Edition, John Wiley & Sons, 2008.

[13] C.B. Ling, "On the Stresses in a Plate Containing Two Circular Holes", Journal of Applied Physics, Vol. 19, 1948.

[14] A.R. Eccles, "Software Development of a Knowledge-Based System for Designing Against Fatigue," MSc Thesis, University of Hull, UK, 1996.

[15] ESDU, "Geometric Stress Concentration Factors: Two Adjacent Unreinforced Circular Holes in Infinite Flat Plates," Engineering Sciences Data Item 75007, 1975.

[16] ESDU, "Stress Concentrations: Interaction and Stress Decay for Selected Cases," Engineering Sciences Data Item 85045, 1985.

[17] R.H. Graham, M. Raines, K.G. Swift, L. Gill, "Prediction of stress concentrations associated with interacting stress-raisers within aircraft design:methodology development and application," Proceedings of the Institution of Mechanical Engineers, Part G: Journal of Aerospace Engineering, 2005.

[18] J. Middendorf, http://www.johnmiddendorf.com/johnmfiles/UNSW/FEA1/index.htm , "Analysis of plate with large elliptical hole and two smaller circular holes," University of New South Wales School of Mechanical Engineering, April 2003.

[19] R.A.W. Haddon, "Stresses in an Infinite Plate with Two Unequal Circular Holes," The Quarterly Journal of Mechanics and Applied Mathematics, Vol. 20, pp. 277-291, 1967.

[20] NASA, "Astronautic Structures Manual, Volume 1", George C. Marshall Space Flight Center, Marshall Space Flight Center, Alabama, 1975.

[21] V.L. Salerno, J.B. Mahoney, "Stress Solution for an Infinite Plate Containing Two Arbitrary Circular Holes under Equal Biaxial Stresses," Trans. ASME, Industry Section, Vol. 90, p. 656, 1968.

[22] A.J. Durelli, R.L. Lake, E. Phillips, "Stress concentrations produced by multiple semi-circular notches in infinite plates under uniaxial states of stress," Proceedings of the Society of Experimental Stress Analysis, Vol. 10, No. 1, 1952.

[23] A.J. Durelli, R.L. Lake, E. Phillips, "Stress distribution in plates under a uniaxial state of stress with multiple semi-circular and flat-bottom notches," Proceedings of the First National Congress on Applied Mechanics, 1952.

[24] C.B. Ling, 1968, "On Stress Concentration Factor in a Notched Strip," Trans. ASME, Applied Mechanics Section, Vol. 90, p. 833, 1968.

[25] A. Atsumi, "Stress Concentration in a Strip under Tension and Containing an Infinite Row of Semicircular Notches," Quarterly Journal of Mechanics and Applied Mathematics, Vol. 11, p. 478, 1958.

[26] M. Isida, "Form Factors of a Strip with an Elliptic Hole in Tension and Bending," Scientific Papers of Faculty of Engineering, Tokushima University, Vol. 4, p. 70, 1953.

[27] M. Hetenyi, "The Distribution of Stress in Threaded Connections," Proceedings of the Society of Experimental Stress Analysis, Vol. 1, No. 1, p. 147, 1943.

[28] R.H. Graham, “Interaction of stress-raising features in aerostructures” PhD Thesis, University of Hull, UK,2002.

[29] K.J. Schulz, "Over den Spannungstoestand in doorborde Platen," (On the State of Stress in Perforated Plates), Doctoral Thesis, Techn. Hochschule, Delft, (in Dutch), 1941.

[30] A. Mori, "Stress Distributions in a Semi-Infinite Plate with a Row of Circular Holes," Bulletin of the Japan Society of Mechanical Engineers,Vol. 15, p. 899, 1972.

[31] R.C. Sampson, "Photoelastic Analysis of Stresses in Perforated Material Subject to Tension or Bending," Bettis Technical Review, WAP-BT-18, 1960.

[32] P. Meijers, "Doubly-Periodic Stress Distributions in Perforated Plates," Dissertation, Tech. Hochschule Delft, Netherlands, 1967.

[33] G. Horvay, "The Plane-Stress Problem of Perforated Plates," Trans. ASME, Applied Mechanics Section, Vol. 74, p.355, 1952.

[34] M. Nishida, "Stress Concentration," Morikita Shuppan, Tokyo, (in Japanese), 1976.

[35] R. Bailey, R. Hicks, "Behavior of Perforated Plates under Plane Stress," Journal of Mechanical Engineering Science, Vol. 2, p. 143, 1960.

[36] L.E. Hulbert, "The Numerical Solution of Two-Dimensional Problems of the Theory of Elasticity,Ohio State University, Eng. Exp. Sta. Bull. 198, Columbus, Ohio, 1965.

[37] L.E. Hulbert and F.W. Niedenfuhr, "Accurate Calculation of Stress Distributions in MultiholedPlates," Trans. ASME, Industry Section, Vol. 87, p. 331, 1965.

[38] H. Kraus, "Stress Concentration Factors for Perforated Annular Bodies Loaded in Their Plane,"Unpublished Report, Pratt and Whitney Company, East Hartford, Connecticut, 1963.

[39] H. Kraus, P. Rotondo, W.D. Haddon, "Analysis of Radially Deformed Perforated Flanges," Trans. ASME, Applied Mechanics Section, Vol. 88, p. 172, 1966.

[40] J.P. Sikora, "A Summary of Stress Concentrations in the Vicinity of Openings in Ship Structures," Department of the Navy, Naval Ship Research and Development Center, Bethesda, Maryland, March, 1973.

[41] CATIA, V5.19, Dassault Systèmes, 1994-2008.

[42] ASTM E466, "Standard Practice for Conducting Force Controlled Constant Amplitude Axial Fatigue Tests of Metallic Materials," ASTM, 1996.

[43] MTS Systems Corporation, www.mts.com, 2013.

[44] ASTM G44-99, "Standard Practice for Exposure of Metal and Alloys by Alternate Immersion in Neutral 3.5% Sodium Chloride Solution," ASTM, 2005.

[45] R.B. Abernethy, "The New Weibull Handbook", Fifth Edition, 2007.

[46] Federal Aviation Administration, "MMPDS-03," Battelle Memorial Institute, Columbus, OH, October, 2006.

[47] Dassault Systèmes, "Generative Structural Analysis User's Guide," Version 5 Release 16, 2005.

[48] M. Niu, "Airframe Structural Design," Conmilit Press Ltd., 1988.

VITA

David Warren Whitley graduated Magna Cum Laude with a Bachelor of Science degree in Mechanical Engineering from the University of Missouri-St. Louis/Washington University joint undergraduate engineering program in 2005. In 2008, he graduated Magna Cum Laude with a Master of Science degree in Aerospace Engineering from Missouri University of Science & Technology. David earned a Doctor of Philosophy in Aerospace Engineering from Missouri University of Science & Technology in 2013. His dissertation title was "Interacting Stress Concentration Factors and their Effect on Fatigue of Metallic Aerostructures", advised by Dr. L. R. Dharani.

David worked as Structural Engineer for ITW, Inc. from 2006 to 2008. He has been employed by Spirit Aerosystems, Inc. as a Fatigue & Damage Tolerance Engineer since 2010.